(NASA-CR-144327) PROGRAM TO DESIGN, FABRICATE, TEST, AND DELIVER A THERMAL CONTROL-MIXING CONTROL DEVICE FOR THE GEORGE C. MARSHALL SPACE FLIGHT CENTER (AIRESEARCH MFG. CO., PHOENIX, ARIZ.) 108 P HC $5.50 G3/35

N76-25540

UNCLAS 42203

PHASES I AND II
TECHNICAL REPORT

PROGRAM TO DESIGN, FABRICATE, TEST, AND DELIVER A THERMAL CONTROL-MIXING CONTROL DEVICE FOR GEORGE C. MARSHALL SPACE FLIGHT CENTER NATIONAL AERONAUTICS AND SPACE ADMINISTRATION (CONTRACT NO. NAS8-31289)

76-411348(1) April 12, 1976

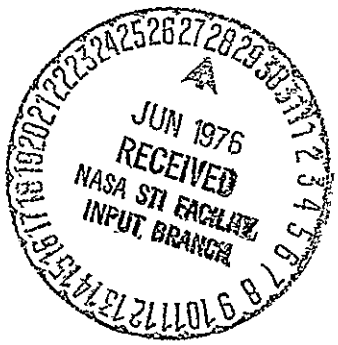

GARRETT

AIRESEARCH MANUFACTURING COMPANY OF ARIZONA
A DIVISION OF THE GARRETT CORPORATION
PHOENIX, ARIZONA

PHASES I AND II
TECHNICAL REPORT

PROGRAM TO DESIGN, FABRICATE,
TEST, AND DELIVER A THERMAL
CONTROL-MIXING CONTROL DEVICE FOR
GEORGE C. MARSHALL SPACE FLIGHT CENTER
NATIONAL AERONAUTICS AND
SPACE ADMINISTRATION
(CONTRACT NO. NAS8-31289)

• 76-411348(1) April 12, 1976 •

Prepared by T. S. Thurston/R. H. Larson

Initial Issue
Approved by L. I. Chambliss/Supvr., Documentation

T. G. Sutton/Ass't. Project Engineer

D. J. Schaffer/Sr. Project Engineer

AIRESEARCH MANUFACTURING COMPANY
A DIVISION OF THE GARRETT CORPORATION
PHOENIX, ARIZONA

REPORT NO. 76-411348(1)

TOTAL PAGES 104

ATTACHMENTS: See Table of Contents.

REV	BY	APPROVED	DATE	PAGES AND/OR PARAGRAPHS AFFECTED

TABLE OF CONTENTS

TABLE OF CONTENTS (CONTD)

LIST OF FIGURES

PHASES I AND II TECHNICAL REPORT

PROGRAM TO DESIGN, FABRICATE, TEST, AND DELIVER A THERMAL CONTROL-MIXING CONTROL DEVICE FOR GEORGE C. MARSHALL SPACE FLIGHT CENTER NATIONAL AERONAUTICS AND SPACE ADMINISTRATION (CONTRACT NO. NAS8-31289)

SECTION 1

INTRODUCTION AND SUMMARY

1.1 INTRODUCTION

This is a technical report that summarizes Phases I and II of the program conducted by AiResearch Manufacturing Company of Arizona, a Division of The Garrett Corporation, for the George C. Marshall Space Flight Center, National Aeronautics and Space Administration, to design, fabricate, test, and deliver a thermal control-mixing control device as outlined in AiResearch Proposal 74-410766. The program was authorized by NASA Contract NAS8-31289 and is being accomplished under AiResearch Master Work Order 3409-248115-01-XXXX. The material in this report summarizes the program progress from initiation of the program on February 19, 1975, through March 10, 1976.

1.2 SUMMARY OF PHASE I, TEMPERATURE SENSOR DEVELOPMENT

Phase I of the program, which consisted of the development of a sensor capable of detecting temperature changes as a function of viscosity changes, has been completed. This type of sensor, consisting of an orifice bridge circuit, has resulted in a device with a threshold above internally generated noise of 0.8C (1.5F). Data was obtained using a "noise free" Freon source provided by an air pressurized bladder.

Tests conducted to operate the sensor from a typical Freon centrifugal pump system employing an air bubble accumulator for noise attenuation disclosed that the sensor could be used only to sense temperature changes greater than 3.3C (6F) because of the excessively noisy output. This was attributed to the high frequency-pressure fluctuations in the Freon supply to the sensor. This temperature sensor was found to be unacceptable for this program because of high pressure noise generated in the Freon pump systems.

An alternate sensor was developed under an AiResearch company-funded Research and Development Program using a fluidic pin amplifier in conjunction with an expansion device. This device is able to sense changes of less than 0.25F with greater than 15:1 signal-to-noise ratio when operating with a typical Freon pump-supplied pressure. The pressure sensitivity of the sensor is approximately 0.0019F/kPa, which is relatively small and can be easily corrected if necessary. The expansion device used is an alcohol-filled bellows.

The filled-bellows pin amplifier temperature sensor has been selected for use in this program and will be integrated with the selected valve in Phase III of this program.

1.3 SUMMARY OF PHASE II, VALVE SELECTION AND DEVELOPMENT

The pulse duration modulation (PDM) diverter valve has been selected as the valve to be incorporated with the temperature sensor in Phase III. The diverter valve has been tested and performed with 100-percent flow diversion. In addition, the valve operates with a flow efficiency of at least 95 percent, with the possibility of attaining 100-percent flow efficiency if the vent flow of the PDM can be channeled through the last stage of the diverter valve.

The proportional-vortex combination mixing valve was built and tested. The flow efficiency of this valve was approximately 45 percent due to large flow losses in the proportional amplifier used to drive the vortex valves. The vortex valves operated very well, with 100-percent flow efficiency and full range mixing capabilities. Because of the flow efficiency of this valve concept (as well as the fact that a special type of heat exchanger capable of handling three flows would be required for Freon cooling), this valve concept was not selected for use in the thermal control loop.

SECTION 2

DESIGN AND EVALUATION OF TEMPERATURE SENSORS

A temperature sensor was to be designed to operate as an integral part of a Freon 21 temperature controller, to be used in a thermal control loop. Two temperature sensors were designed and evaluated for this application. This sensor is required to operate in Freon 21 and to have the temperature sensitivity necessary to control temperature to 50 ±3F. The results of this effort is discussed in the following subparagraphs.

2.1 ORIFICE BRIDGE VISCOSITY CHANGE TEMPERATURE SENSOR

The design and analysis of the orifice bridge viscosity change temperature sensor is presented in the following subparagraphs. This sensor uses a resistive bridge network to sense viscosity changes due to temperature.

2.1.1 Operation of the Orifice Bridge Viscosity Change Temperature Sensor

The orifice bridge sensor shown in Figure 1 consists of two types of restrictors, capillary (R_1 and R_4) and vortex (R_2 and R_3).

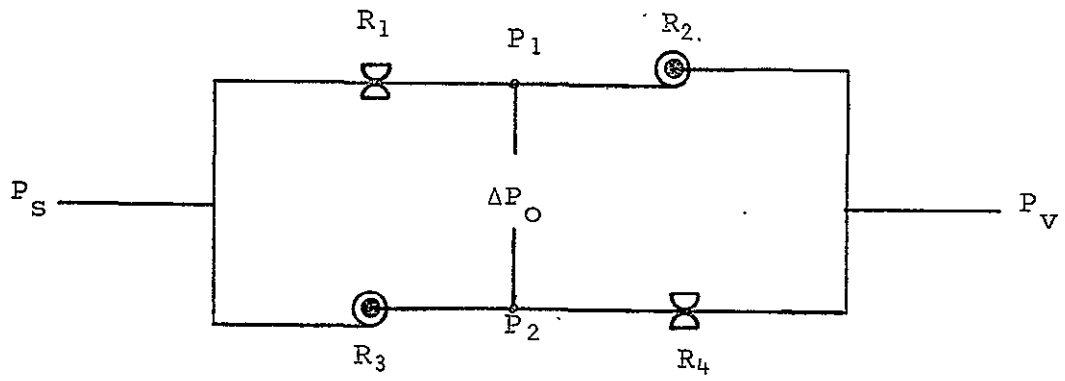

FIGURE 1

ORIFICE BRIDGE SENSOR

The effective resistance of the restrictors will change as a function of viscosity. The effect of viscosity change on a vortex restrictor is somewhat different than on a capillary restrictor. Two dissimilar restrictors placed in series like R_1 and R_2 in Figure 1 will produce a change in P_1 that is proportional to viscosity or temperature. By reversing the order of R_1 and R_2 relative to supply and vent, R_3 and R_4 would produce an opposite effect. In the orifice bridge circuit, the differential pressure, ΔP_o, represents a pressure gain twice that of the series restrictors.

The performance of the orifice bridge sensor with a noise-free power supply (Figure 2) is shown in Figure 3.

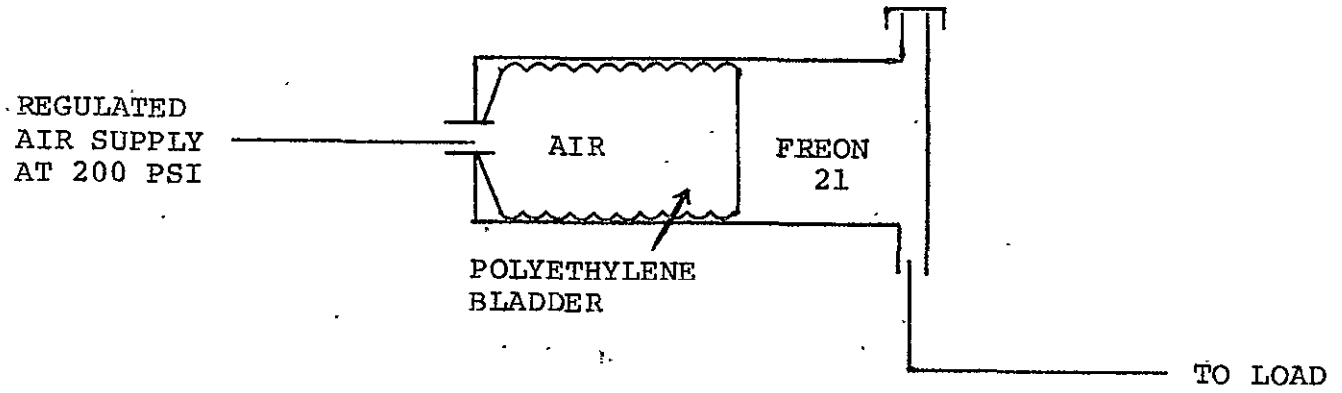

FIGURE 2

BLADDER USED IN NOISE-FREE POWER SUPPLY

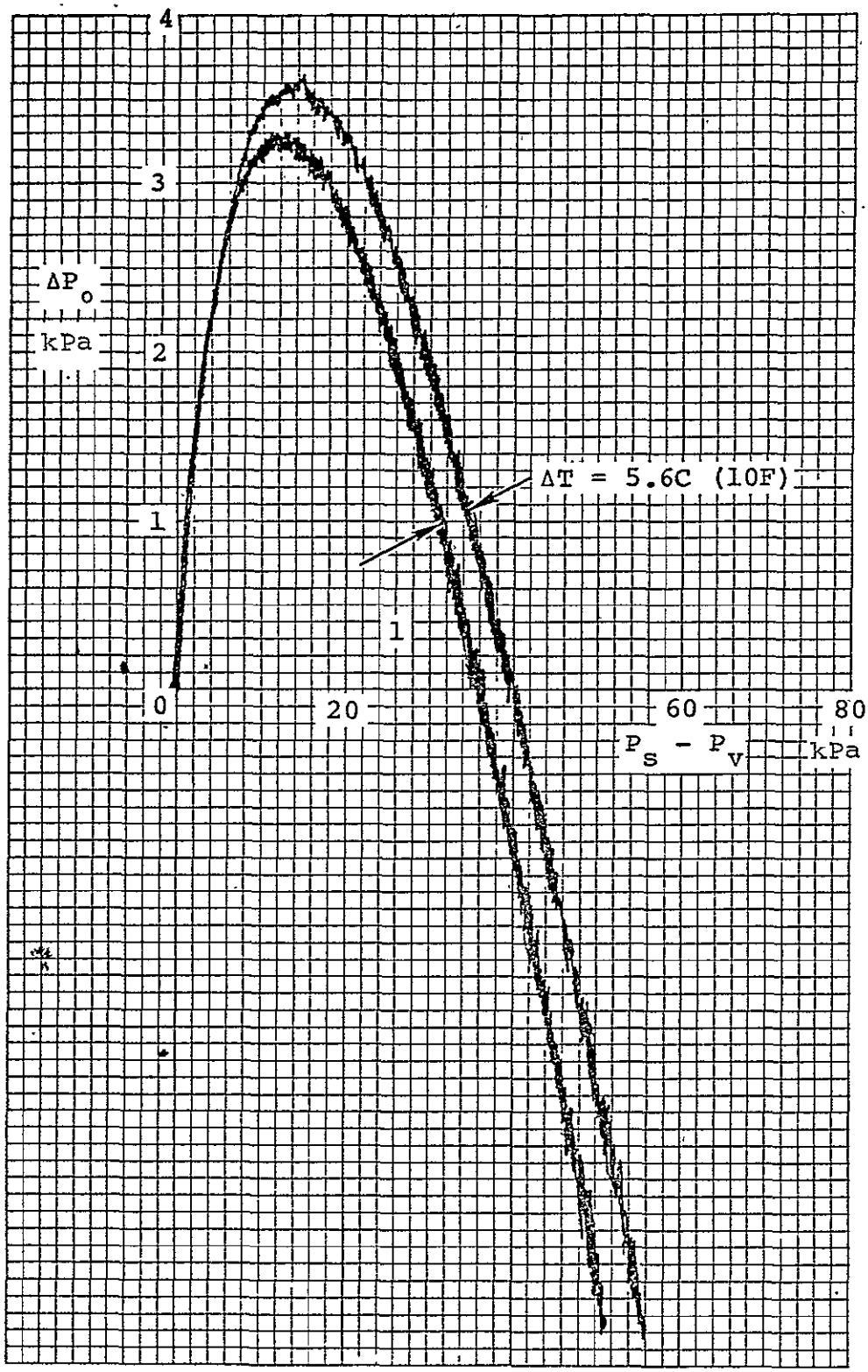

FIGURE 3

OUTPUT OF TEMPERATURE SENSOR

2.1.2 Analysis of the Orifice Bridge Viscosity Change Temperature Sensor

The analyses and theory presented herein were applied to a simple circuit employing two dissimilar restrictions connected in series as shown in Figure 4.

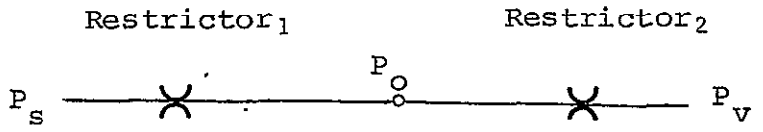

FIGURE 4

DISSIMILAR RESTRICTIONS
CONNECTED IN SERIES

where

P_s = Supply pressure

P_v = Vent pressure

P_o = Output pressure

Starting with the basic flow equation for incompressible flow through a restriction, and by assuming that the flow is dependent upon a Reynolds number, the following equation for flow along a differential length of a restriction is obtained.

$$\frac{-dP}{d\ell} = C_f \frac{\rho V^2}{2} = C_f \frac{\omega^2}{2\rho A^2}$$

where

dP = Differential pressure drop

$d\ell$ = Differential length

C_f = Flow coefficient (dependent on Reynolds number and restrictor geometry)

ρ = Fluid density

V = Fluid velocity

ω = Weight flow rate

A = Flow area

By separating the variables and integrating the equation along the length of the restriction, the incompressible theory yields:

$$\int_{P_i}^{P_o} -dP = \int_{o}^{\ell} \frac{\omega^2}{2A^2\rho} C_f \, d\ell = \frac{\omega^2}{2A^2\rho} \int_{o}^{\ell} C_f \, d\ell$$

where

P_o = Pressure downstream of restriction

P_i = Pressure upstream of restriction

T = Fluid temperature

P = Local pressure

where the term $\int_{o}^{\ell} C_f \, d\ell$ is proportional to the Reynolds number at the B power.

For Reynolds number similitude and fixed geometry

$$P_i - P_o \propto R_e^{\beta}\ \omega^2 T$$

where

R_e = Reynolds number

β = Assumed Reynolds number exponent

By substituting $\frac{\rho V d}{\mu}$ for R_e, assuming that $\mu \propto T^K$ and $\rho V \propto \omega$, and then solving the flow rate, we obtain:

$$\omega \propto (P_i - P_o)^{\eta}\ T^{\alpha}$$

where

$\eta = \frac{1}{\beta + 2}$ and $\alpha = \frac{K\beta}{\beta + 2}$

μ = Fluid viscosity

K = Exponent on viscosity temperature term

It is interesting to note that the pressure exponent, η, and the temperature exponent, α, are not independent.

Temperature gain, supply sensitivity, the determination of η and α, and bridge temperature sensors analyses follow.

2.1.2.1 Temperature Gain, $\frac{\partial P_o}{\partial T}$ - By adjusting the flow in the two series restriction to equal each other, then taking the partial derivitive with respect to temperature and solving for $\frac{\partial P_o}{\partial T}$, the following gain is obtained.

$$\text{Incompressible:}\quad \frac{\partial P_o}{\partial T} = \frac{\alpha_1 - \alpha_2}{T\left[\left[\frac{\eta_1}{P_s - P_o}\right] + \left[\frac{\eta_2}{P_o - P_v}\right]\right]} \qquad (1)$$

2.1.2.2 Supply Sensitivity, $\frac{\partial P_o}{\partial P_s}$ - By again adjusting the flow in the two series restrictions equal to each other, taking the partial derivitive with respect to P_s, and solving for $\frac{\partial P_o}{\partial P_s}$, the following is obtained.

$$\text{Incompressible:} \quad \frac{\partial P_o}{\partial P_s} = \frac{\eta_1}{\eta_2\left[\frac{P_s - P_o}{P_o - P_v}\right] + \eta_1} \tag{2}$$

2.1.2.3 Determination of α and η - After defining the temperature gain and supply sensitivity above as functions of η and α for the two restrictions, the last step was to determine these values. Since α and η are both defined functions of β, the only required values were the values of β for each restriction. β can be determined from the flow/pressure data of each restriction.

NOTE: If η is known, β may be solved for and used to find α.

$$\text{Incompressible:} \quad \beta = \frac{1}{\eta} - 2$$

$$\alpha = \frac{K\beta}{\beta + 2} = K\eta\left(\frac{1}{\eta} - 2\right)$$

2.1.3 Bridge Circuit Performance

Using the previously derived equations for gain and supply sensitivity (and with all parameters defined at zero ΔP_o), the bridge circuit performance is defined as follows:

2.1.3.1 Gain

$$\text{Incompressible:} \quad \frac{\partial \Delta P_o}{\partial T} = \left[\frac{\alpha_1 - \alpha_2}{\eta_1 + \eta_2}\right]\left[\frac{P_s - P_v}{T}\right] \tag{3}$$

where

$$\left(P_s - P_o\right) = \left(P_o - P_v\right) \text{ for maximum gain.}$$

2.1.3.2 Supply Sensitivity

$$\text{Incompressible:} \quad \frac{\partial \Delta P_o}{\partial P_s} = \frac{\eta_1 - \eta_2}{\eta_1 + \eta_2} \tag{4}$$

Since null of the bridge circuit occurs at a particular temperature, which is a function of supply pressure, the sensitivity of the set point temperature changes as a function of supply pressure, $\frac{\partial T_{set}}{\partial P_s}$, as defined below.

2.1.3.3 Setpoint Pressure Sensitivity

$$\frac{\partial T_{set}}{\partial P_s} = - \frac{\partial \Delta P_o}{\partial P_s} \quad \frac{\partial \Delta P_o}{\partial T}$$

$$\text{Incompressible:} \quad \frac{\partial T_{set}}{\partial P_s} = \left[\frac{T}{P_s - P_v}\right]\left(\frac{1}{2K}\right) \tag{5}$$

NOTE: The sensitivity of the setpoint temperature to supply pressure is a function of the sensitivity of the fluid viscosity to temperature and is independent of the flow characteristics of the restrictions used.

2.1.4 Bridge Circuit Operating on Freon 21

The gain of the bridge circuit shown in Figure 1 can be determined from the equation derived in the previous sections. The following values have been determined experimentally for Freon, capillary restrictors, and vortex restrictors.

Freon 21	$K = 2.38$
Capillary restrictors	$\beta_c = -0.37$; $\alpha_c = 0.54$; $\eta_c = 0.61$
Vortex restrictors	$\beta_v = 0.22$; $\alpha_v = -0.24$; $\eta = 0.45$

With $(P_s - P_v)$ of 100kPa (14.5 psi) and a setpoint temperature of 283K (50F), the anticipated temperature sensor gain is approximately 0.26kPa/K (0.021 psi/F). The anticipated setpoint pressure sensitivity is approximately 0.59K/kPa (7.32F/psi) for the same conditions.

Since an entire control band of 50 ±3F was specified, it is reasonable to allow ±0.56C (±1F) of sensor inaccuracy due to supply pressure variations. Solving Equation (5) for the allowable supply pressure variations, it was found that:

$$\Delta(P_s - P_v) = 2K \frac{\Delta T_{set}}{T_{set}} (P_s - P_v)$$

NOTE: The symbol, Δ, is used to represent allowable parameter variations.

Therefore, the allowable supply variation is 0.93 percent.

2.1.5 Performance of the Orifice Bridge Viscosity Change Temperature Sensor

The performance of the bridge circuit with a noise-free power supply was shown in Figure 3. The set point conditions of this sensor is approximately 283K (50F) with $(P_s - P_v)$ at approximately 40kPa (5.8 psi). The temperature sensitivity of the sensor is approximately 1.25kPa/K (0.1 psi/F) and the setpoint pressure sensitivity is approximately 1.6K/kPa (20F/psi). These values were within 15 percent of those estimated by analysis.

The noise present on the output signal of the bridge circuit corresponds to approximately 0.8C (1.5F). This noise is assumed to be flow noise and could be reduced.

Figure 5 shows the performance of a bridge circuit which has approximately ±10kPa (±1.45 psi) noise in the supply pressure. The noise level generates approximately 6C variation in the temperature signal. This also makes it apparent that the noise on the supply pressure be eliminated to allow the sensor to operate within the prescribed control bands.

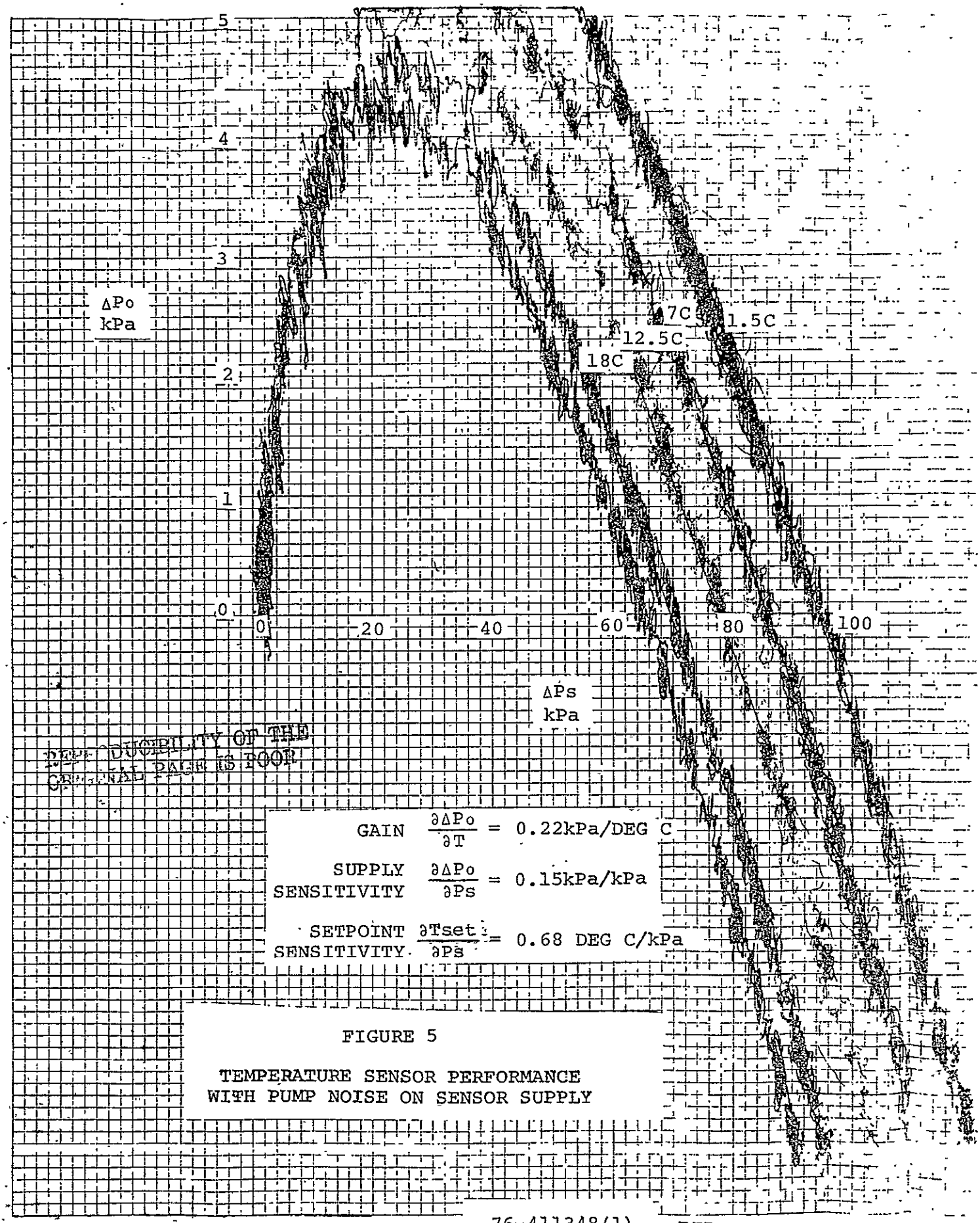

REPRODUCIBILITY OF THE ORIGINAL PAGE IS POOR

GAIN $\frac{\partial \Delta Po}{\partial T}$ = 0.22kPa/DEG C

SUPPLY SENSITIVITY $\frac{\partial \Delta Po}{\partial Ps}$ = 0.15kPa/kPa

SETPOINT SENSITIVITY $\frac{\partial Tset}{\partial Ps}$ = 0.68 DEG C/kPa

FIGURE 5

TEMPERATURE SENSOR PERFORMANCE
WITH PUMP NOISE ON SENSOR SUPPLY

2.2 DEVELOPMENT TESTING OF THE ORIFICE BRIDGE VISCOSITY CHANGE TEMPERATURE SENSOR

2.2.1 Argon-Freon Innerface Power Supply

Regulated argon was used to pressurize a Freon bottle, in the interest of saving time and expense, as shown in Figure 6. The pressurized Freon was used through a heat exchanger as the supply to the bridge circuit.

When the system was tested, the output of the sensor was too noisy to provide useful information needed in the sensor development. It was then discovered that the Freon was absorbing argon.

A conclusion made at this time was that the argon came out of solution in the passages of the bridge circuit. This was believed to be the cause of the noise in the sensor. The argon-Freon innerface power supply was abandoned at this time.

2.2.2 Freon Vapor Pressure Power Supply

The next approach in creating a power supply is shown in Figure 7. A pressure difference was produced by heating the supply reservoir and cooling the vent reservoir.

This method of producing a power supply also created noise on the sensor's output. It was concluded that the pressure which the sensor operated was too low to assure the Freon was not in two phases while in the passages of the sensor. At this point it was decided that all further Freon testing would be done with a 100kPa (14.5 psi) pressure differential with the supplyppressure at 1400kPa (200 psig) to eliminate any problems associated with Freon being in two phases.

2.2.3 Freon Pump Power Supply

A pump had to be acquired that would operate in a Freon 21 environment because of the corrosive properties of Freon 21. Time to acquire this pump resulted in a delay in the program schedule.

A schematic diagram of the test setup is shown in Figure 8. A centrifugal pump is used in this system with a flow rate of 15.1 litre/min (4.6 gpm) at 1370kPa (200 psia). During testing, it was discovered that the pump was generating noise in the supply pressure. The amplitude of this noise is shown in Figure 9A and was approximately ±43kPa (±6 psi) at a frequency of 250 Hz. The sensor was unable to meet the sensitivities needed for this application with the noise level present in the Freon supply.

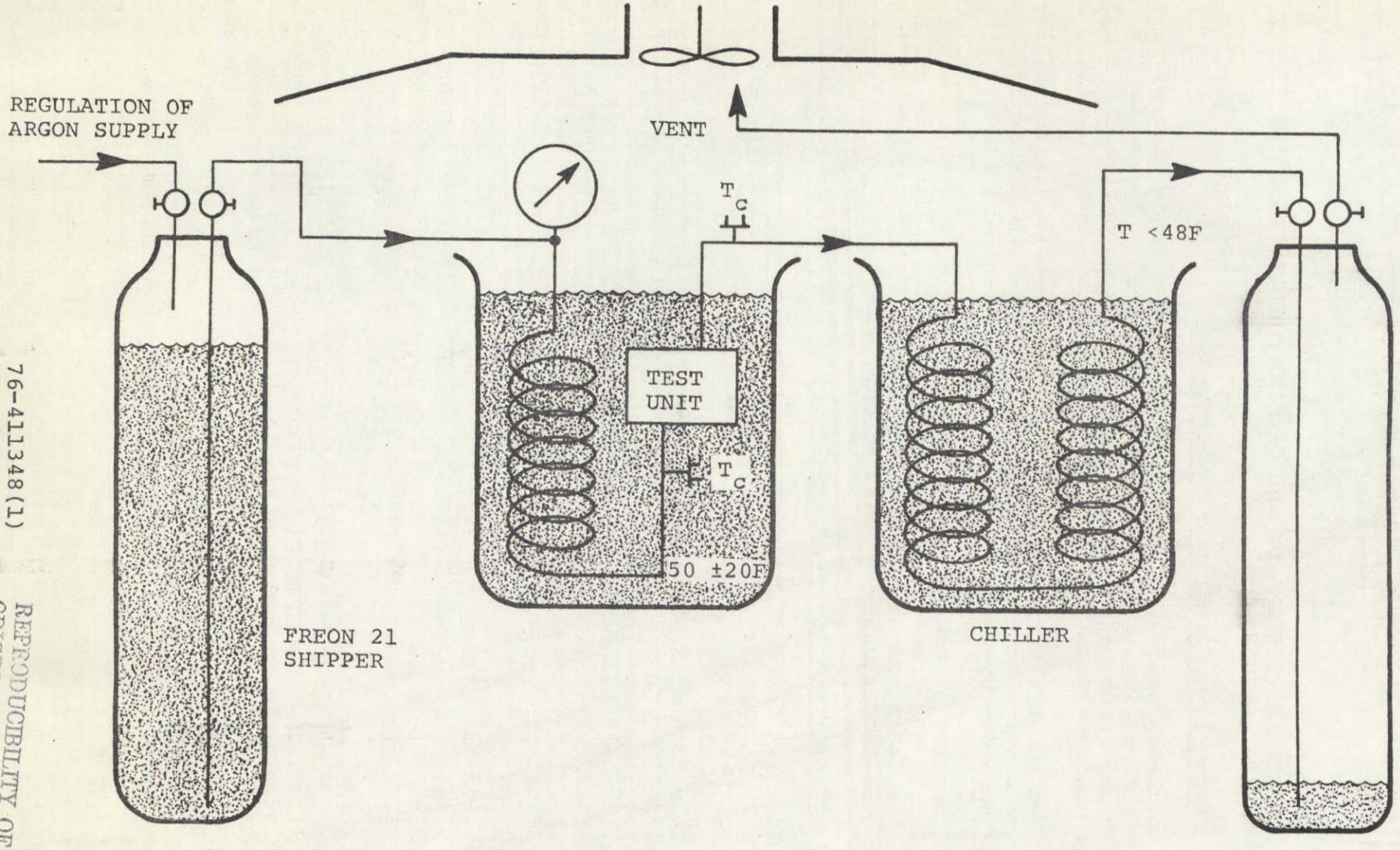

FIGURE 6

TEMPERATURE SENSOR TEST SETUP
PHASE I

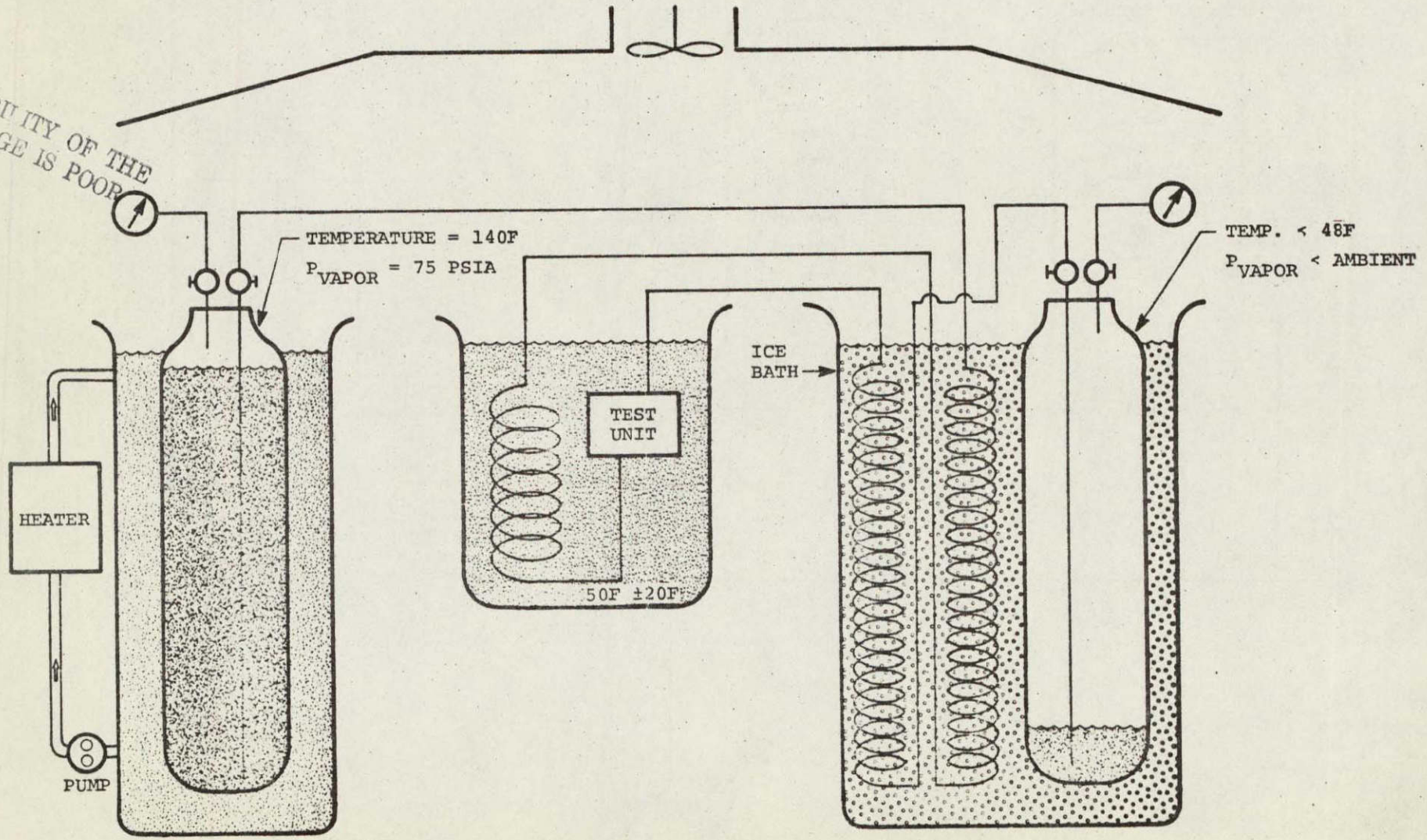

FIGURE 7

MODIFIED TEMPERATURE TEST SETUP
PHASE I

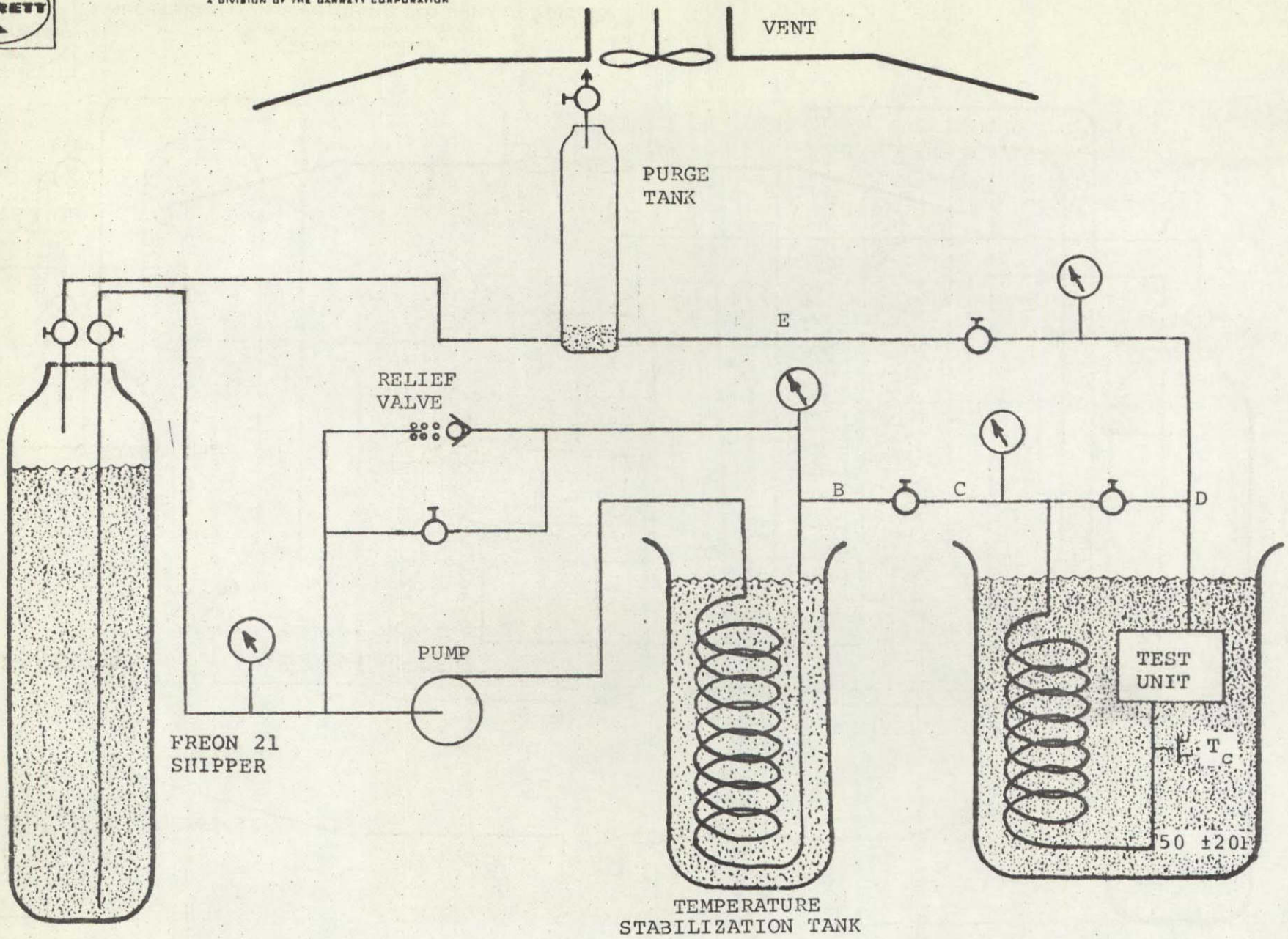

FIGURE 8

FREON PUMP POWER SUPPLY

SCALE: HORIZONTAL - 5 MS/DIV
VERTICAL - 35kPa/DIV (5 PSI/DIV)

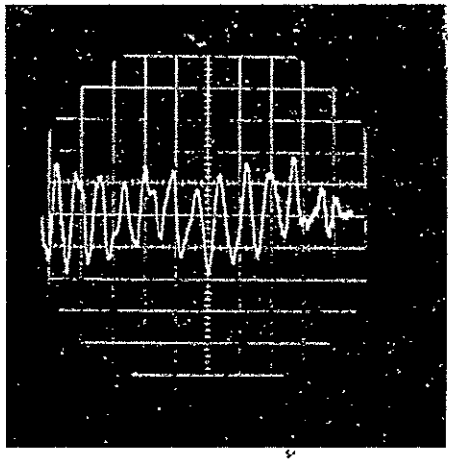

A

FREON PUMP OUTPUT

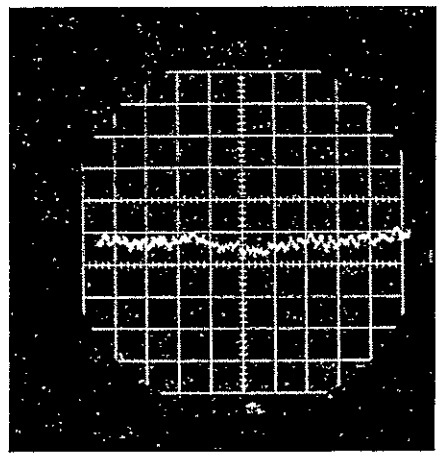

B

OUTPUT WITH AIR BUBBLE IN A VOLUME AT THE PUMP OUTLET

FIGURE 9

FREON PUMP OUTPUT NOISE

The only way that the bridge type viscosity sensor will operate on Freon 21 to meet the design tolerances would be if the supply pressure noise level is below 0.93 percent of the bridge circuit differential pressure ($P_s - P_v$). Since there are no pumps available that can provide such a power supply, the only solution was to provide an acceptable level.

Various types of attenuation were investigated. The response requirement of an attenuator needed for this application immediately eliminated all mechanical accumulators with moving parts of appreciable mass. Off-the-shelf accumulators capable of high frequency response are typically of the bladder type; however, Freon 21 compatibility problems prevented the use of these accumulators.

An air bubble accumulator was introduced into the system at point B of Figure 8. Ideally the air bubble accumulator will provide the best filtering effect in that there is a negligible mass interface between the air and Freon. However, this type of accumulator can not be used in a real life system because the air is slowly absorbed into the Freon. This accumulator was used only to determine the approximate amount of filtering that could be achieved. The results of this type of filtering is shown in Figure 9B.

It is estimated that an accumulator with a polyethylene bladder which is not affected by the corrosive action of Freon 21 could be constructed with a noise amplitude of less than ±7kPa. A schematic diagram of the accumulator is shown in Figure 10.

2.2.4 Noise-Free Power Supply Using Polyethylene Bladder

A schematic diagram of the noise-free power supply is shown in Figure 11. This supply provides a noise-free pressure to the bridge for a short period of time. This is not a closed loop system and was used only to eliminate the supply pressure noise.

By eliminating the supply pressure noise, the temperature circuit may be tested and examined for its sensitivities, gain, and any other noise present in the circuit.

The remaining noise on the sensor output could be assumed to be the result of turbulent fluid flow in the sensor passages. The bridge output under this condition is shown in Figure 3, and reveals that the flow noise corresponds to approximately 1.5F (0.8C). This noise level was reduced from that found in previously built sensors by modifying the transfer passages within the fluidic stack. It can be assumed that further improvement in this area is possible.

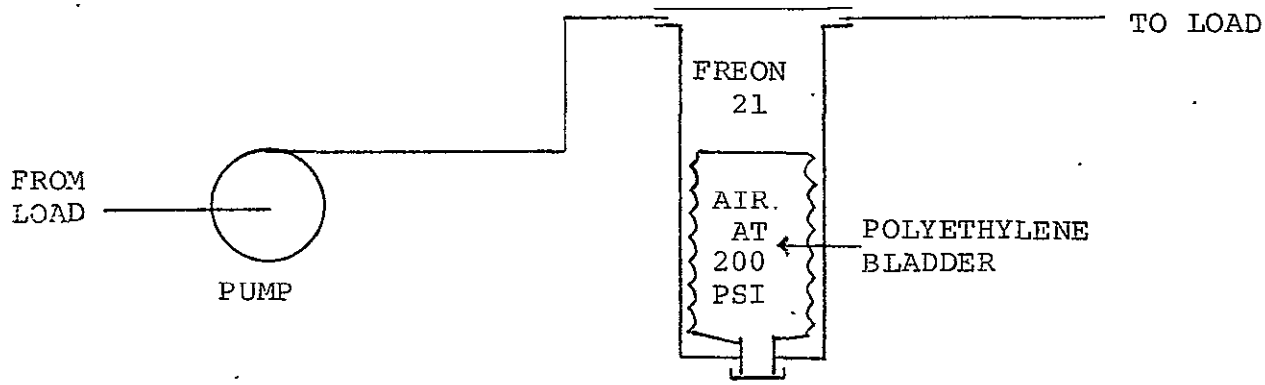

FIGURE 10

BLADDER USED IN NOISE ATTENUATOR

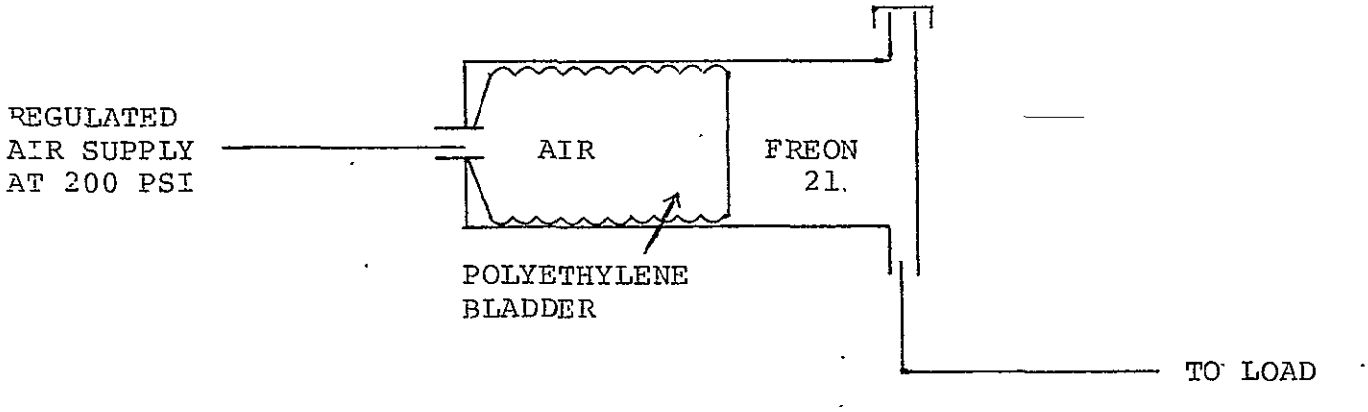

FIGURE 11

BLADDER USED IN NOISE-FREE
POWER SUPPLY

2.2.5 Conclusions of the Orifice Bridge Viscosity Change Temperature Sensor Development Testing

The pressure sensitivity of bridge circuit temperature sensors operating on Freon 21 is not compatible with the noise level on the pump output, in that the desired control accuracy cannot be achieved even while using the most effective known methods of noise attenuation.

By filtering the supply such that pressure variation would be maintained within ±0.93 percent, a bridge-type temperature sensor could be developed with tolerances capable of controlling temperature to an estimated ±2.8C(±5F). An additional 0.56C(1F) would be added to the control tolerance for each additional 0.93 percent pressure variation in the supply.

The temperature sensor desired for this system should be insensitive to supply variation, so that the effect of noise generation in the power supply is eliminated.

2.3 BELLOWS-DRIVEN PIN AMPLIFIER FLUIDIC TEMPERATURE SENSOR

In the following subparagraphs, the design and development of a bellows-driven pin amplifier fluidic temperature sensor is described. This sensor is insensitive to the fluid properties whose temperature is being sensed. It has high accuracy and is less sensitive to supply-to-vent-pressure differential than other fluidic temperature sensors.

2.3.1 Design Approach

Due to the high sensitivity required, the pin amplifier appeared to be an ideal choice as the main component on the sensor. Figure 12 shows the pin amplifier and output characteristics. The pin amplifier consists of a fluid amplifier that has no control ports. The control action is obtained by introducing a pin in the interaction region. As the pin is moved from the center position, one of the receivers is blocked off more, while the other one is exposed more to the jet. The result is a differential pressure output.

The second critical part of the sensor is the actuation system that moves the pin as a function of temperature. Several bimetallic configurations were analyzed; however, in order to get the required displacement for a one-degree F temperature change, the size of the bimetallic element was too large and susceptible to vibration. A different approach was to use a bellows assembly filled with an incompressible fluid. This latter approach was utilized. Figure 13 shows a schematic of the sensor and the bellows assembly.

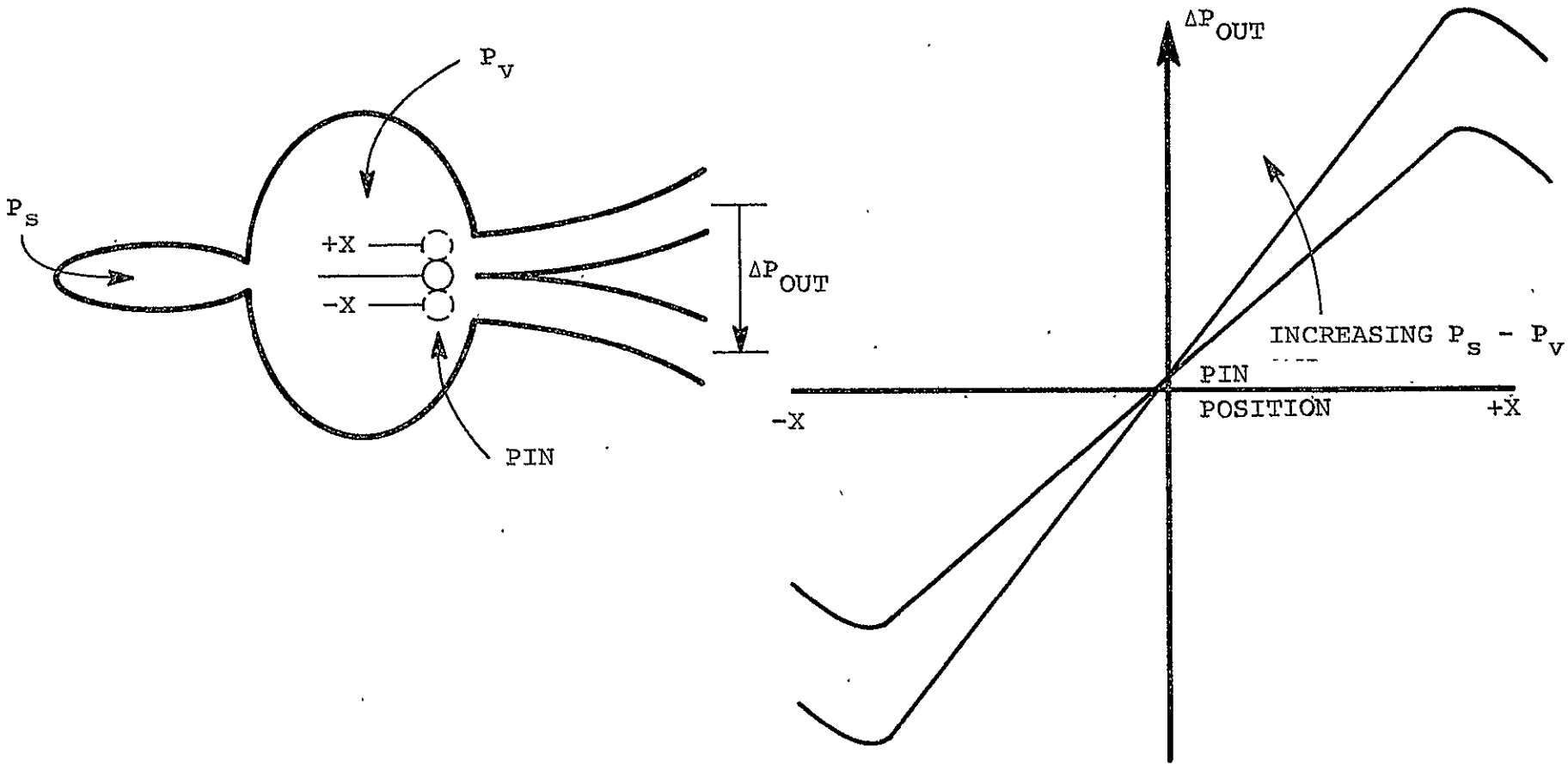

FIGURE 12

PIN AMPLIFIER

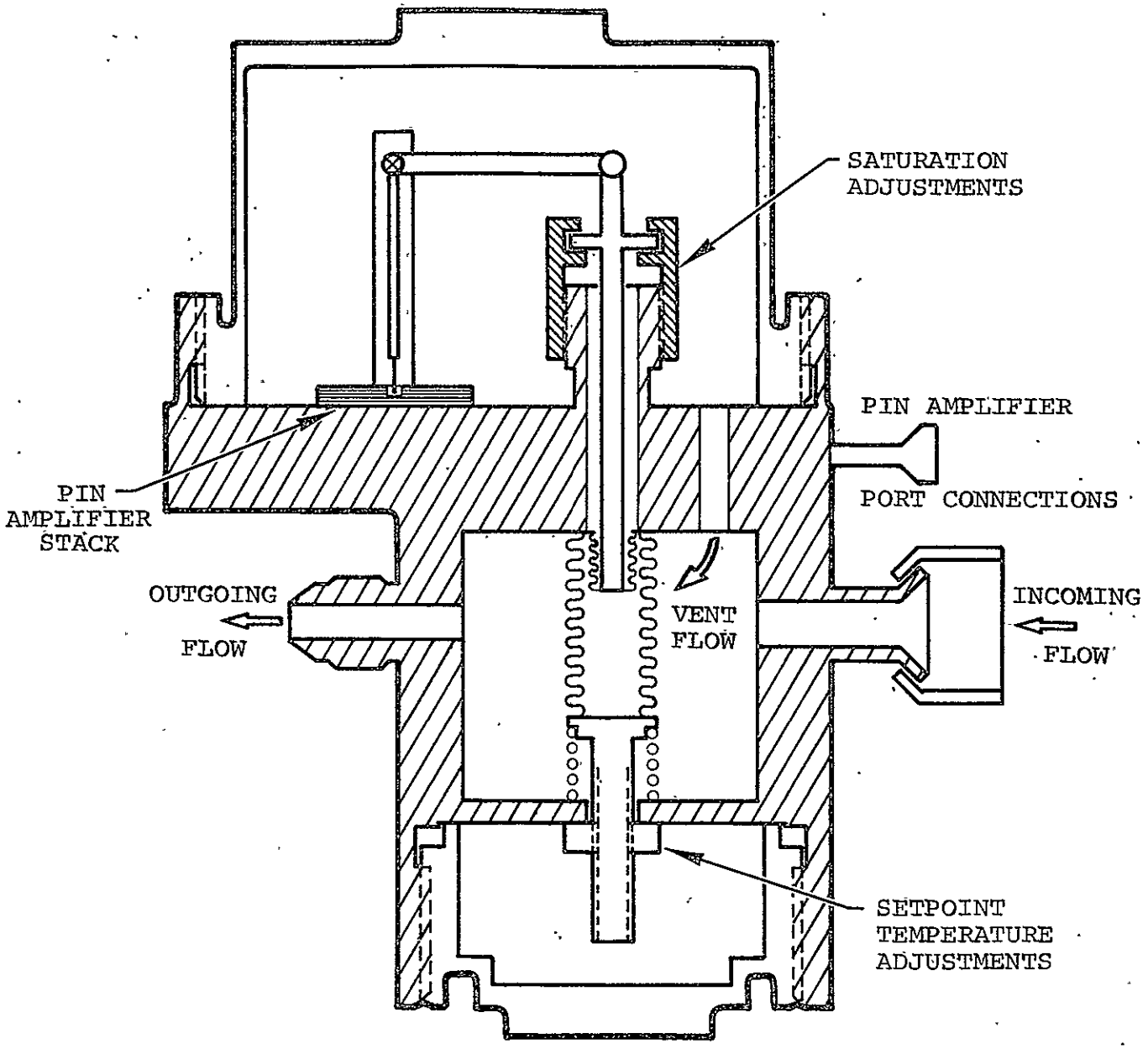

FIGURE 13

BELLOWS-DRIVEN PIN AMPLIFIER
FLUIDIC TEMPERATURE SENSOR

The bellows assembly consists of two bellows filled with methyl alcohol. This liquid was selected since it is virtually incompressible and, thus, is not affected by the pressure outside the bellows. Methyl alcohol was chosen particularly because it does not freeze at minus 65F and it has a high coefficient of cubic thermal expansion.

The small bellows and the amplifier pin move only during the operating range of 47 to 53F. The movement of the small bellow was designed to drive the amplifier pin from one end of saturation to the other in 6F. Motion is constrained by two stops. The anticipated output characteristics of the sensor are shown in Figure 14.

As the temperature goes above 53F, the linkage connected to the small bellows moves against one of the stops. The pressure inside the bellow assembly increases to a value sufficient to overcome the spring preload on the large bellows. Then, expansion of the alcohol is absorbed by an expansion of the large bellows. When the temperature drops below 47F, the linkage connected to the small bellows moves against the other stop. As the temperature decreases, the liquid inside the bellows assembly contracts. However, neither of the two bellows can move since both of them are against the stops. The result is a rapid decrease in pressure inside the bellows assembly. Once this pressure reaches the vapor pressure of the alcohol, the alcohol begins to evaporate such that alcohol vapor will occupy the remaining volume. As the temperature increases again, the vapor will condense and the alcohol again will become all liquid. Figure 15 illustrates the behavior of the pressure inside the bellows as a function of temperature and the phase diagram of methyl alcohol.

The bellows assembly is located in the flow stream to maximize response time. The bellows assembly, due to the shape of the bellows, is an excellent heat exchanger and is sized to contain the required volume of alcohol necessary to provide the expansion at the operating range.

The sensor has two main flow ports: an inlet and outlet port for the fluid temperature being sensed. There is very small pressure drop across the sensor since the only restriction is the bellows assembly. By reducing the flow area around the bellows, a larger fluid velocity is obtained; this improves heat transfer and response time, but results in a larger pressure drop. Three additional ports are required for the pin amplifier: one for the supply flow and two for the output signal. The vent flow from the interaction region is directed first to the upper cavity of the sensor, then through a passage to the lower cavity where it is mixed with the incoming flow. While this feature is desired in this particular application, it can be modified, if desired, by isolating the upper and lower cavities and adding an additional vent port to the upper cavity.

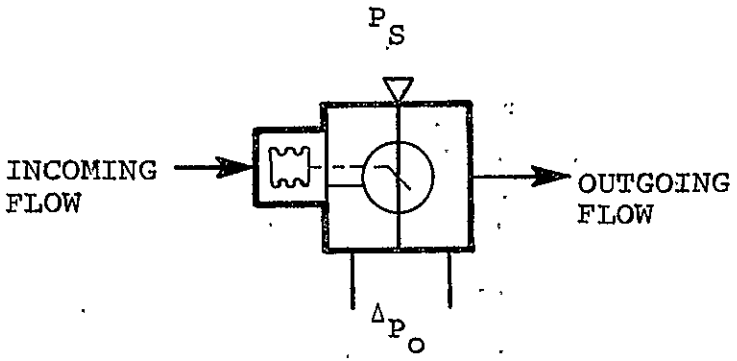

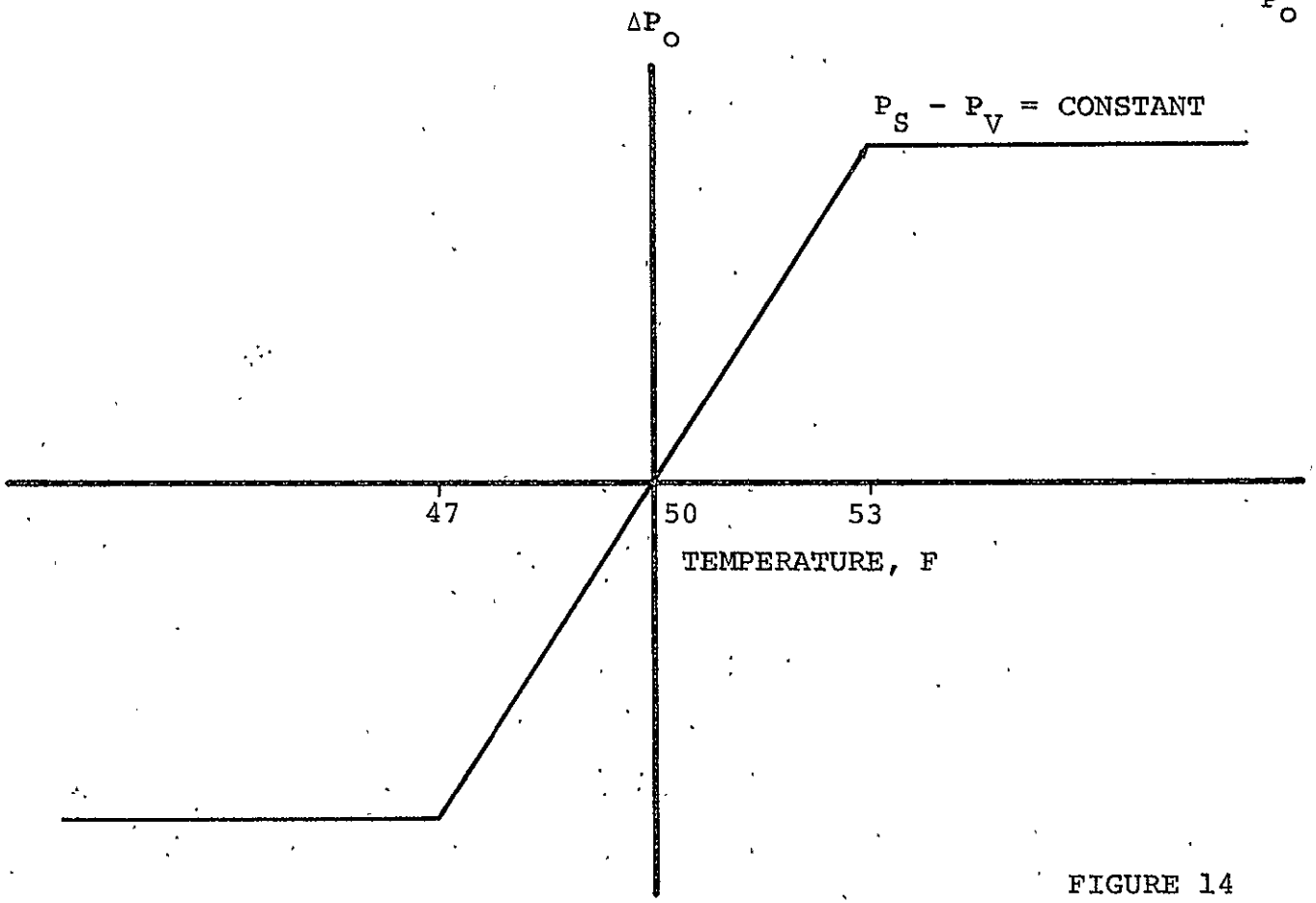

FIGURE 14

EXPECTED OUTPUT CHARACTERISTICS
OF THE BELLOWS-DRIVEN PIN AMPLIFIER
FLUIDIC TEMPERATURE SENSOR

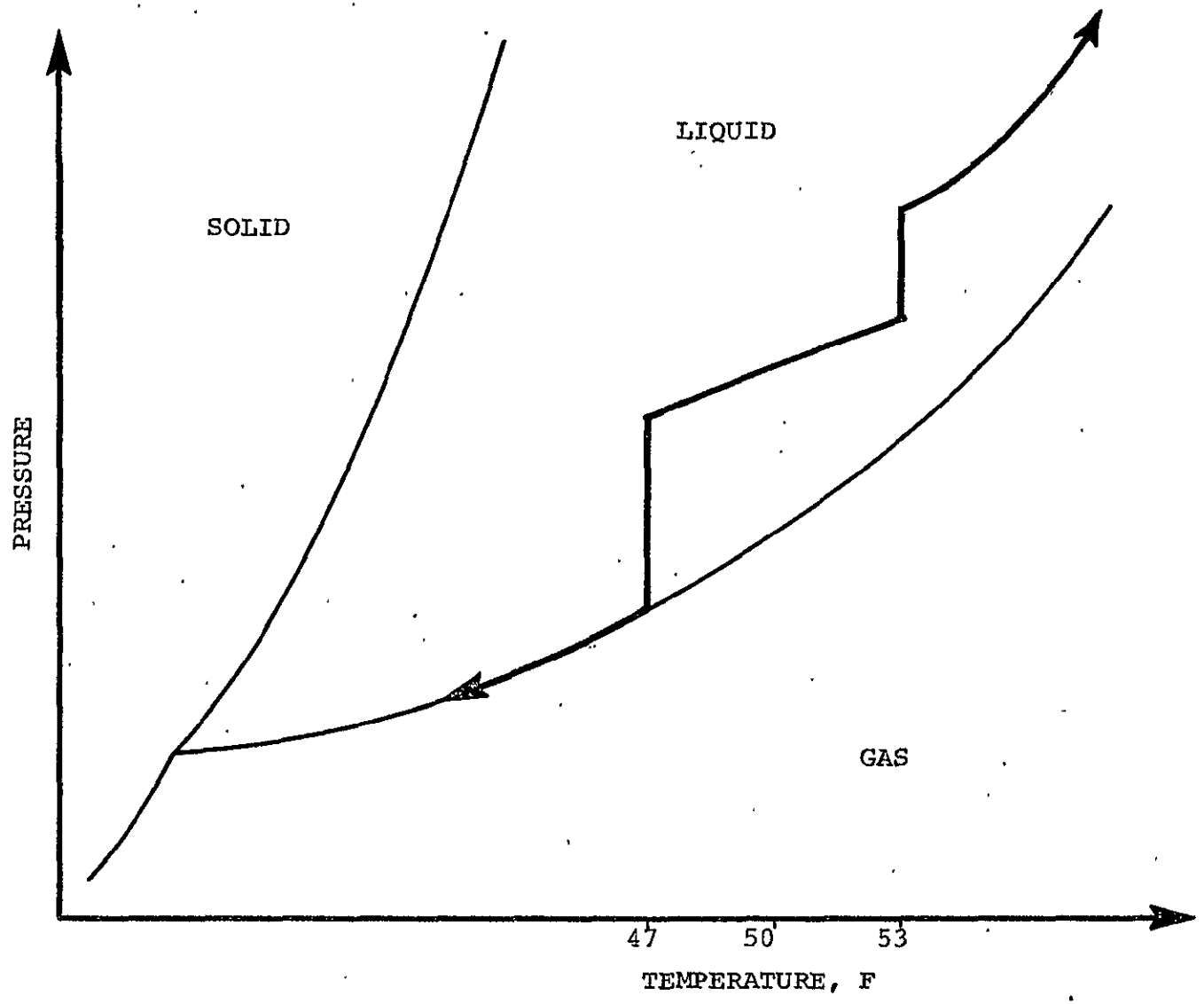

FIGURE 15

PHASE DIAGRAM FOR METHYL ALCOHOL AND PRESSURE
INSIDE BELLOWS ASSEMBLY AS A FUNCTION OF TEMPERATURE

One of the outstanding features of this sensor is that it can be adjusted easily for any set point temperature within the range of minus 65F to plus 150F. Figure 13 shows the saturation stop and set point temperature adjustments.

For a different application, it may be desirable to change the gain of the sensor. This can be accomplished in several ways.

- Changing the expanding fluid inside the bellows assembly
- Changing the size of the pin amplifier
- Raising the position of the amplifier and thus reducing the lever arm

2.3.2 Design Analysis

2.3.2.1 Pin Amplifier - Figure 16 shows the separate laminates and pin amplifier stack. For this particular pin amplifier design, the distance that the pin has to be moved from the center position to obtain saturation is 0.0075 inch (0.19 mm). Thus, the total travel required is 0.015 inch (0.38 mm).

A study was performed to investigate the fluid forces on the pin using water as the supply fluid. The results indicated that the forces were negligible and would have no effect on the performance.

2.3.2.2 Bellows Assembly - A model was used to determine the volume necessary to yield the required motion of the small bellows. This model simulated:

- Spring constant of the small bellow
- Container (bellows assembly) elasticity
- Container (bellows assembly) thermal expansion
- Fluid (alcohol) compressibility
- Fluid thermal expansion
- Effect of external pressure

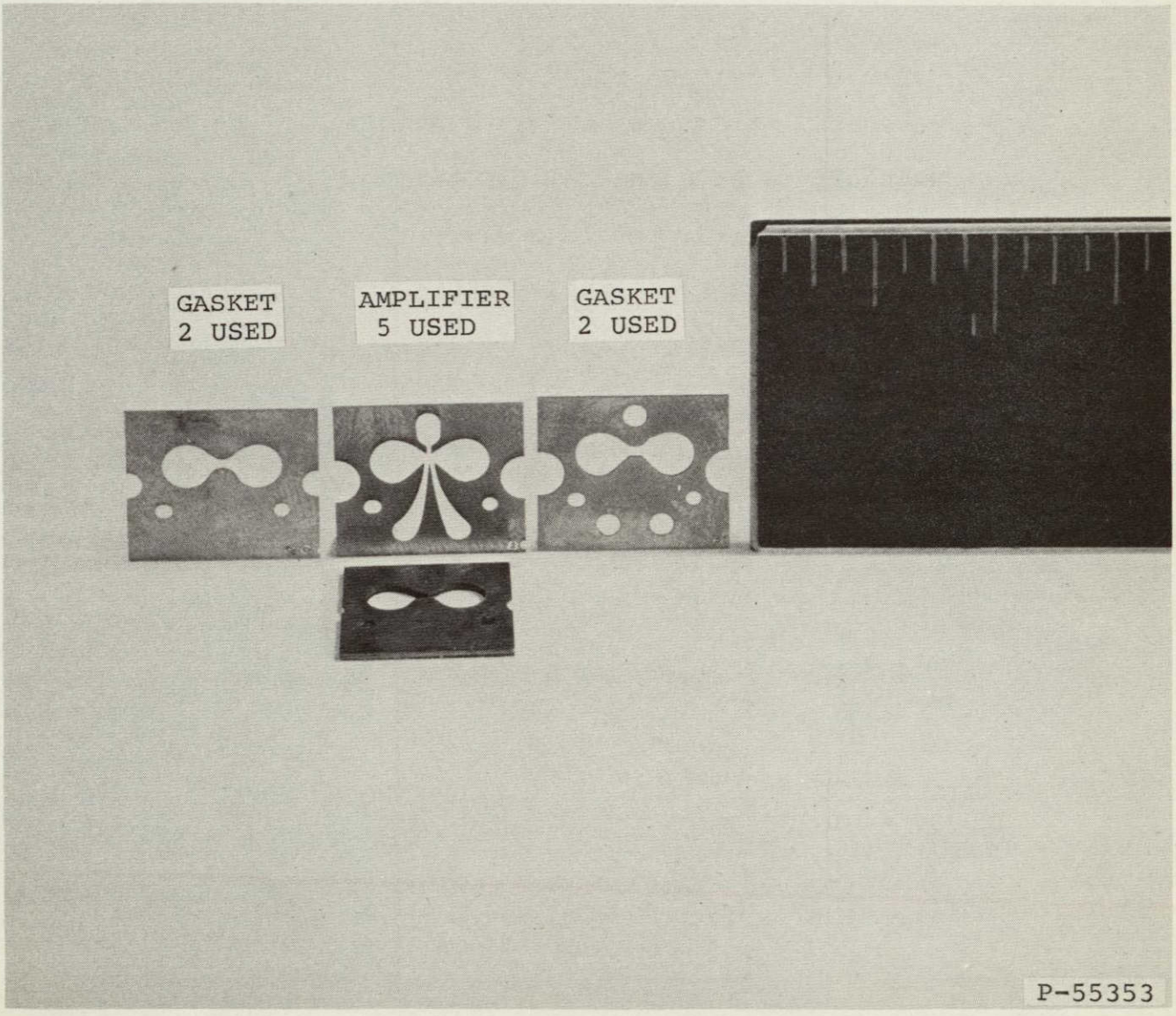

FIGURE 16

PIN AMPLIFIER LAMINATE AND STACK

The model is illustrated on Figure 17. The distance between the center position and the pin is given by:

$$X = \frac{(P_c - P_e)\ A_{EFF}}{K} \qquad (6)$$

assuming that the small bellows is at its free position where the pin is at the center position

where:

X = Distance between the center position and the pin

P_c = Pressure inside the bellows assembly

P_e = Pressure outside the bellows assembly

A_{EFF} = Effective area of small bellows

K = Spring constant of small bellows

The volume, V_c, of the container can be linearly approximated as

$$V_c = V_{c_o} \left[1 + C_1\ (T - T_o) + C_2\ (P_i - P_e) \right] \qquad (7)$$

where

V_c = Volume of the container

V_{c_o} = Initial volume of container

T = Temperature

T_o = Initial temperature

P_i = Inside pressure

P_e = Outside pressure

C_1 = 3 x linear thermal expansion coefficient of the large bellow (nickel)

$C_2 = \frac{D_o}{t\ E}$

D_o = Diameter of large bellows

t = Thickness of large bellows

E = Modulus of elasticity

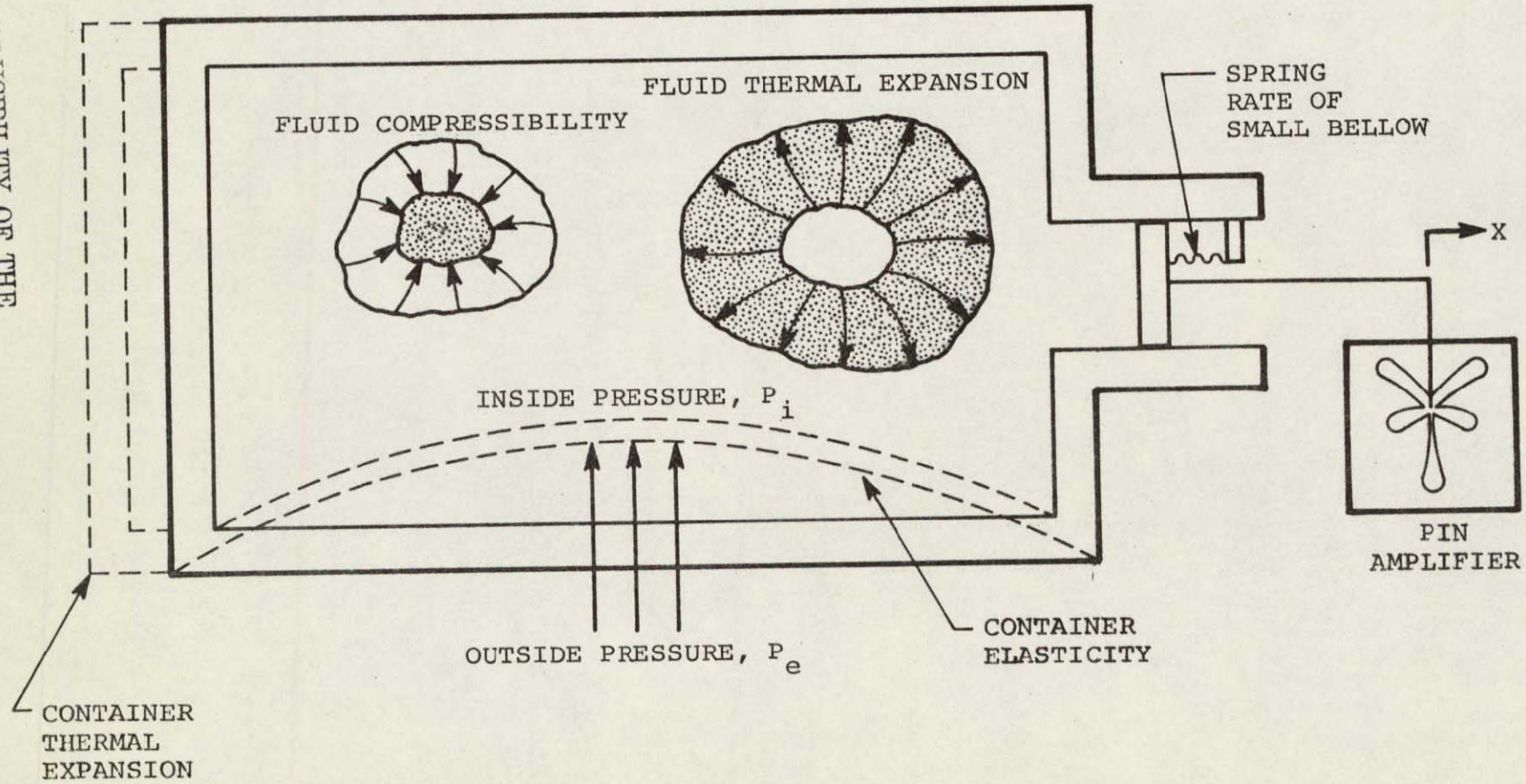

FIGURE 17

MODEL OF BELLOWS ASSEMBLY

The volume of the expanding liquid can be linearly approximated as

$$V_F = \frac{M_F}{\rho_F} \cong \frac{M_F}{\rho_{F_o}\left[1 - f_1\ (T - T_o) + f_2\ (P_i - P_o)\right]}$$

$$\cong \frac{M_F}{\rho_o} \cdot \left[1 + f_1\ (T - T_o) - f_2\ (P_i - P_o)\right] \qquad (8)$$

where

M_F = Mass of the fluid

ρ_F = Density of the fluid

ρ_{F_o} = Initial density of the fluid

f_1 = Coefficient of cubic thermal expansion for the expanding liquid (alcohol)

T = Temperature

T_o = Initial temperature

f_2 = Compressibility of the expanding liquid

$= \frac{1}{\beta}$; f = bulk modulus

P_i = Pressure inside the container

P_o = Initial pressure inside the container

The final basic equation is

$$X = \frac{1}{A_{EFF}}\ (V_F - V_c) \qquad (9)$$

where

X = Distance between the center position and the pin

A_{EFF} = Effective area of small bellows

V_F = Volume of the fluid

V_c = Volume of the container

Equations (6) through (9) are combined to yield

$$X = \frac{\frac{V_{c_o}}{A_{EFF}} \left[(f_1 - C_1) (T - T_o) + f_2 (P_o - P_e) \right]}{1 + \frac{V_{c_o} \; k \; (C_2 + f_2)}{A_{EFF}^2}} \qquad (10)$$

where all the terms are described in Equations (6) through (9).

By taking the partial derivative of Equation (10) with respect to T, the following is obtained

$$\frac{\partial X}{\partial T} = \frac{\frac{V_{c_o}}{A_{EFF}} (f_1 - C_1)}{1 + \frac{V_{c_o} \; k \; (C_2 + f_2)}{A_{EFF}^2}} \qquad (11)$$

The desired value of $\frac{\partial X}{\partial T}$ is

$$\frac{\partial X}{\partial T} \cong \frac{\Delta X}{\Delta T} = \frac{0.015 \text{ in.}}{6F} = 0.0025 \frac{\text{in.}}{F} \; (0.0635 \frac{\text{mm}}{F})$$

Solving Equation (11) for V_{c_o} and substituting values, a value for V_{c_o} of 0.0759 in.^{3} (1.24 cm^3) is obtained. This value is 10 percent higher than the value obtained by the simple formula

$$V_{c_o} \cong \frac{\Delta X \; A_{EFF}}{\Delta T \; f_1}$$

$$\cong \frac{(0.015) \; (0.0179)}{(6F) \; (6.48 \times 10^{-4} \; \frac{1}{F})} = 0.0690 \text{ in.}^3 \; (1.13 \text{ cm}^3)$$

The bellows assembly has an internal volume of 0.0775 in.^{3} (1.27 cm^3).

Although alcohol is a liquid, most liquids are slightly compressible; therefore, some set point sensitivity with pressure will result. Taking the partial derivative of Equation (10) with respect to P_e, the following is obtained

$$\frac{\partial X}{\partial P_e} = \frac{-\frac{V_{c_o}}{A_{EFF}} f_2}{1 + \frac{V_{c_o} \; k \; (C_2 + f_2)}{A_{EFF}^2}}$$

After substituting the corresponding values

$$\frac{\partial X}{\partial P_e} = 2.29 \times 10^{-5} \; \frac{\text{in.}}{\text{psi}}$$

and since

$$\frac{\partial T_{SET}}{\partial P_e} = \frac{\partial T}{\partial X} \cdot \frac{\partial X}{\partial P_e}$$

$$= \frac{1}{(0.0025 \; \frac{\text{in.}}{\text{F}})} \left(2.28 \times 10^{-5} \; \frac{\text{in.}}{\text{psi}} \right)$$

$$= 0.0092 \; \frac{\text{F}}{\text{psi}} \; (0.0013 \; \frac{\text{F}}{\text{kPa}})$$

However, the actual figure will probably be larger since any impurities or air entrained in the alcohol will increase the compressibility.

2.3.3 Development Unit

Figure 18 shows the bellows-driven pin amplifier fluidic temperature sensor. Figure 19 shows a bottom view of the sensor and the ports. Figure 20 shows the uncovered top view with the saturation adjustments and the pin amplifier. Figure 21 shows the uncovered bottom view with the set point adjustment. Figure 22 is a reduced outline drawing of the sensor.

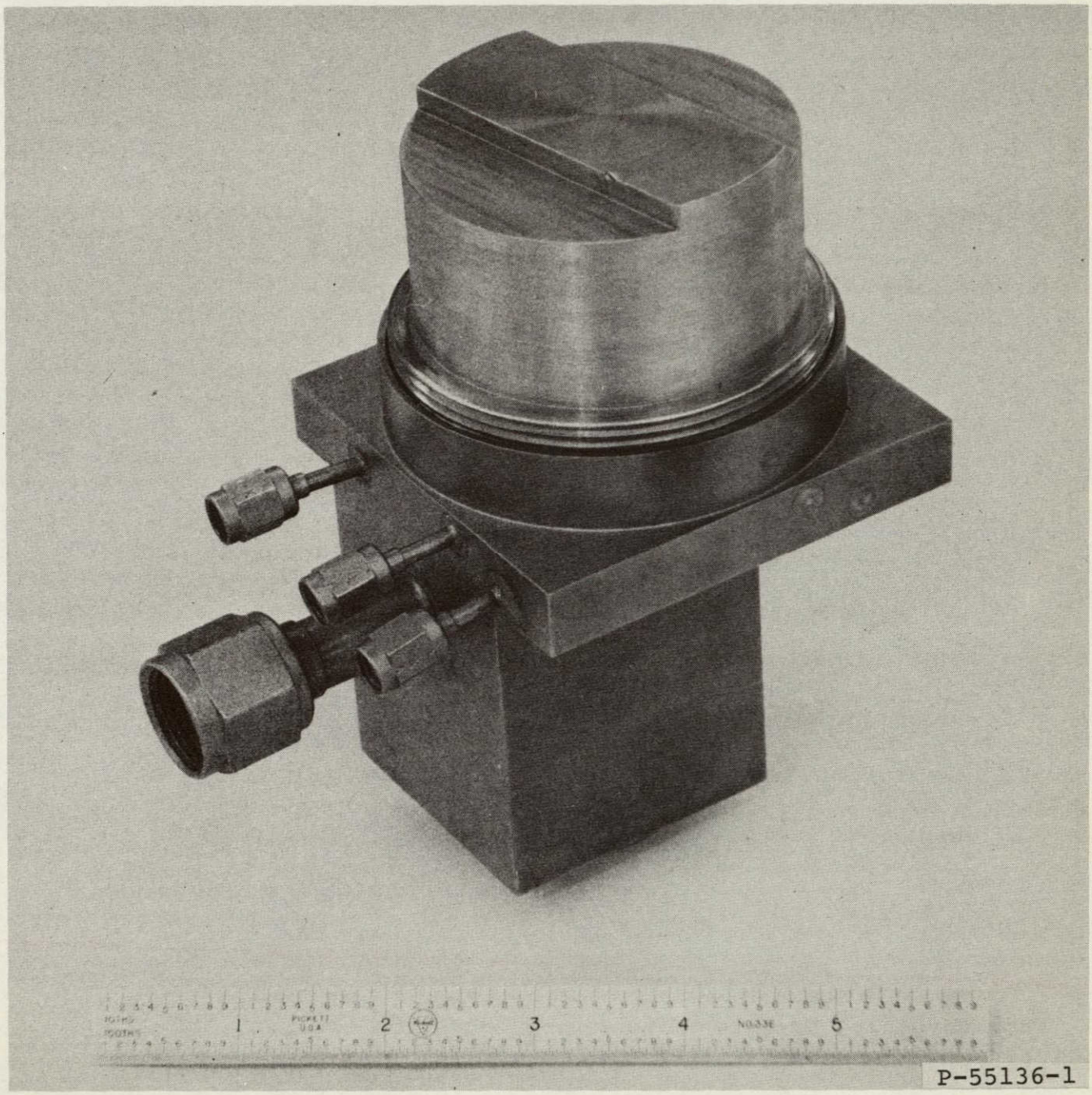

FIGURE 18

BELLOWS-DRIVEN PIN AMPLIFIER
FLUIDIC TEMPERATURE SENSOR

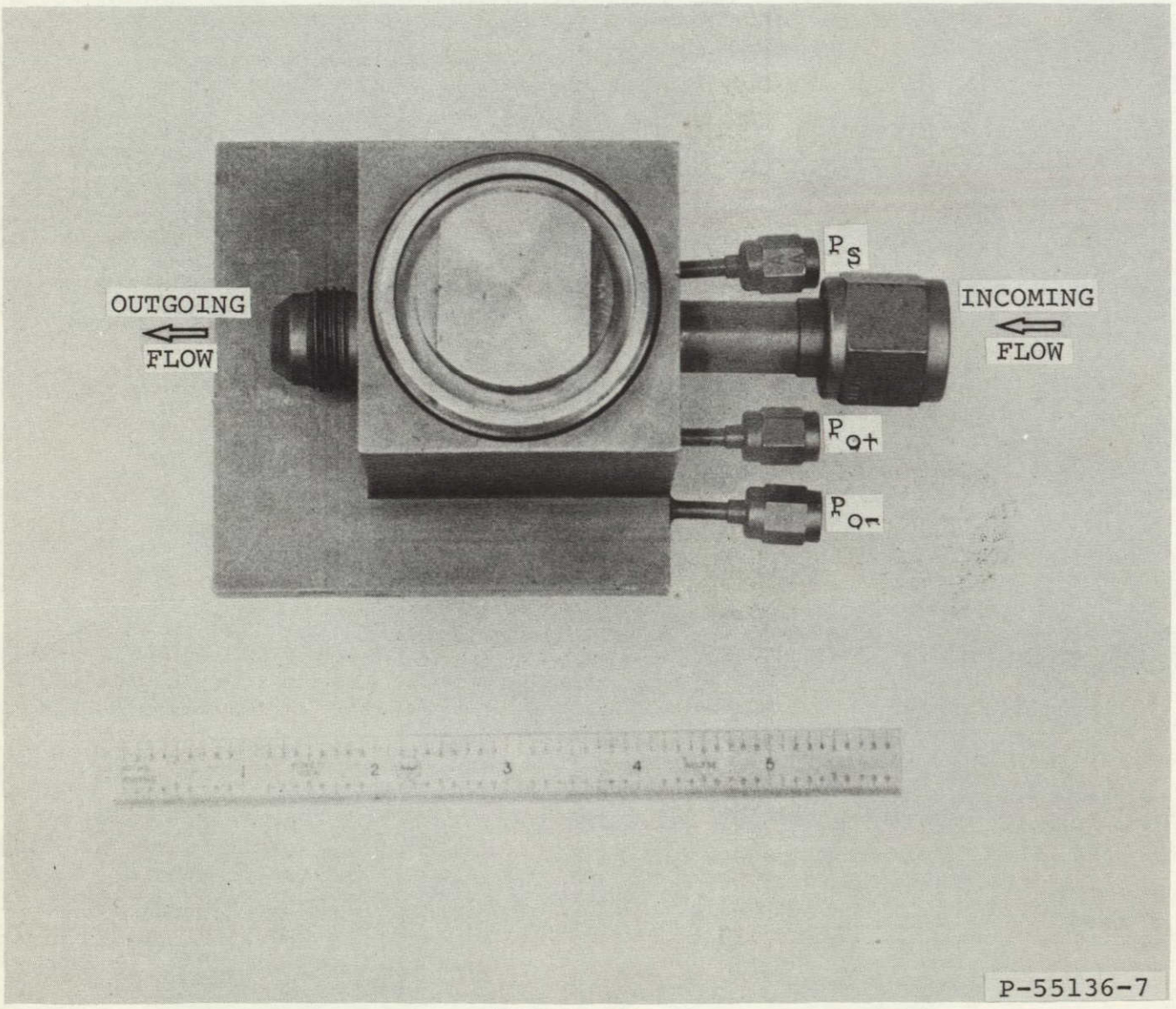

FIGURE 19

BOTTOM VIEW OF FLUIDIC TEMPERATURE SENSOR

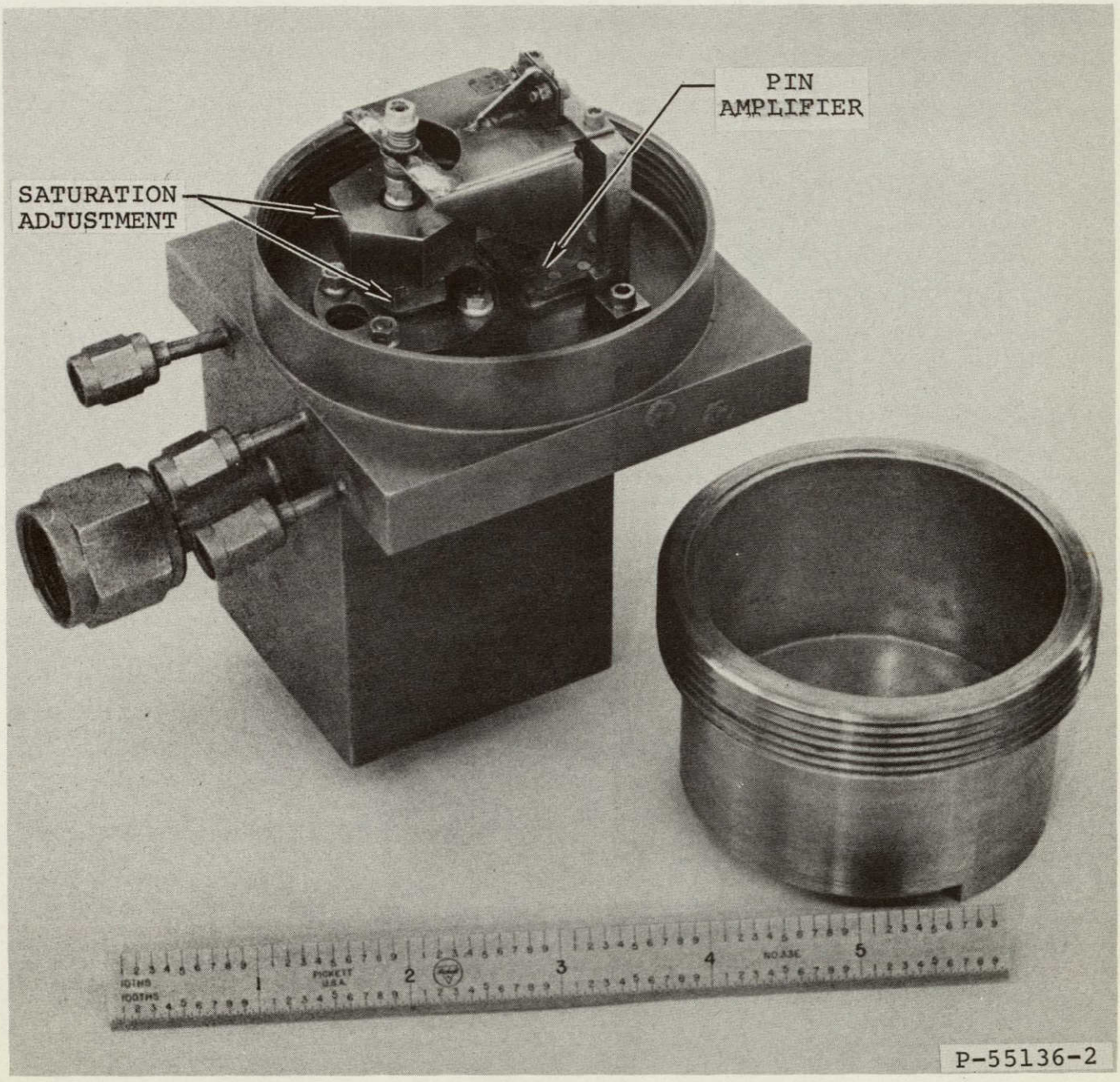

FIGURE 20

UNCOVERED TOP VIEW OF FLUIDIC TEMPERATURE SENSOR
SHOWING SATURATION ADJUSTMENT AND PIN AMPLIFIER

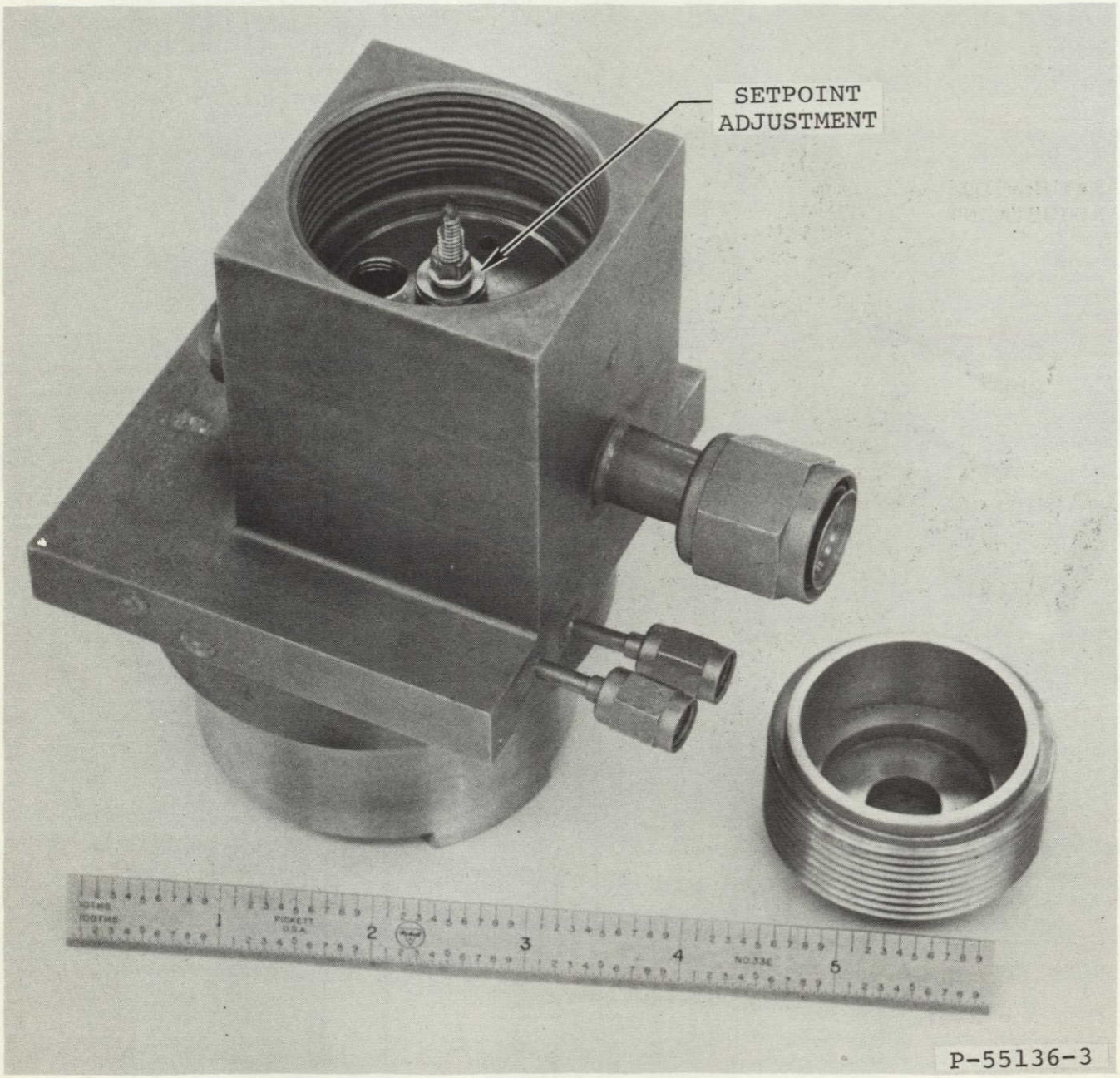

FIGURE 21

UNCOVERED BOTTOM VIEW OF FLUIDIC TEMPERATURE SENSOR
SHOWING SET POINT ADJUSTMENT

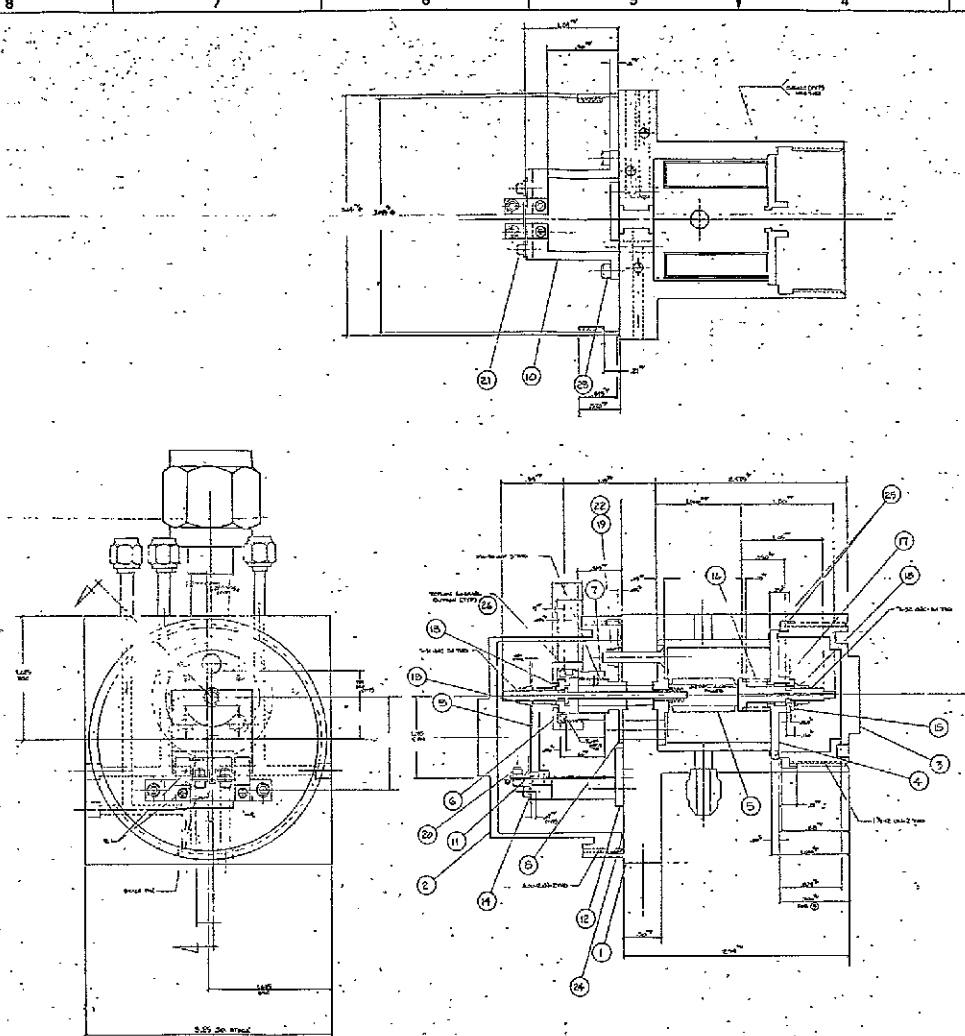

FIGURE 22
TEMPERATURE CONTROLLER

L710548

2.4 DEVELOPMENT TESTING OF THE BELLOWS-DRIVEN PIN AMPLIFIER FLUIDIC TEMPERATURE SENSOR

2.4.1 Testing with Water

Preliminary tests were performed with water. Figure 23 shows the test setup used to test the unit in water and Figure 24 shows the test results. To obtain a curve like that shown in Figure 24, the temperature must be varied very slowly. If this is not done, the resulting curve will exhibit an apparent "hysteresis" due to thermal lag.

2.4.2 Testing with Freon 114

Once the unit was operating satisfactorily in water, tests were begun with Freon 114. Figure 25 shows the test circuit. Using this circuit, only the Freon inside the sensor is lost when the unit is removed from the circuit. Figure 26 shows a characteristic curve for the sensor. As with the tests with water, if the temperature is not changed very slowly, an apparent hysteresis will appear due to the thermal lag of the sensor.

Freon tests revealed that the unit was noisier than expected. There was some noise anticipated outside the set point temperature, since the gain of the pin amplifier is proportional to $P_S - P_V$. However, at the set point temperature (pin is at the center of the interaction region), the output pressure, ΔP_o, is zero for any $P_S - P_V$ even though P_o+ and P_o- will both increase or decrease with increasing or decreasing $P_S - P_V$, respectively. Yet, results indicate that ΔP_o is not noise free at the set point temperature. It is suspected that the output impedances are not the same; consequently, the pressure transducer will sense an increase in P_o+ faster than P_o- (or vice versa). Although there is some noise in the output signal, the signal-to-noise ratio is high enough that no problems are expected when the sensor is integrated in the rest of the system. Figure 27 shows an oscilloscope picture of the supply vent pressure and output noise.

It was expected that the sensor would be slightly sensitive to the pressure around the bellows because of the compressibility of the alcohol. Experimental results indicate that the set point sensitivity with pressure outside the bellows was 0.0129 $\frac{F}{psi}$ (0.0019 $\frac{F}{kPa}$).

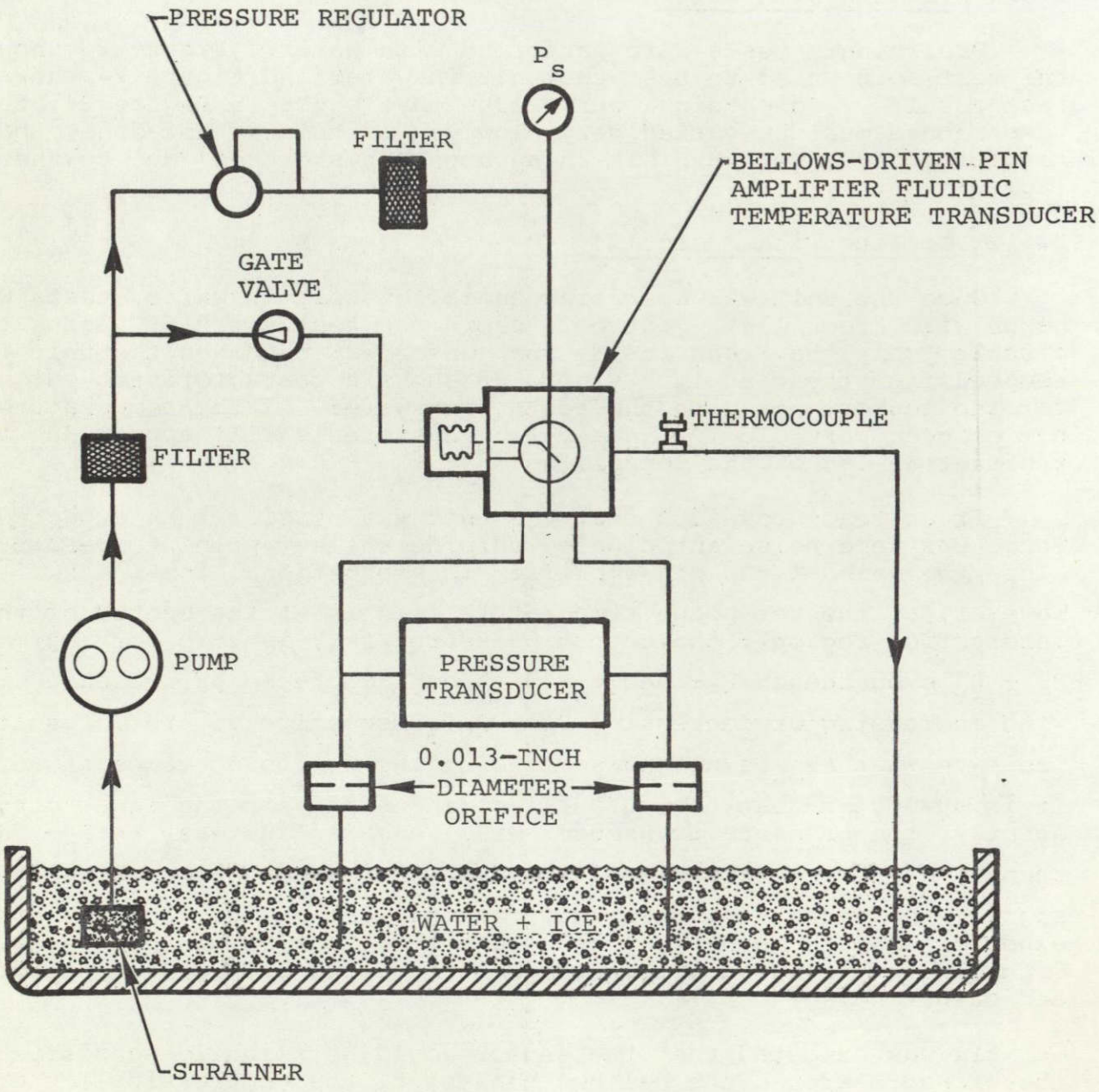

FIGURE 23

WATER TEST CIRCUIT

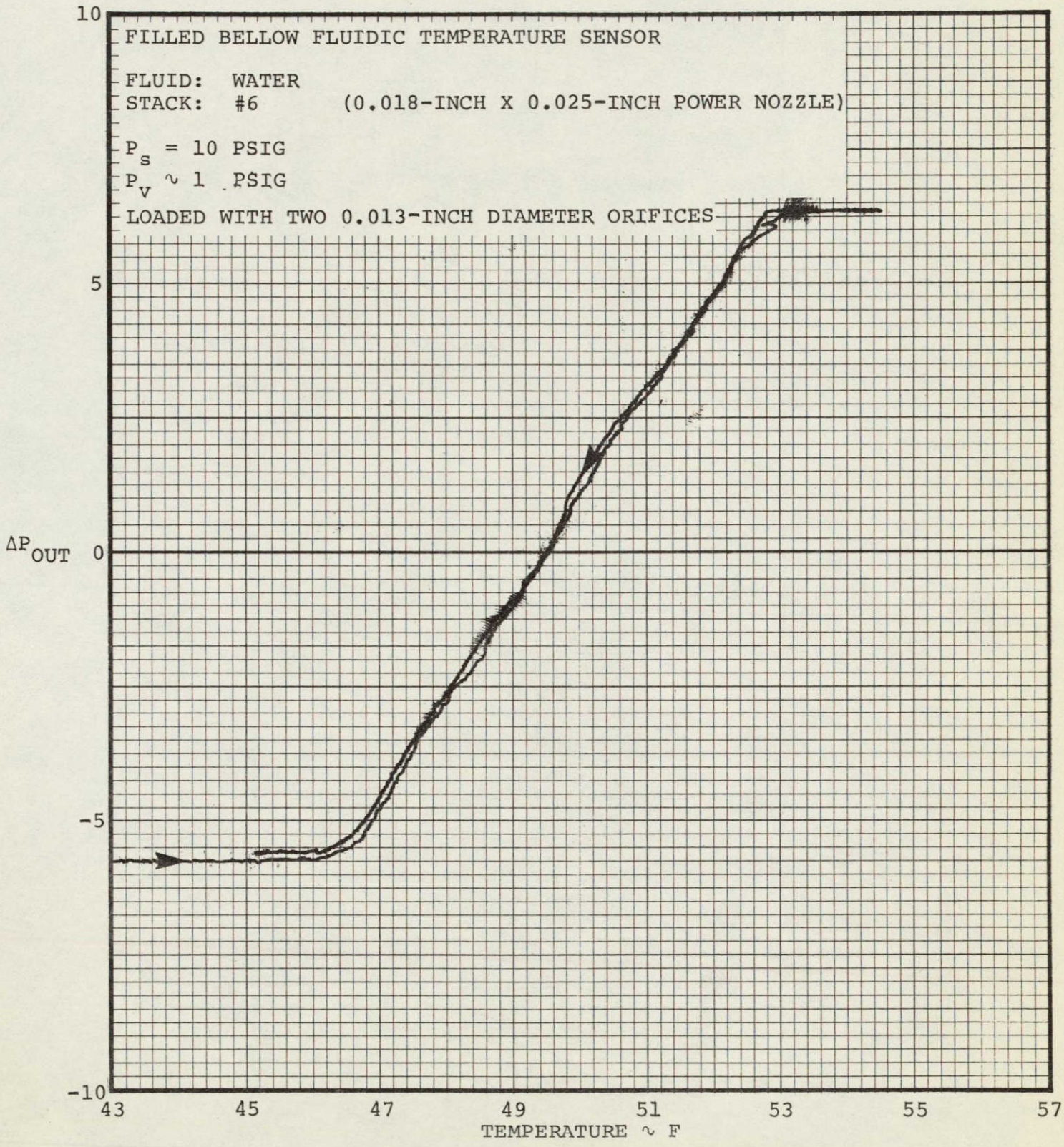

FIGURE 24

FILLED BELLOWS FLUIDIC TEMPERATURE SENSOR
REPRODUCIBILITY OF THE OUTPUT CHARACTERISTICS IN WATER

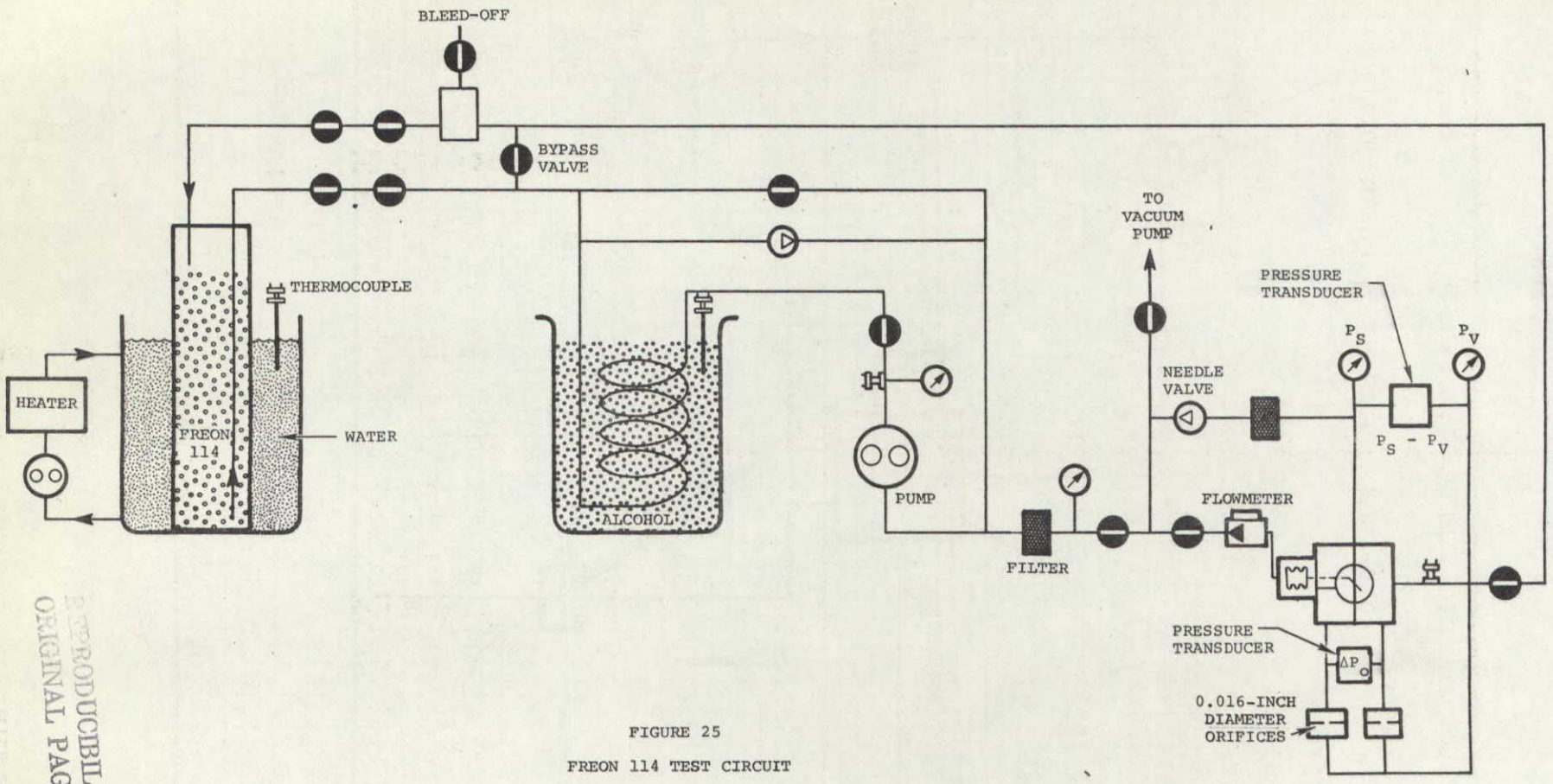

FIGURE 25

FREON 114 TEST CIRCUIT

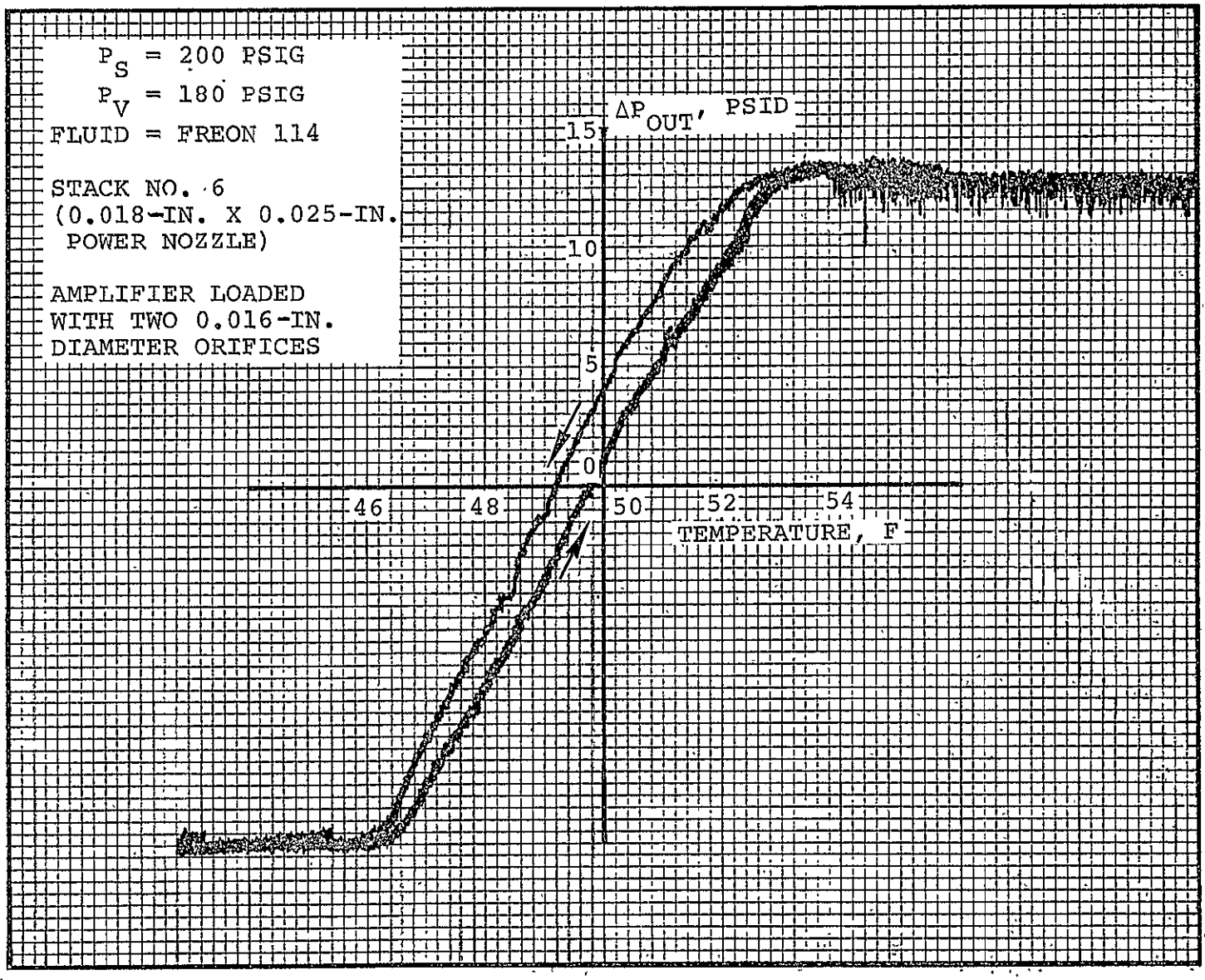

FIGURE 26

CHARACTERISTIC CURVE OF THE SENSOR

SCALE: HORIZONTAL - $P_S - P_V$, 10 PSI/DIV

ΔP_o, 1.25 PSI/DIV

VERTICAL - 5 MSEC/DIV

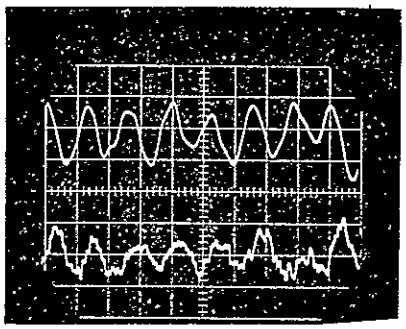

$P_S - P_V$

ΔP_o

FIGURE 27

$P_S - P_V$ AND ΔP_o NOISE OF THE SENSOR

2.4.3 Conclusion of the Bellows-Driven Pin Amplifier Fluidic Temperature Sensor Development Testing

This temperature sensor is capable of providing the temperature-sensing function required for the thermal control loop. The output sensitivity of the temperature sensor is approximately 14 kPa/F with a 70 kPa supply. This far exceeds the sensitivity that can be attained by oscillator or bridge-type fluidic temperature sensors. This temperature sensor when operating on Freon has a signal-to-noise ratio of approximately 15, which is adequate for use in the thermal control system.

SECTION 3

DESIGN AND EVALUATION OF DIVERTER AND MIXING VALVES

3.1 VALVE DESIGNS

Several valve concepts were considered for this application. The major factors chosen for selecting the valve to be used were reliability, efficiency, and range of control. The desired reliability and efficiency of the valve would be as high as possible, whereas the range of control of the valve must exceed a minimum value established by the temperature control band and the worst temperature case of the system. The worst case is established when the hot flow is 53F and the cold flow is minus 65F. The valve must be able to control the temperature to 50 ±3F by mixing the hot and cold flow. The minimum required diverting or mixing capability of the valve is approximately 95 percent hot flow and 5 percent cold flow. This would result in a mixed flow temperature of 47F.

The following sections discuss the operation and capability of the valves that were considered for this application.

3.1.1 Proportional Fluidic Diverter Valve

A proportional valve, as shown on Figure 28, may be operated with or without a vented interaction region. Venting the interaction region would be accomplished by providing a flow path between the interaction region of the valve and the pump inlet. This flow path may be restricted or regulated such that a constant pressure drop may be maintained across the valve.

The valve vent flow returned to the pump inlet is considered lost flow since the flow could not be used in the remainder of the thermal control loop. Figure 29 indicates the flow paths if the valve is vented.

Operating with a vented interaction region, the flow that is recovered through the output of the valve will be approximately 50 percent of the flow entering the supply and control ports of the valve. It is possible, however, to divert 100 percent of the recovered flow, either to or bypassing the cool sink.

When the valve is operated with a nonvented interaction region, the only flow paths available are through the entire control loop. This allows the valve to have 100-percent flow recovery or efficiency. However, the characteristic that renders this approach inadequate is that 95-percent flow diversion cannot be obtained.

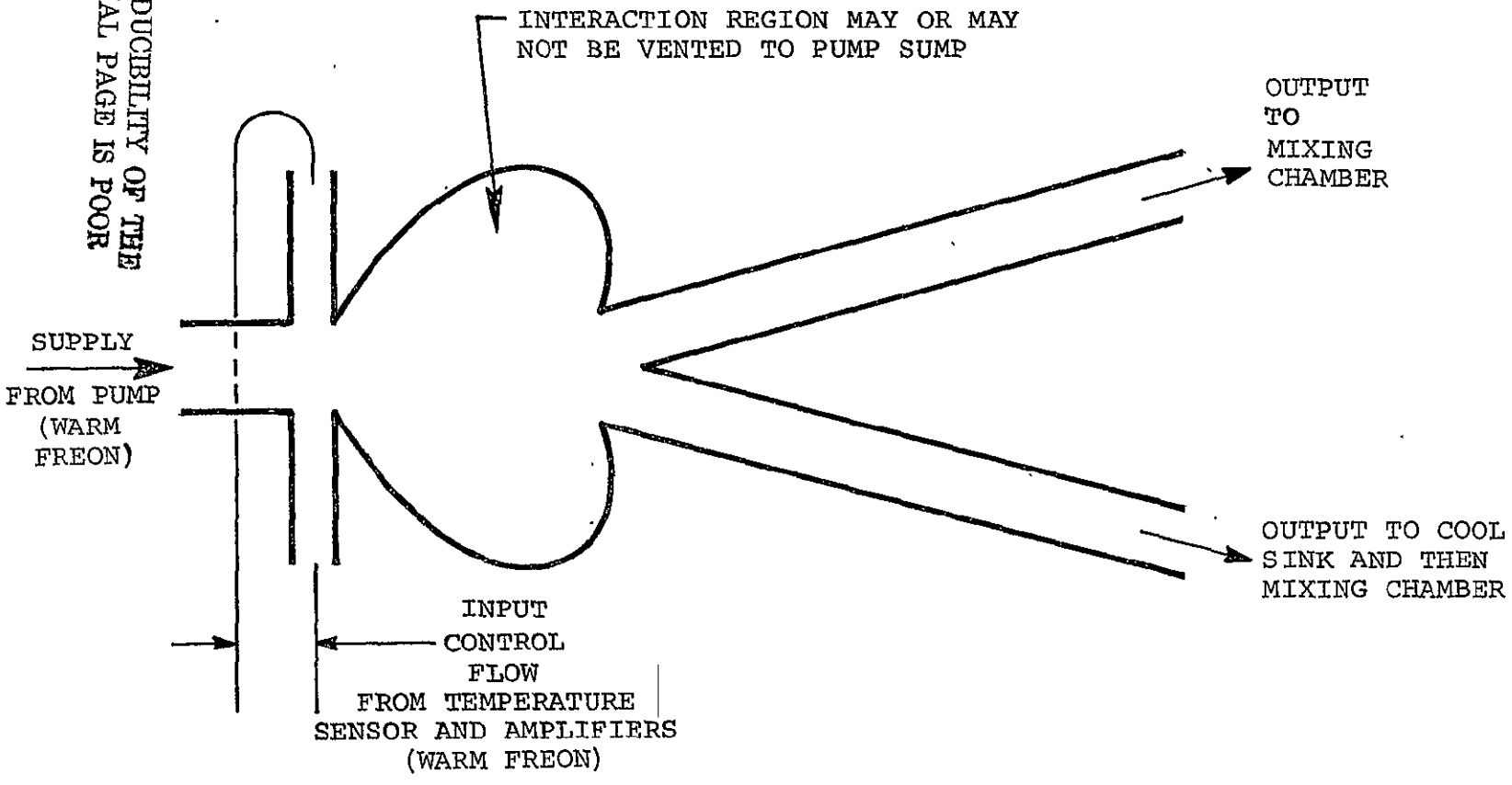

FIGURE 28

PROPORTIONAL VALVE

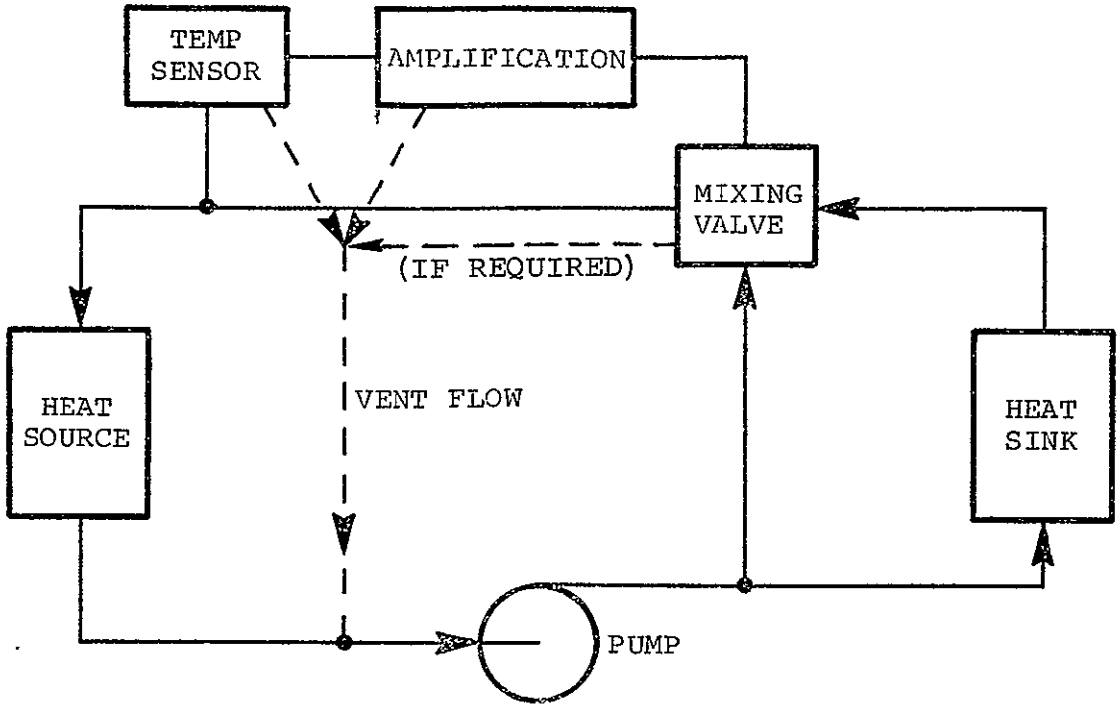

(a)

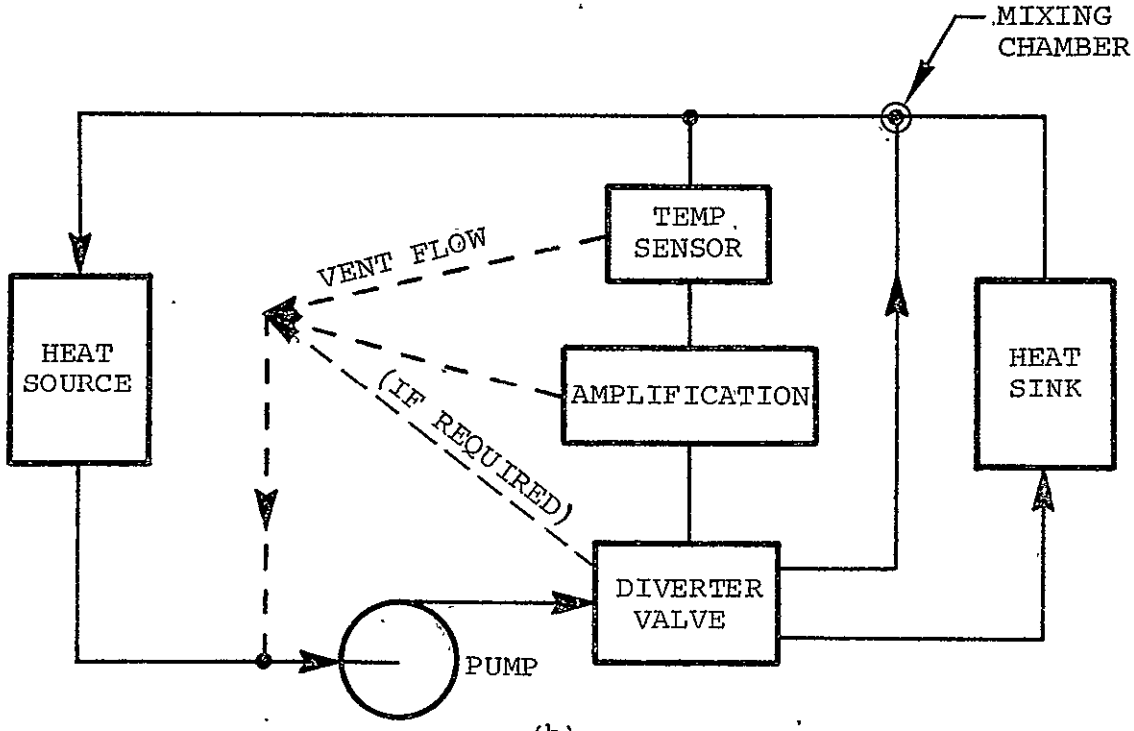

(b)

FIGURE 29

SYSTEM BLOCK DIAGRAMS OF THERMAL CONTROL SYSTEMS

The nonvented valve is not suitable for the thermal control loop application. The vented valve will operate and meet the range of control requirements of the system. However, the factor to be considered would be the flow efficiency of the valve, which is approximately 50 percent.

3.1.2 Vortex Valves

The flow characteristics of the vortex valve are shown on Figure 30. This valve may be vented by placing a vent port surrounding the output port of the amplifier as shown on Figure 31.

The nonvented vortex valve can attain flow gains of approximately five to six, but cannot be used as a diverter valve since the maximum flow diversion a pair of vortex valves can achieve is approximately 75 percent, as compared to the 95 percent required for the system. The vented vortex valve can attain approximately the same flow gain and meet the flow diversion requirement. As with the proportional flueric diverter valve, the vent flow is considerable and flow efficiency will be approximately 50 percent or less.

Another vortex valve characteristic that should be considered is control pressure (P_c) which must be higher than the supply pressure (P_s) for the vortex valve to operate as intended. This means that the output of any device that would be used to drive the vortex valve must be capable of creating vortex control port pressures greater than the vortex valve supply port pressure. Figure 32 is a schematic of a vortex cascade that could be used as a diverter valve. Notice that $\Delta P_c'$ is the output of the vortices driven by ΔP_c and supplied with P_s. The pressure levels of $\Delta P_c'$ is lower than P_s, which is lower than the pressure level ΔP_c. This is similarly true for Stages 2 and 3. It can also be shown that P_s must be greater than P_s', which must be greater than P_s''. P_s, P_s', and P_s'' must be regulated, or by some means held constant at three separate levels. This could require additional pump head as well as possible implementation of low reliability, moving-part pressure regulators to operate the valve.

3.1.3 Proportional-Vortex Combination Mixing Valve

This mixing valve arrangement (as shown in Figure 33) utilizes two vortex valves, which are controlled oppositely by the output of a vented proportional amplifier. In this system, Vortex A functions with hot supply flow (W_{sA} at 53F to 100F), which arrives at the vortex from the Freon pump through Restrictor R_1, and with a cold

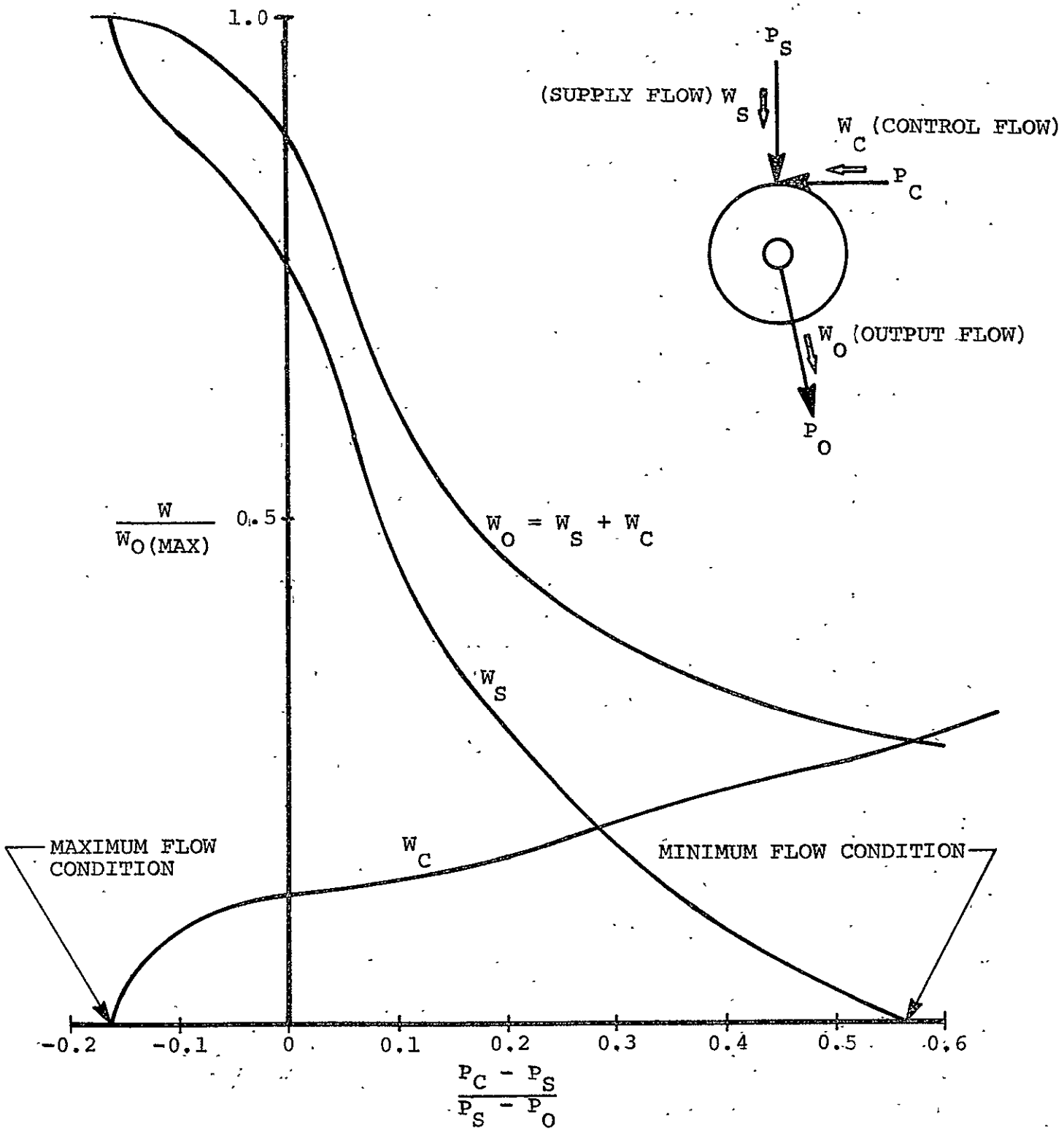

FIGURE 30

VORTEX VALVE FLOW CHARACTERISTICS

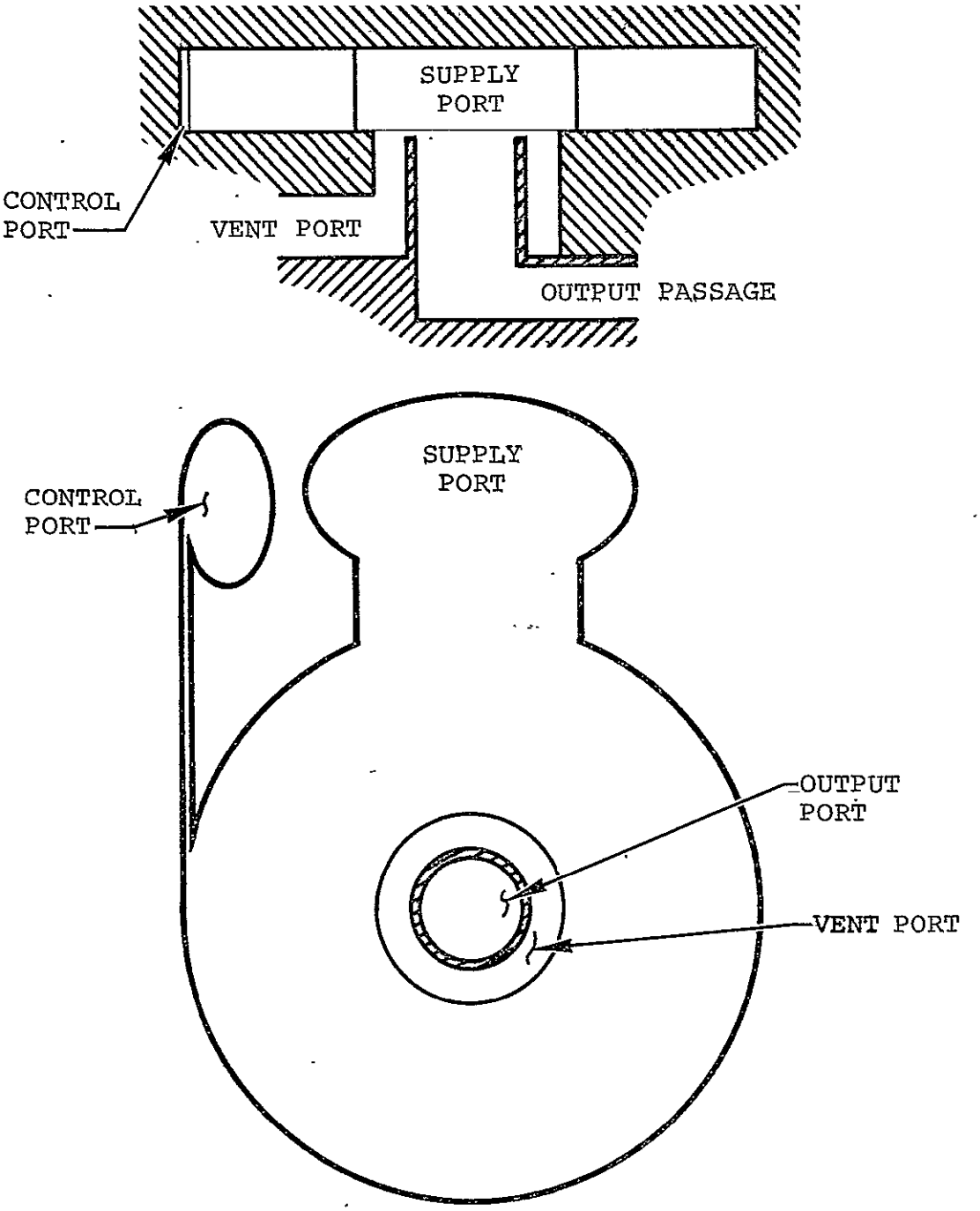

FIGURE 31

VENTED VORTEX VALVE

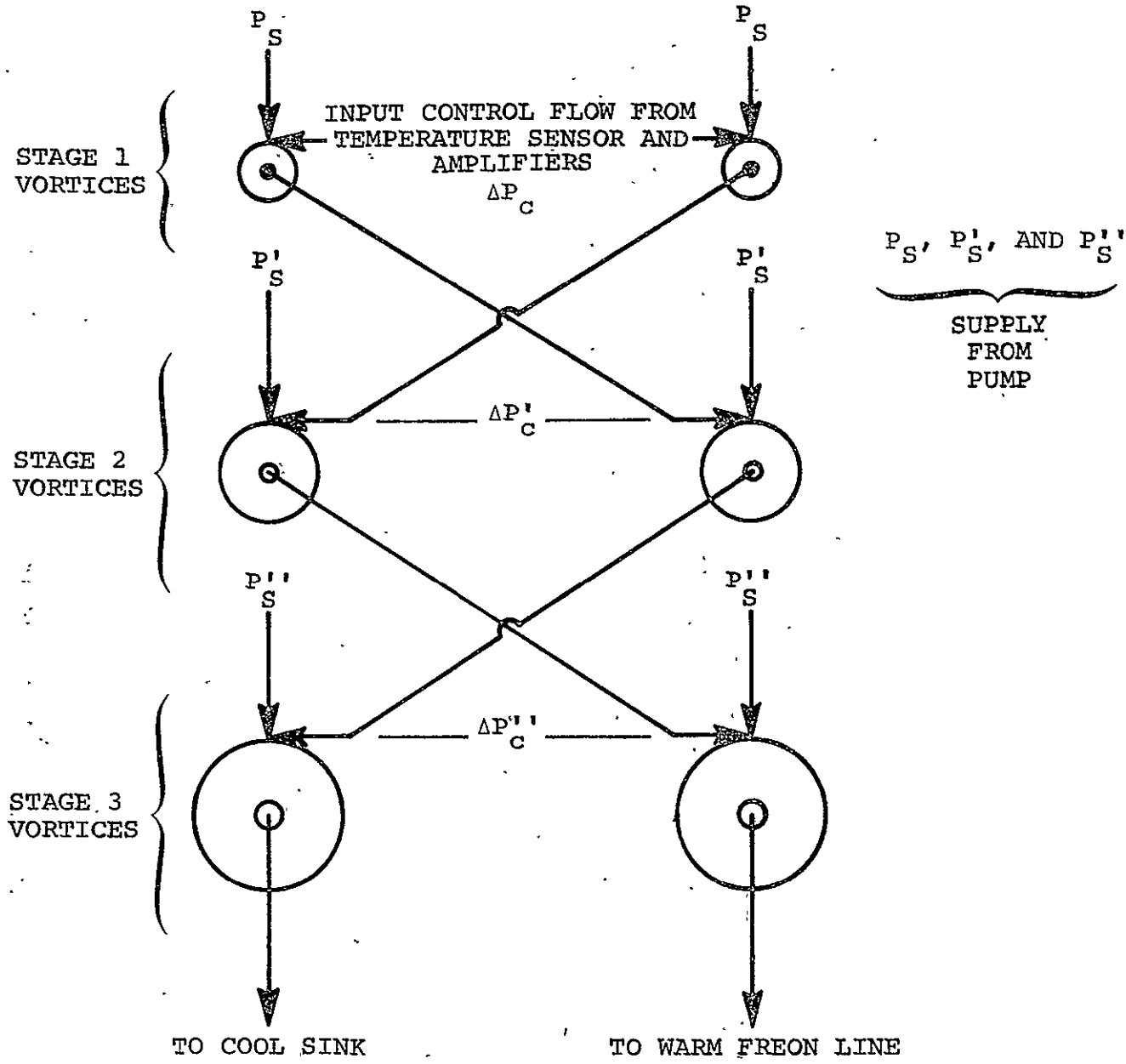

FIGURE 32

VORTEX DIVERTER VALVE

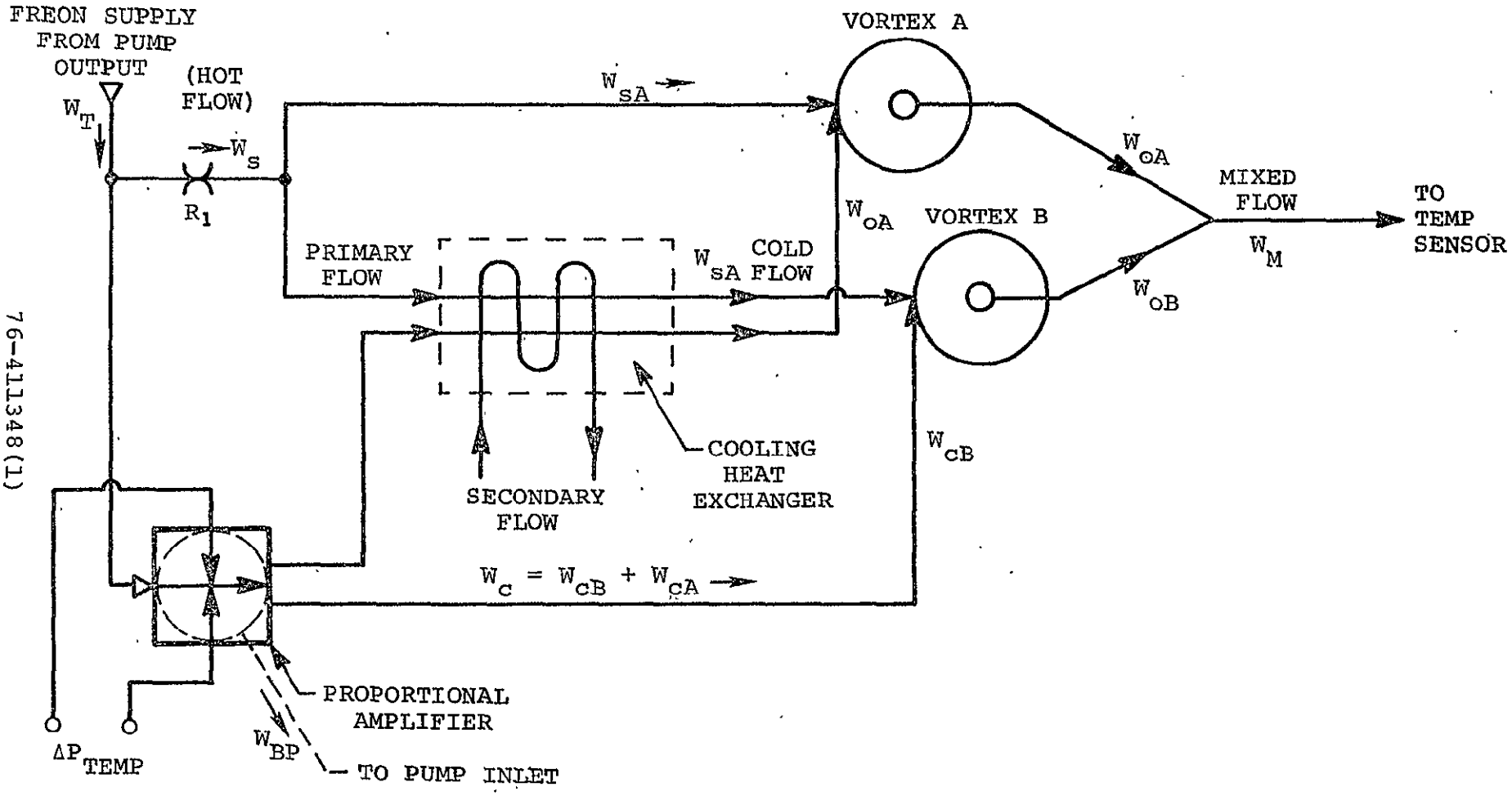

FIGURE 33

PROPORTIONAL-VORTEX COMBINATION MIXING VALVE

control flow (W_{cA} at 47F to minus 65F), which was hot flow from the output of the proportional amplifier before passing through the cooling heat exchanger. Vortex B functions with a cold supply flow (W_{sB} at 47F to minus 65F), which is hot flow from the Freon pump through Restrictor R_1 before being passed through the cooling heat exchanger, and with a hot control flow (W_{cB} at 53 to 100F), which is hot flow from the output of the proportional amplifier.

The supply flow (W_s) of the vortex valve may be shut off completely as seen in Figure 30. At this condition, the minimum flow condition,

$$W_{o(min)} = W_s + W_c = W_c$$

since

$$W_s = 0$$

Similarly, the control flow will be zero when the supply flow (W_s) equals the output flow (W_o). At this condition, the maximum flow condition,

$$W_{o(max)} = W_s + W_c = W_s$$

since

$$W_o = 0.$$

By modulating the control flows to each vortex valve such that the output flow of Vortex A (W_{oA}) is a maximum when the output flow of Vortex B (W_{oB}) is a minimum, the total flow (W_m) would consist entirely of hot flow since,

$$W_m = W_{oB(min)} + W_{oA(max)}$$

and $W_{oA(max)} = W_{sA} + \cancel{W_{cA}}^{zero} = W_{sA}$ (hot flow)

$$W_{oB(min)} = \cancel{W_{sB}}^{zero} + W_{cB} = W_{cB} \text{ (hot flow)}$$

then $W_m = W_{sA} + W_{cB}$ (both are hot flow {53F to 100F})

The opposite would be true by modulating to the condition where

$$W_T = W_{oB(max)} + W_{oA(min)}$$

$$W_{oA(min)} = \cancel{W_{sA}}^{zero} + W_{cA} = W_{cA} \text{ (cold flow)}$$

$$W_{oB(max)} = W_{sB} + \cancel{W_{cB}}^{zero} = W_{sB} \text{ (cold flow)}$$

then $W_T = W_{sB} + W_{cA}$ (both are cold flows {47F to minus 65F})

Modulation of the vortex valves in the fashion described above can be provided by a vented proportional amplifier, which would be driven by the output of the temperature sensor. It is theoretically possible by this means of control to mix any proportion of hot and cold flow from either 100 percent hot or 100 percent cold flow.

The vortex valves of the mixing valve operate with full flow recovery. The overall flow efficiency of this mixing valve arrangement will be reduced by the flow efficiency of the vented proportional amplifier used to drive the vortices. The flow bypassed to pump inlet (W_{BP}) is considered lost flow since it will not be used as cooling or heating flow in the rest of the system. Tests using water as the test medium indicate flow efficiencies of staged proportional amplifiers at approximately 40 to 50 percent. Since the supply flow of the vortex valves (W_s) constitutes approximately 70 percent of the total mixed flow (W_m) and the output of the vented proportional amplifier (W_c) constitutes the remaining 30 percent of the mixed flow, the overall flow efficiency of this valve arrangement is estimated in the range of 69 to 77 percent as calculated from the following equation:

$$\eta_w = \text{Overall Flow Efficiency} = \frac{W_s + W_c}{W_s + W_c + W_{BP}} \times 100 \text{ percent}$$

$$= \frac{W_m}{W_T} \times 100 \text{ percent}$$

The flow efficiency of this valve concept will be of significant importance in the selection of a valve for this program.

3.1.4 Pulse Duration Modulation (PDM) Diverter Valve

The pulse duration modulation is a means of providing a proportional control of either flow or pressure, in this case flow, of a two-position valve. This is accomplished by modulating the relative length of time that the valve exists in either one or the other of the valve positions, at a switching frequency much faster than the remaining components of the system (in this case, the temperature sensor) can react to. Figures 34 and 35 show schematically the operation of the PDM's function in providing a proportion flow control. The PDM diverter valve will divert pulses of flow, either through the cooling heat exchanger, mixing chamber and temperature sensor, or bypassing the cooling heat exchanger to the mixing chamber and then to the temperature sensor. The duration of the pulses in the two flow paths are modulated oppositely from zero to 100 percent of the period of oscillation of the PDM. In Case No. 1 (see Figure 34), the duration of the pulse that bypasses the cooling heat exchanger is 0.75 t. Similarly, the duration of the pulse to the cooling heat exchanger would be 0.25 t. The average flow rate in each flow path for Case No. 1 would be 75 and 25 percent of the maximum flow rate, or 75 percent flow diversion to the path bypassing the cool heat exchanger and 25 percent flow diversion to the path to the cooling heat exchanger. Case No. 2 indicates 50 percent flow diversion to either flow path. The average flow rate in each path is 50 percent of maximum and the pulse duration in each path is 0.5 t. Case No. 3 would be the exact opposite of Case No. 1.

It should be noted that, if the duration of the pulse in a path is 1.0 t, the pulsing has stopped and 100 percent flow diversion to that path has been achieved.

The schematic of the PDM diverter valve is shown on Figure 35. The schematic of this valve arrangement indicates three sections: the oscillator, the output staging of the PDM, and the bistable diverter valve. Operation of these devices is discussed in the following subparagraphs.

The flow efficiency of this valve arrangement is dependent upon the amount of flow that must be bypassed to the pump inlet. In Figure 35, the oscillator and PDM output of the PDM diverter valve use vented amplifiers which constitute flow losses. As described in paragraph 3.1.4.3, the bistable diverter valve may operate unvented with 100 percent flow recovery or may be flow amplified so that the oscillator and PDM output staging may operate with low power consumption and low vent flow. It is expected that the flow efficiency of this type of valve arrangement may exceed 95 percent.

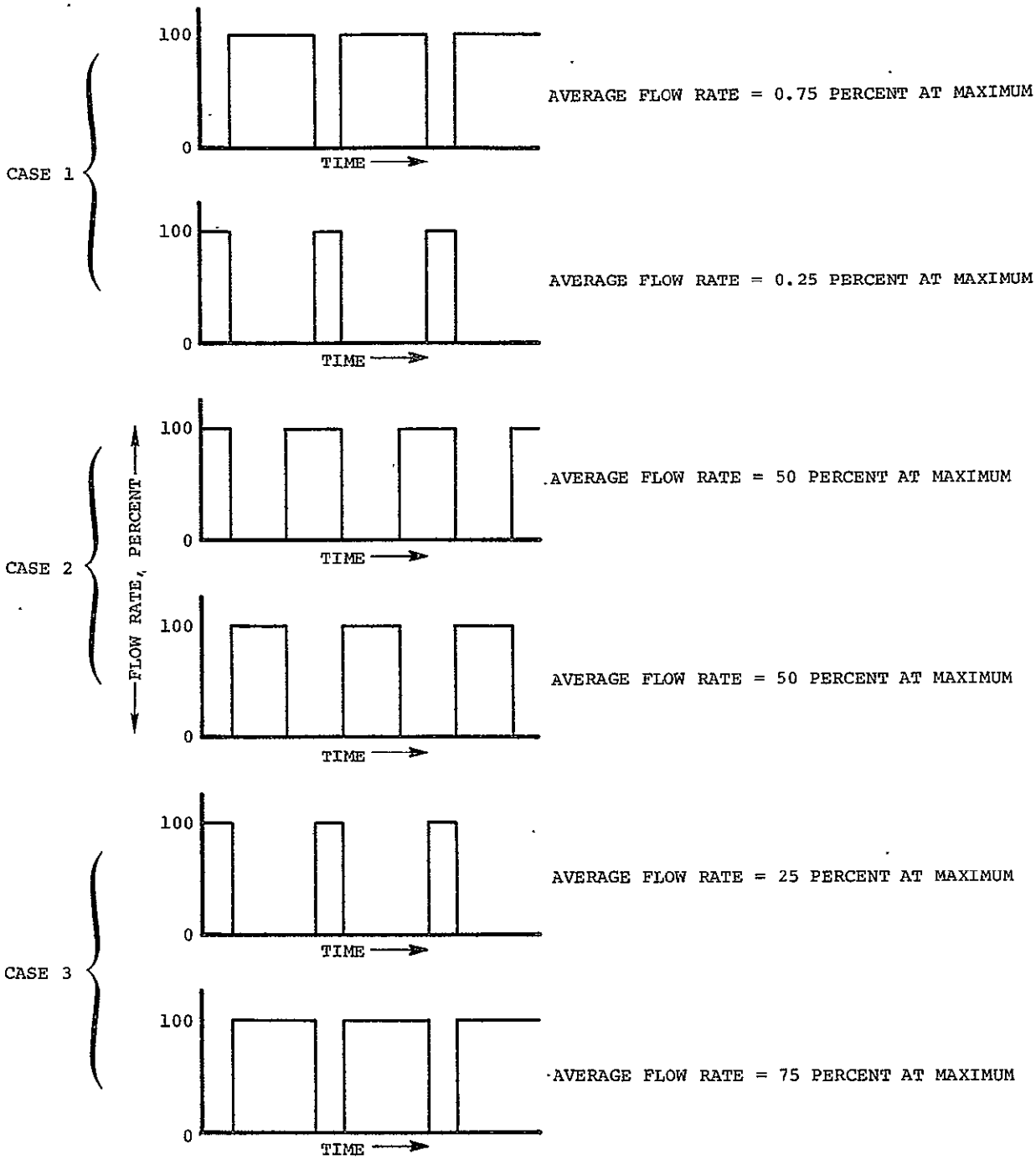

FIGURE 34

PDM PULSE MODULATION CHARACTERISTICS

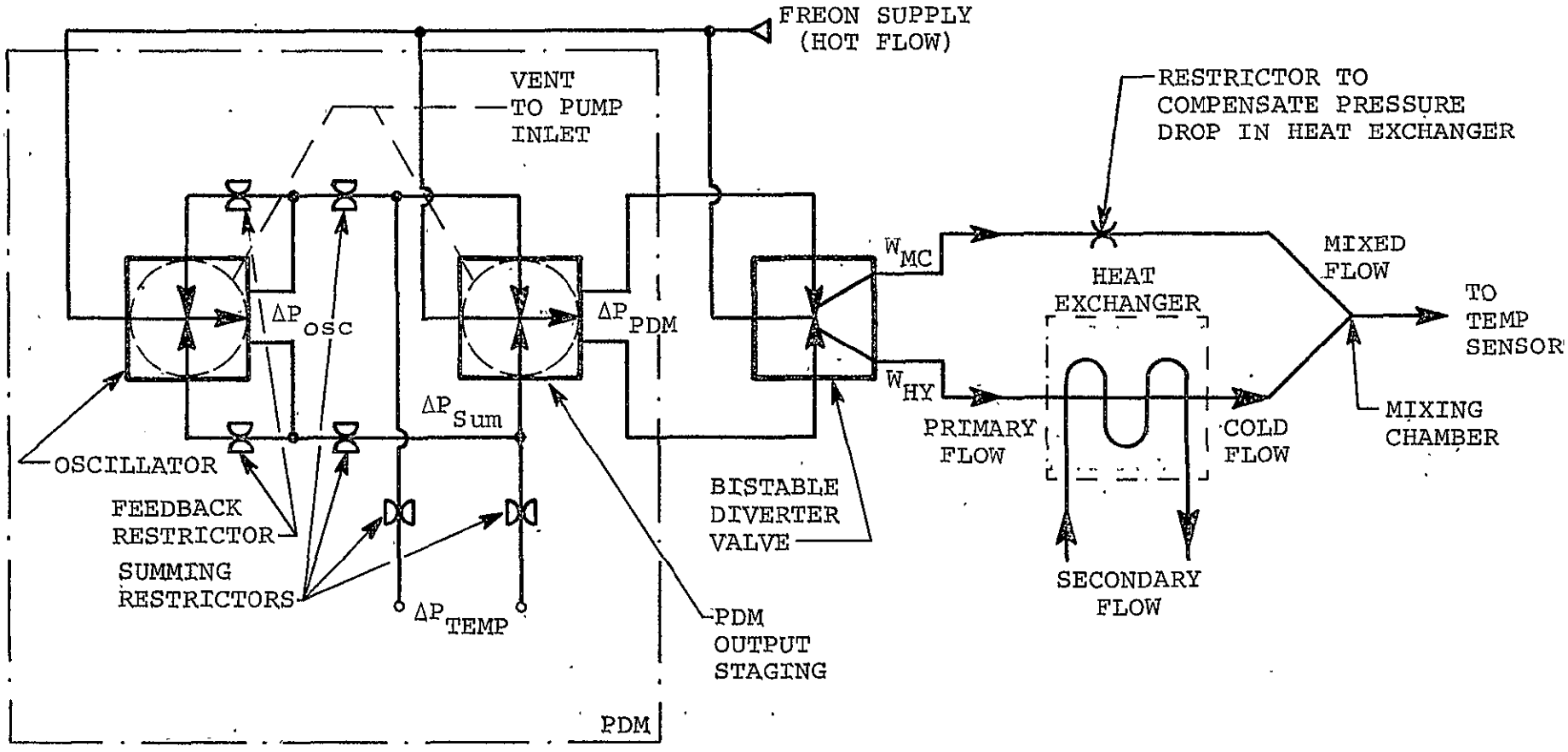

FIGURE 35

PULSE DURATION MODULATION
DIVERTER VALVE

A potential problem in coupling of this system with the temperature sensor is the possibility of noise being generated from the switching of the diverter valve, thereby generating excess noise in the temperature sensor output.

3.1.4.1 Oscillator - The oscillator circuitry provides a base frequency for the PDM. The oscillator consists of a high-gain amplifier cascade with a time delayed negative feedback such that the amplifier is unstable and will oscillate at a frequency determined by the amount of time delay that is introduced into the feedback. The time delay is mainly generated in the transport lags that exist in the amplifiers and the feedback restrictors.

3.1.4.2 PDM Output Staging and Modulation Control - The PDM output staging is nothing more than a two-position switch that will have an output characteristic as shown in Figure 36, where ΔP_{Sum} is the input to the switch and ΔP_{PDM} is the output.

ΔP_{Sum} is a function of the output of the oscillator (ΔP_{osc}) and the modulation control. Modulation control in this application is the output of the temperature sensor (ΔP_{Temp}). The summing restrictors reduce the gain and superimpose the oscillator output and the temperature sensor output such that the ΔP_{Sum} and ΔP_{PDM} have a characteristic as shown in Figure 37. Superimposing of the oscillator output and the temperature output enables the output of the PDM to have a modulated pulse width.

3.1.4.3 Bistable Diverter Valve - This flueric valve has a two-position output which will divert 100 percent of the flow to either of the output flow paths. The direction of diversion is commanded by the output of the PDM. This valve is not vented, which means 100-percent flow recovery. The valve can be staged such that low control flow from the PDM may drive the diverter valve. This is important in maintaining a high flow efficiency in the PDM diverter valve. Figure 36 indicates the approximate characteristic of the bistable diverter valve. The output flow of the diverter valve is shown in Figure 37(c) and (d).

3.1.5 Jet Pipe Diverter Valve

A schematic of this valve is shown in Figure 38. This diverter valve uses the temperature signal (ΔP_{Temp}) to position the nozzle of the jet pipe over the nozzle receivers, which diverts the flow as either hot flow or as flow to the cooling heat exchanger.

The jet pipe valve can operate without vents and thus maintain 100-percent flow efficiency. It is expected that 95-percent flow diversion can be attained.

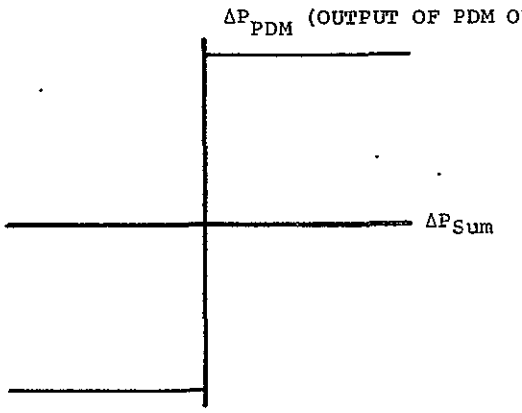

FIGURE 36

PDM OUTPUT STAGE CHARACTERISTICS

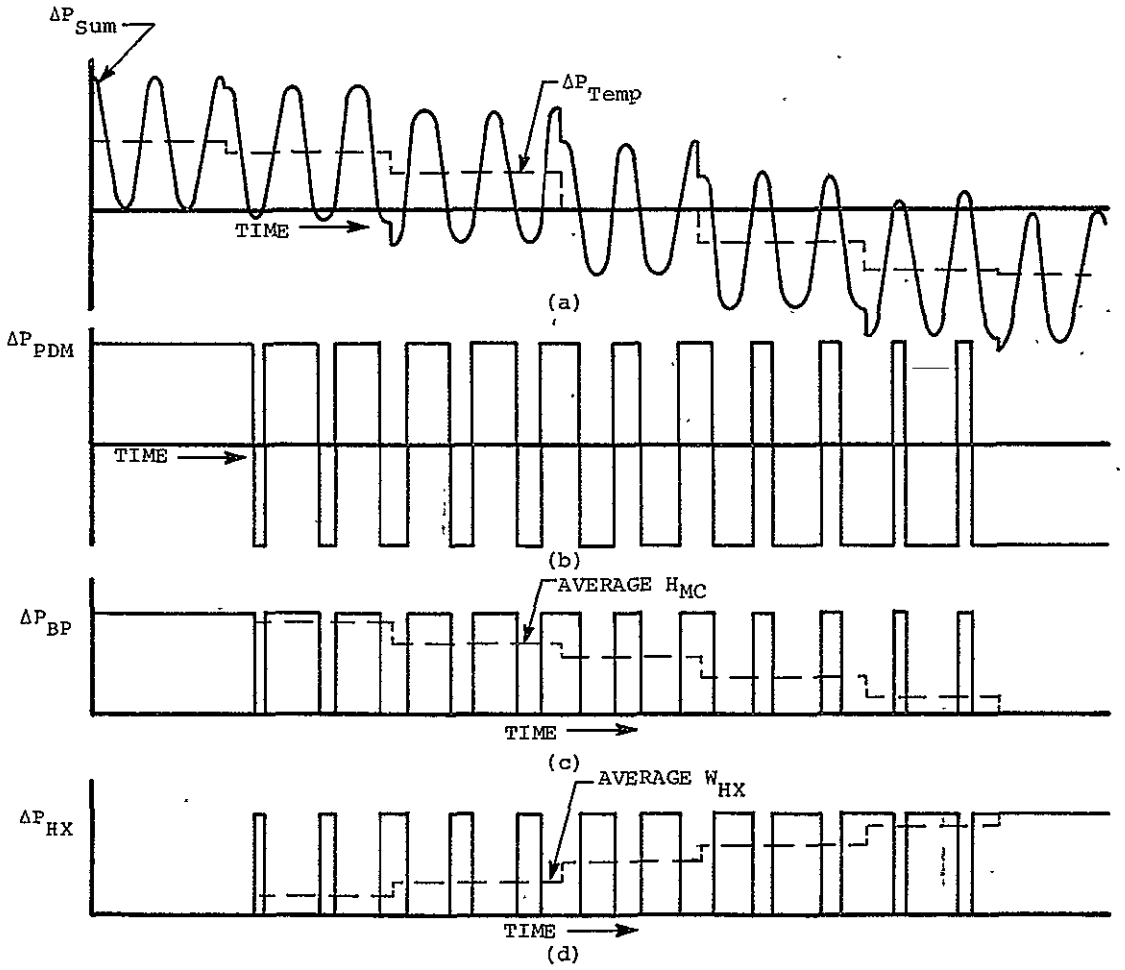

FIGURE 37

PDM CHARACTERISTICS

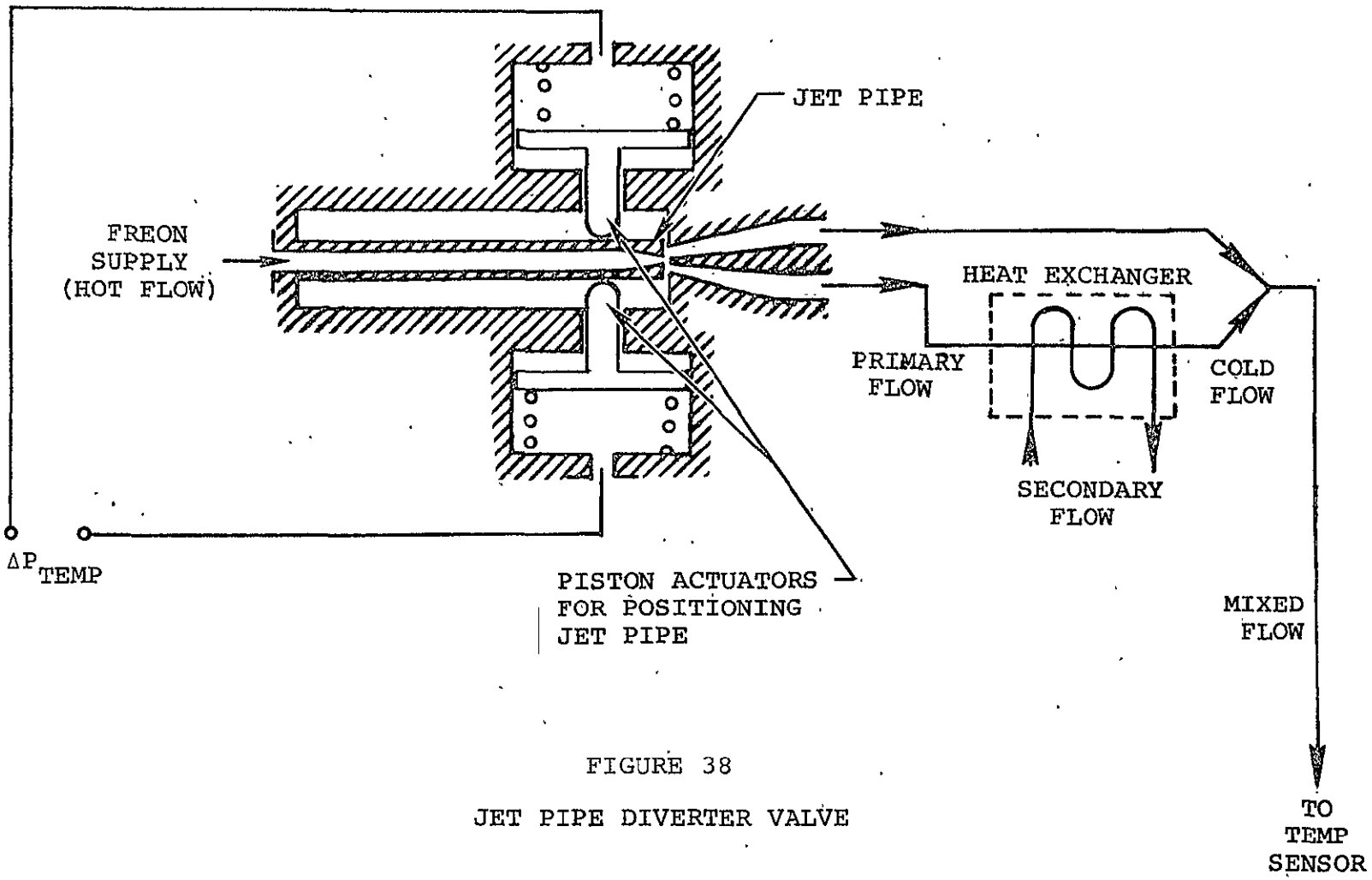

FIGURE 38

JET PIPE DIVERTER VALVE

3.2 DEVELOPMENT TESTING OF VALVES

In evaluation of the valves considered for this program, the proportional amplifier and the vortex valve were immediately rejected because they could not meet the required system performance. The jet pipe diverter valve, which has possibilities of meeting the requirements, was not evaluated because of inherent low reliability of the moving parts as compared to non-moving part flueric valves.

It was decided that the PDM diverter valve and the proportional-vortex mixing valve would be partially constructed and tested for confirmation of expected performances. The points of interest in the development testing of these valves were achieving high flow efficiency and meeting the diversion or mixing requirements.

3.2.1 Development and Testing of the Proportional-Vortex Combination Mixing Valve

The fluidic schematic of the proportional-vortex valve is shown in Figure 39. This valve requires flow amplification of the temperature sensor output, which is provided by Amplifiers No. 1 through 4. The output of the No. 4 amplifier drives into the control ports of the vortices. Note that supply flow of Vortex A and the output leg of Amplifier No. 4, which feed the control port of Vortex B, both flow through the cooling heat exchanger and that orifice Restrictors 1 and 3 have been stationed so as to compensate equally for any pressure drop that may be encountered in the heat exchanger. Flow Restrictor 2 is used to drop the vortex supply pressures to levels lower than the control port pressure levels for proper operation of the vortices.

Development testing of this valve concept was accomplished in two parts: one to define the performance of the vortex valves when coupled in this manner, and the other to define the size of the proportional amplifier (No. 4) needed to drive the vortex valves.

The following subparagraphs discuss the design, procedure of test, performance, hardware, and problems present in this valve concept.

3.2.1.1 Vortex Valve Design - A conceptual diagram of a vortex valve is shown in Figure 40. This represents the major design parameters and flows of vortex valves. These parameters have been nondimensionally mapped for design purposes as shown in Figure 41. The parameters used are defined as follows:

r_o - The outer radius of the chamber.

r_e - The exit port radius.

h - The chamber height.

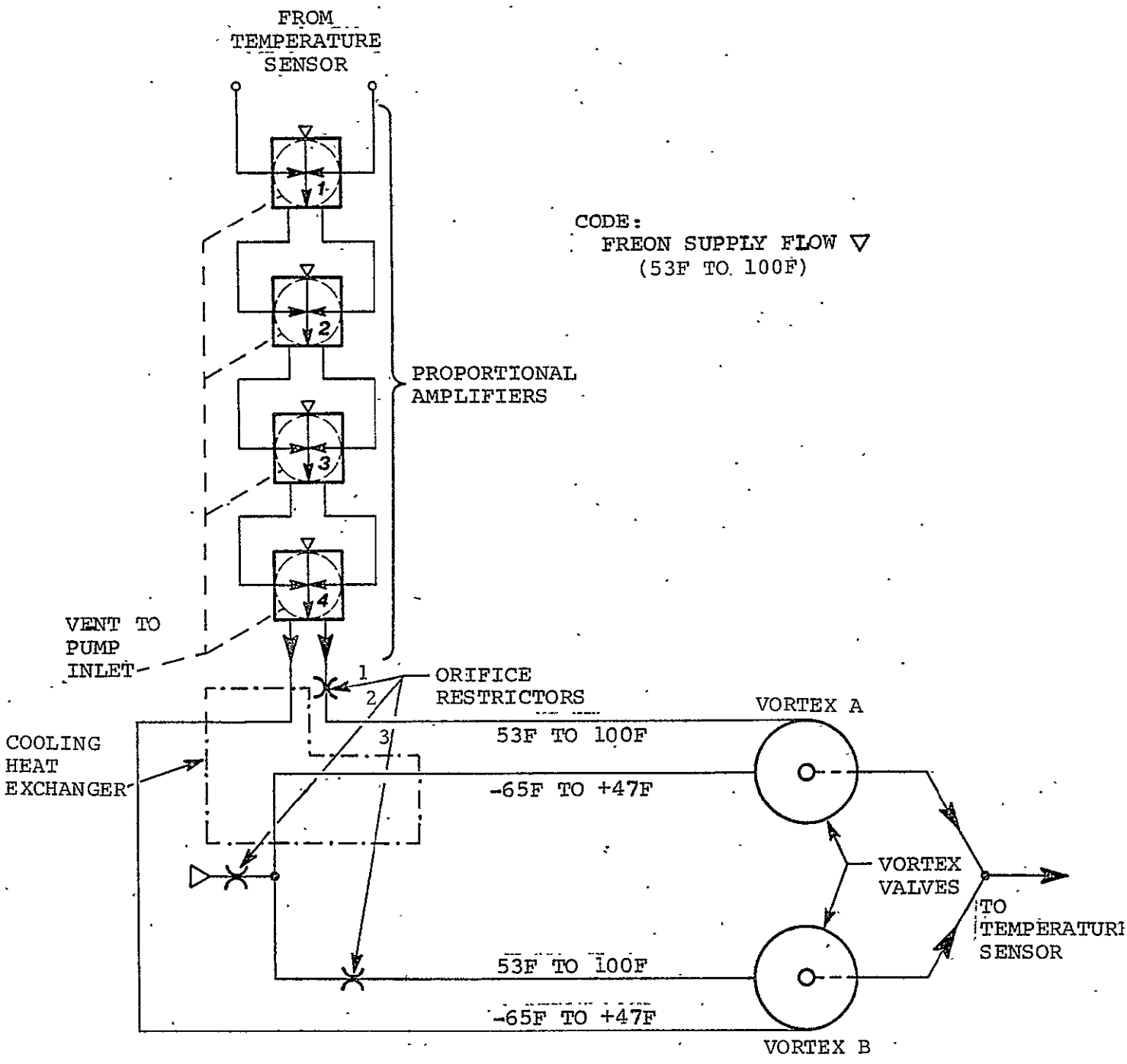

FIGURE 39

PROPORTIONAL-VORTEX MIXING VALVE

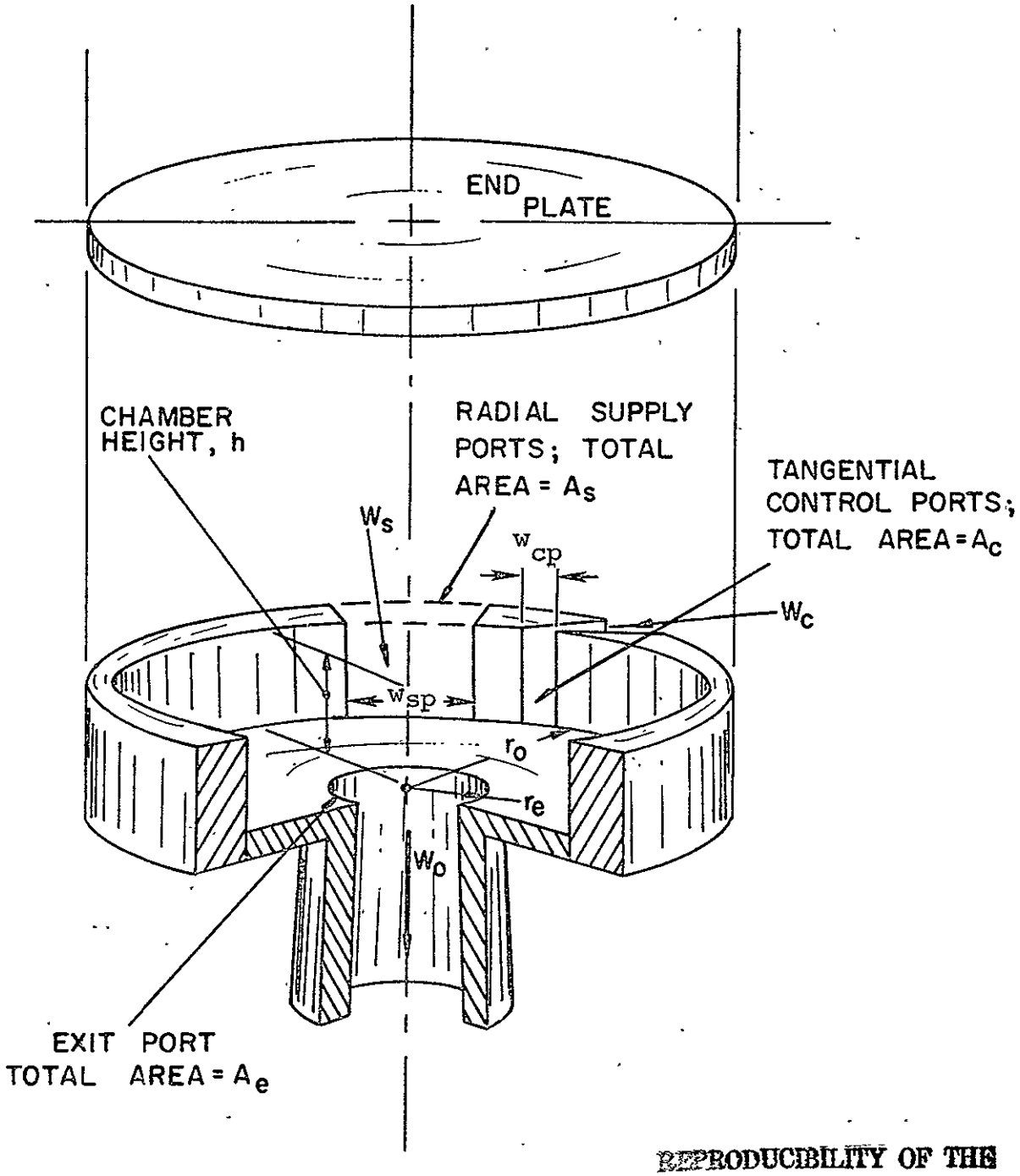

FIGURE 40

CONCEPTUAL DIAGRAM OF A VORTEX VALVE

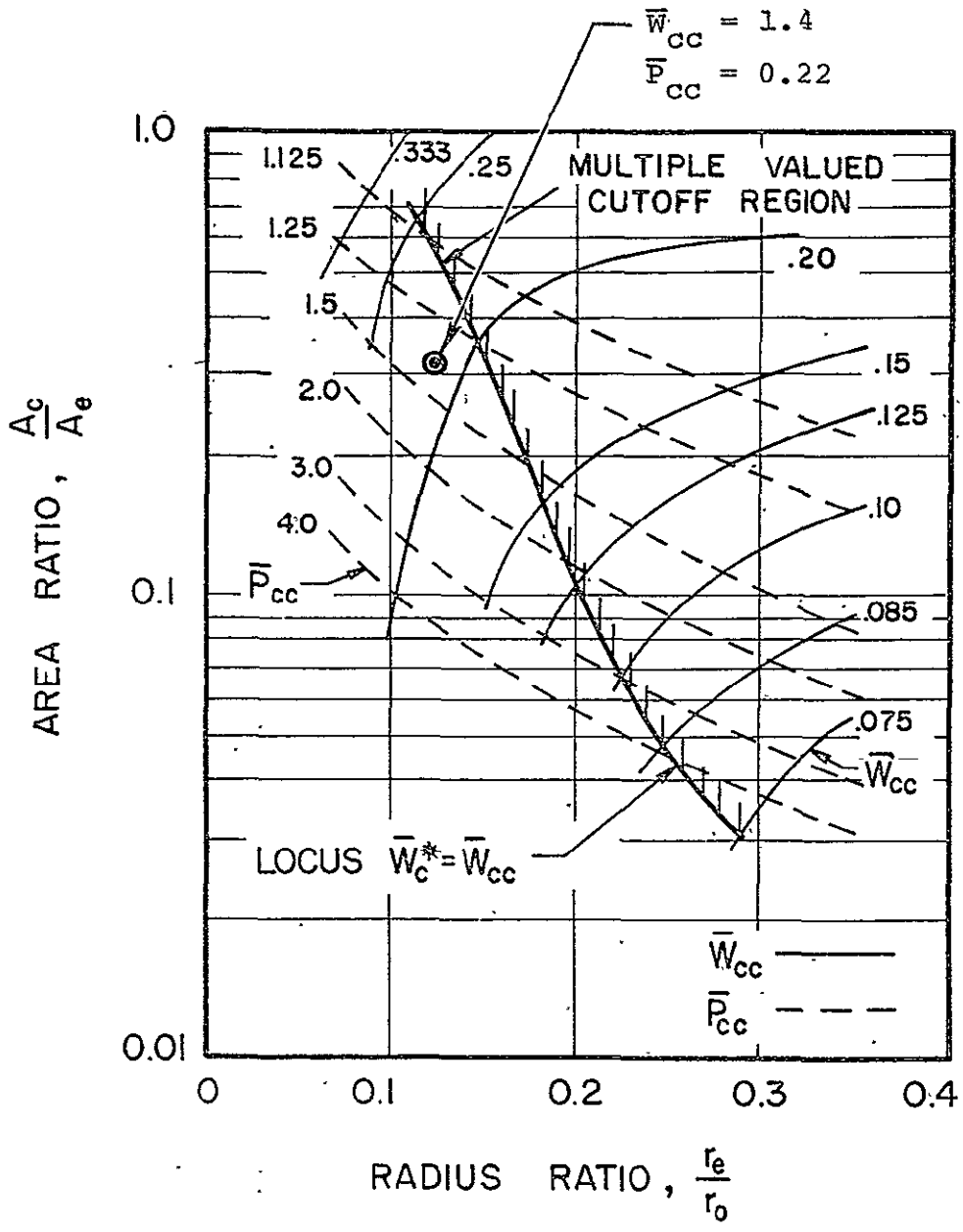

FIGURE 41

VORTEX VALVE CUTOFF FLOW
AND PRESSURE CHARACTERISTICS

A_s - The total area of the supply ports.

A_c - The total area of the control ports.

A_e - The total area of the exit ports.

P_s - The supply pressure differential between supply and exhaust ports.

W_m - The maximum valve output mass flow.

P_{cc} - The maximum control pressure difference between the control and exhaust ports; this is also the cutoff control pressure.

W_{cc} - The maximum control mass flow available to actuate the valve; the minimum or cutoff total flow for the valve.

$$\overline{W}_{cc} = \frac{W_{cc}}{W_m}$$

$$\overline{P}_{cc} = \frac{P_{cc}}{P_s}$$

$$A_s/A_e > 3$$

$$0.144 < \frac{h}{r_o} < 0.64$$

$$\frac{h}{r_e} > 2$$

The multiple-valued cutoff region of the vortex valve cutoff flow and pressure characteristic is used for the design of bistable action vortex valves. Design in this area was avoided since continuous modulation of the supply flow was needed for the mixing action.

Using the characteristics of Figure 41, development testing of the vortex valve was developed in the following manner.

a. The desired supply port difference was selected as

$$P_s = 100 \text{ kPa } (14.5 \text{ psi})$$

with the maximum control pressure

$$P_{cc} = 140 \text{ kPa } (20 \text{ psi})$$

This yields

$$\overline{P}_{cc} \approx 1.4$$

b. It is desired that $\overline{W}_{cc}$ be as low as possible to increase flow yet maintain a margin of safety from the multiple-valued cutoff region. Thus

$$\overline{W}_{cc} = 0.22$$

was selected.

c. With $\overline{W}_{cc}$ and $\overline{P}_{cc}$ plotted on the vortex map in Figure 40, the area ratio and radius ratio are indicated for meeting the $\overline{W}_{cc}$ and $\overline{P}_{cc}$ requirements.

$$\text{Area Ratio, } \frac{A_c}{A_e} \approx 0.33$$

$$\text{Radius Ratio, } \frac{r_e}{r_o} \approx 0.13$$

d. The total flow rate desired of the two vortices (W_{Total}) operating oppositely should total approximately 15 lpm (4 gpm)

Then

$$W_{Total} = W_{cc} + W_m = 0.22\ W_m + W_m$$

$$W_m = \frac{W_{Total}}{1.22} = 12.3 \text{ lpm } (3.25 \text{ gpm})$$

With W_m, P_s, and knowing the operating fluid (for development testing this was water), A_e was determined by the following relationship

$$A_e = \frac{W_m}{C_e \frac{\sqrt{2\rho P_s}}{g}}$$

where

C_e = The discharge coefficient of exit port, $C_e \approx 0.75$

ρ = Density of fluid

g = Gravitational constant

This yields

$A_e \approx 0.196$ cm^2 (0.030 in.^{2})

and

$r_e \approx 0.25$ cm (0.098 in.).

e. For $r_e/r_o \approx 0.13$

$r_o \approx 1.92$ cm (0.75 in.).

f. h of the vortex supply port must fall between the following limits

0.5 cm (0.196 in.) < h < 1.18 cm (0.465 in.)

h was selected at 1.02 cm (0.4 in.).

g. Since A_c/A_e should equal 0.33

$A_c = 0.066$ cm^2 (0.010 in.^{2})

and control port width would be

$w_{cp} = 0.064$ cm (0.25 in.).

h. For the requirement of $A_s/A_o > 2.5$, the width of the supply port must be

$$w_{sp} > 0.38 \text{ cm } (0.150 \text{ in.}).$$

Through this analysis, the vortex was designed to the following dimensions

$$r_e = 0.1 \text{ in. } (0.254 \text{ cm})$$

$$r_o = 0.8 \text{ in. } (2.03 \text{ cm})$$

$$w_{sp} = 0.170 \text{ in. } (0.432 \text{ cm})$$

$$w_{cp} = 0.025 \text{ in. } (0.064 \text{ cm})$$

$$h = 0.4 \text{ in. } (1.02 \text{ cm})$$

This design is shown in Figure 42.

Due to a dimensional error in manufacturing tooling, the control port width (w_{cp}) was doubled, resulting in an area ratio of 0.67 instead of 0.33. By referring to Figure 41, it can be seen that the expected performance of the vortex valve with the area ratio of 0.67 and radius ratio of 0.125 would be

$$\overline{W}_{cc} \approx 0.25$$

$$\overline{P}_{cc} \approx 1.125$$

$$W_m \approx 12.3 \text{ lpm } (3.25 \text{ gpm})$$

$$W_{cc} = 3.08 \text{ lpm } (0.81 \text{ gpm})$$

$$P_{cc} = 113 \text{ kPa}$$

3.2.1.2 Proportional Amplifier Design for Driving the Vortex Valve - Since the required output flow of each leg of the proportional amplifier was zero to approximately 3.8 lpm (1 gpm), a vented proportional amplifier would be required since a nonvented proportional amplifier is not capable of achieving this flow requirement. An amplifier design capable of achieving the required flows was in existence and was used for development testing of this valve concept. This proportional amplifier is shown in Figure 43.

AIRESEARCH MANUFACTURING COMPANY OF ARIZONA
A DIVISION OF THE GARRETT CORPORATION

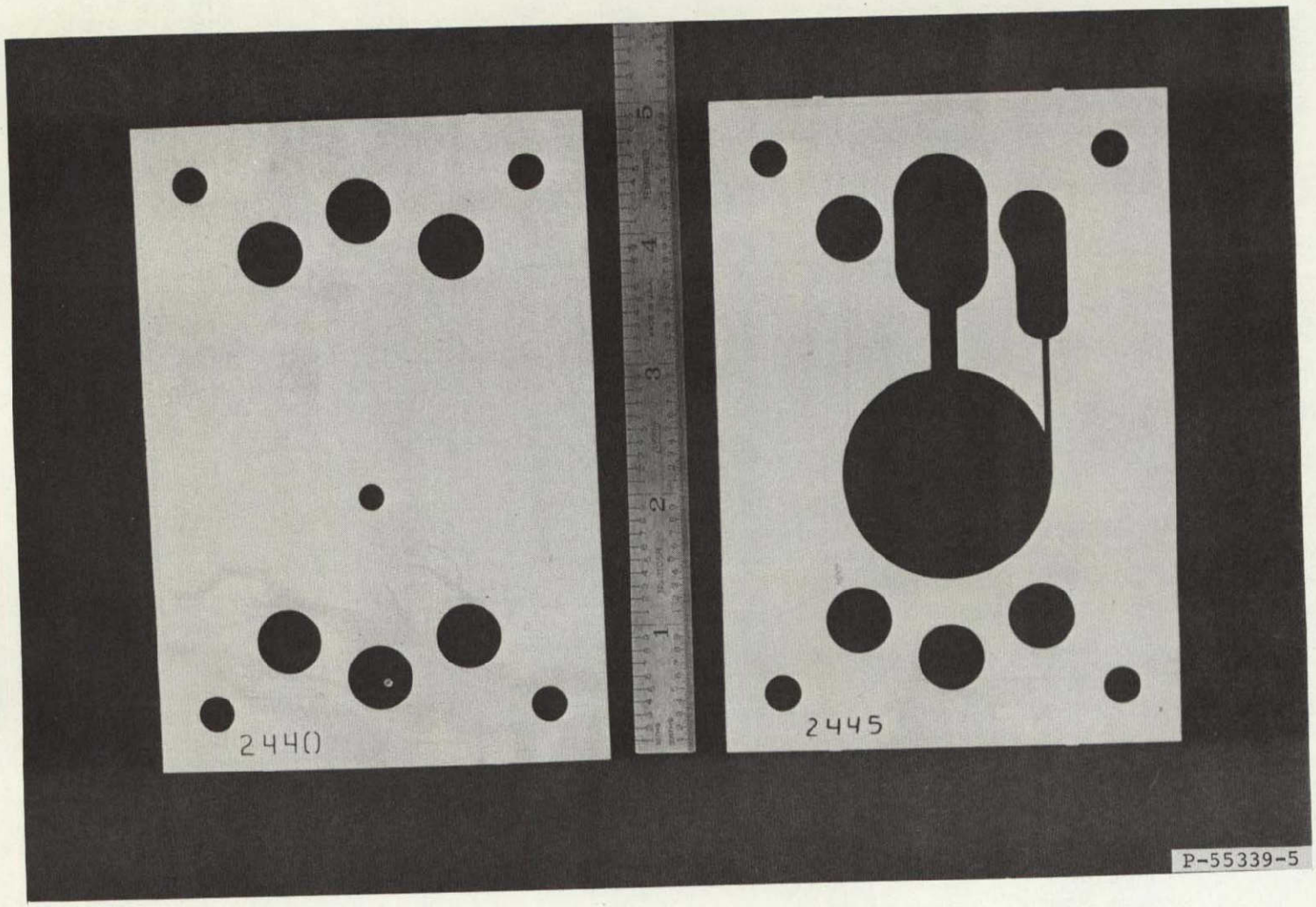

FIGURE 42

VORTEX VALVE

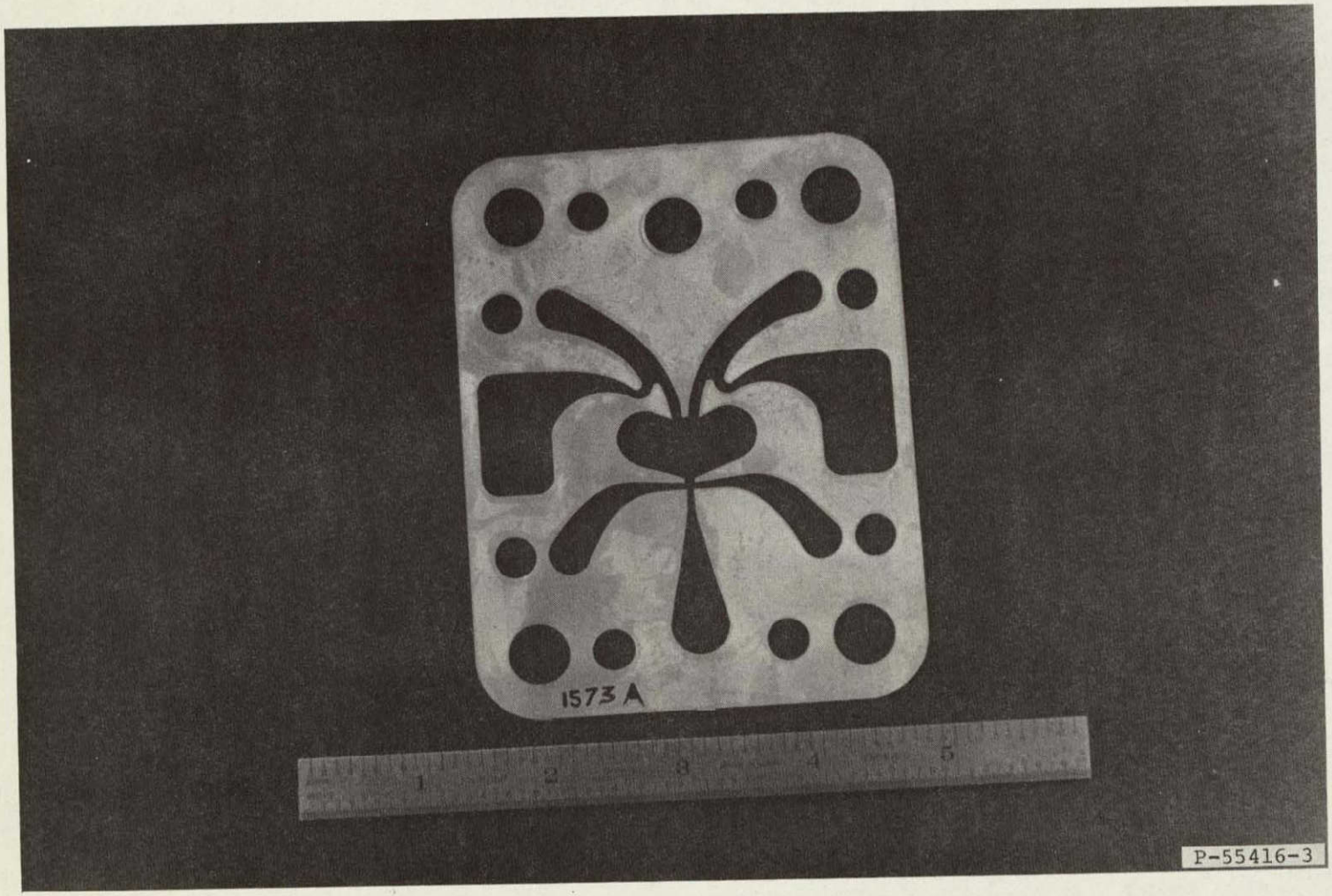

FIGURE 43

PROPORTIONAL AMPLIFIER

3.2.1.3 Development Testing and Test Results of the Vortex Valves - To simplify the complexity of integrating heating and cooling loop in the test setup, the vortex valves were operated with the working fluid at ambient temperature. Water was used for all testing for ease of operation of the system, to reduce development costs resulting from loss of Freon in switching test fixtures, and to avoid the additional expense required to build and bond fluidic circuitry to eliminate Freon leakage. The effect of the fluid on the performance of the valves and amplifiers will be proportional to the relative density of the fluids.

Figures 44 and 45 present, respectively, the schematic and photograph of the test setups for testing vortex valves. This setup was arranged to simulate loading of the valves when operating with the heat exchanger and being driven by the proportional amplifier. Flowmeters and gauges were placed in this system such that the control, supply, output flows, and pressures could either be determined or read directly. Ball valves BV_2 and BV_3 were used in this test setup to simulate the pressure drop created by the cooling heat exchanger and its compensation resistance (Orifice Restrictor 3 in Figure 39). It was assumed that the pressure drop of the heat exchanger would be negligible; therefore, both ball valves BV_3 and BV_2 were opened. BV_1 was adjusted for approximately a 10-psi drop to simulate the approximate pressure drop produced by Orifice Restrictor 2 of Figure 39.

The purpose of this test was to determine if the vortex valves could be operated in this fashion, if the vortex valves were capable of attaining the flow mixing requirements, and if so, what were the required driving forces needed to operate the valves.

These tests were performed by modulating the control pressures (P_{c_1} and P_{c_2}) oppositely such that the mean control pressure (P_{mean}) was constant.

$$P_{mean} = \frac{P_{c_1} + P_{c_2}}{2} = \text{constant.}$$

Figure 46 presents the test results by representing the supply flows (W_{s_1} and W_{s_2}) and control flows (W_{c_1} and W_{c_2}) versus the pressured differential, ΔP_c, on the two vortex control ports.

$$\Delta P_c = P_{c_1} - P_{c_2}.$$

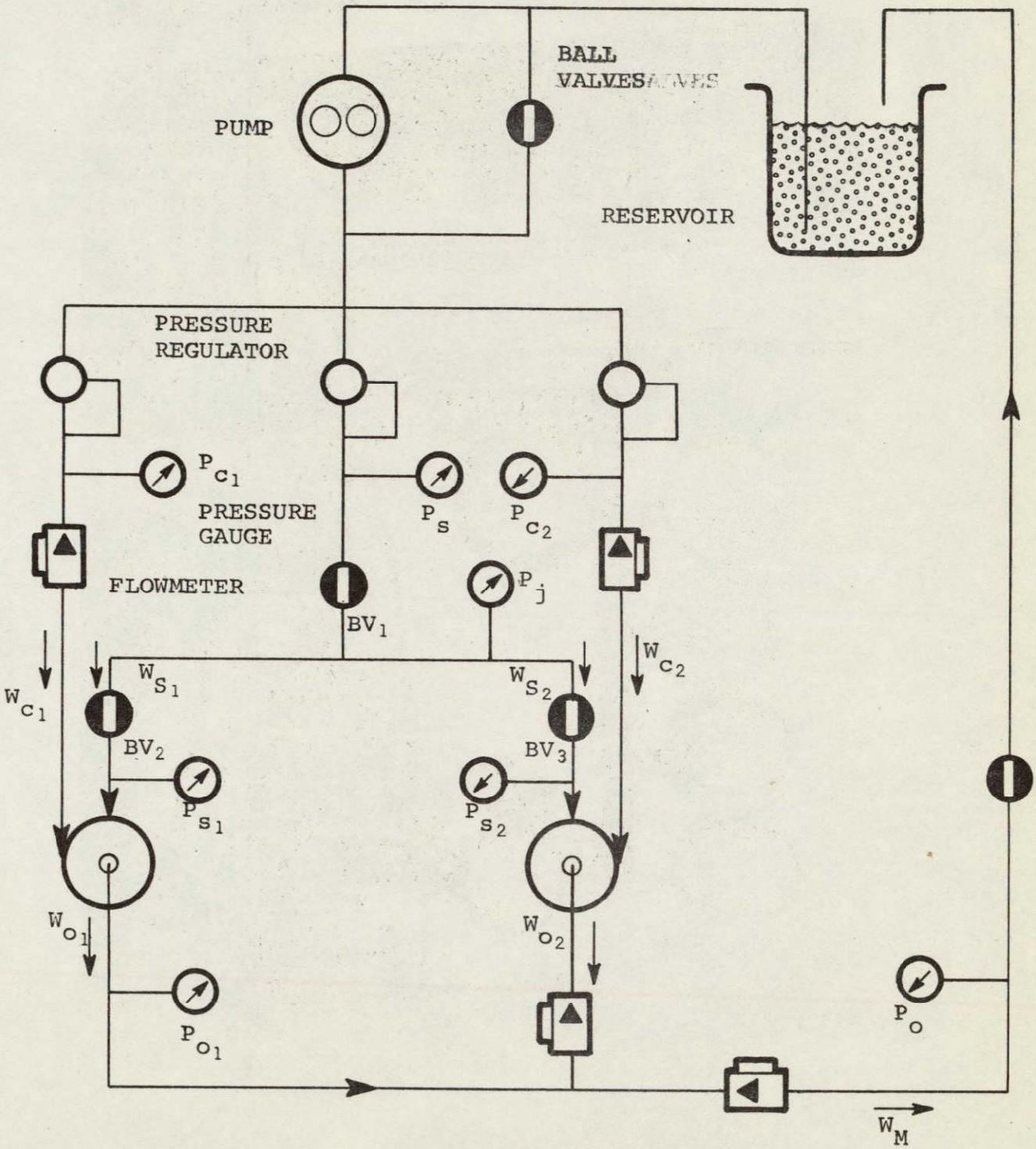

FIGURE 44

SCHEMATIC OF TEST SETUP
FOR TESTING VORTEX VALVES

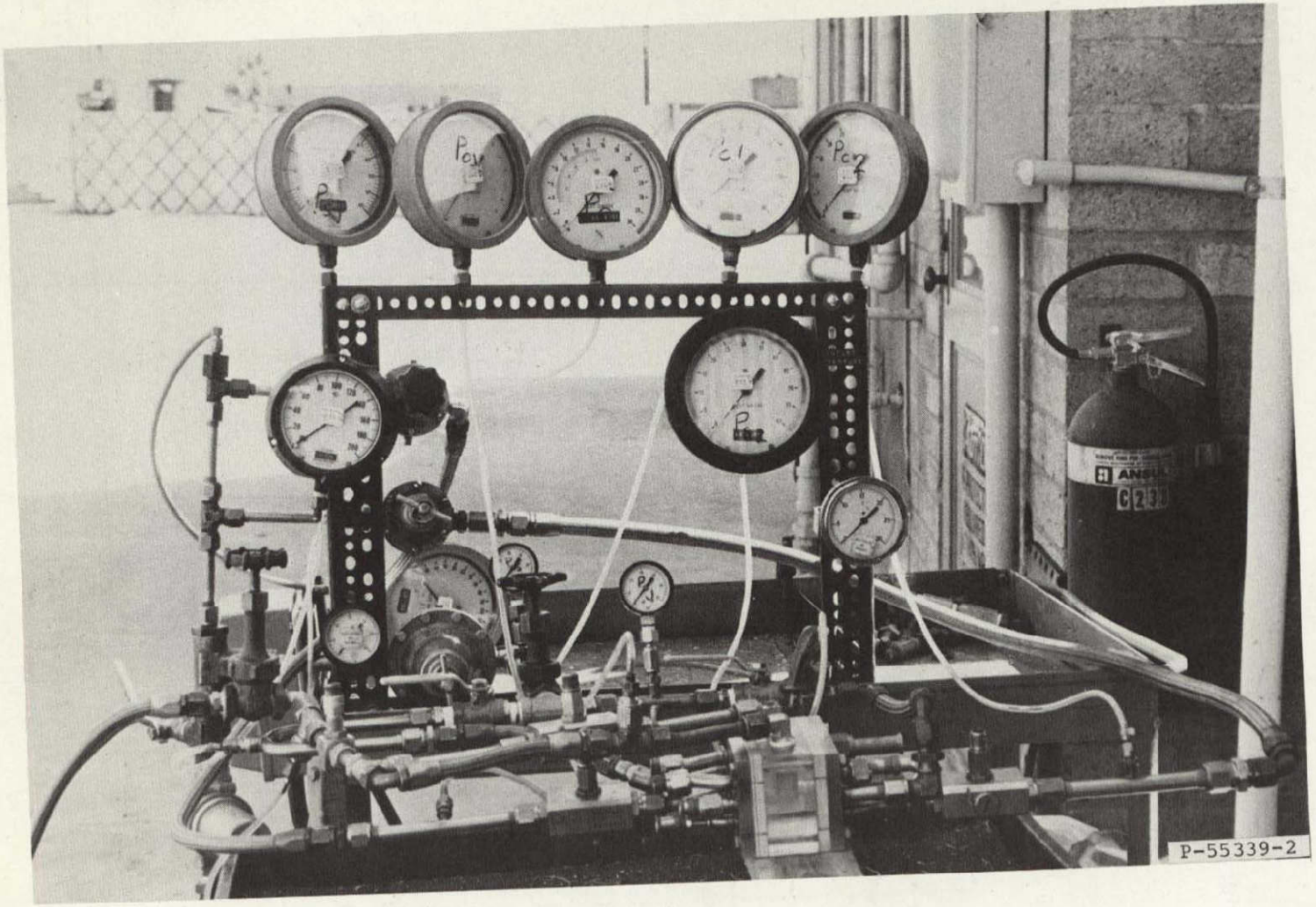

FIGURE 45

PHOTOGRAPH OF TEST SETUP
FOR TESTING VORTEX VALVES

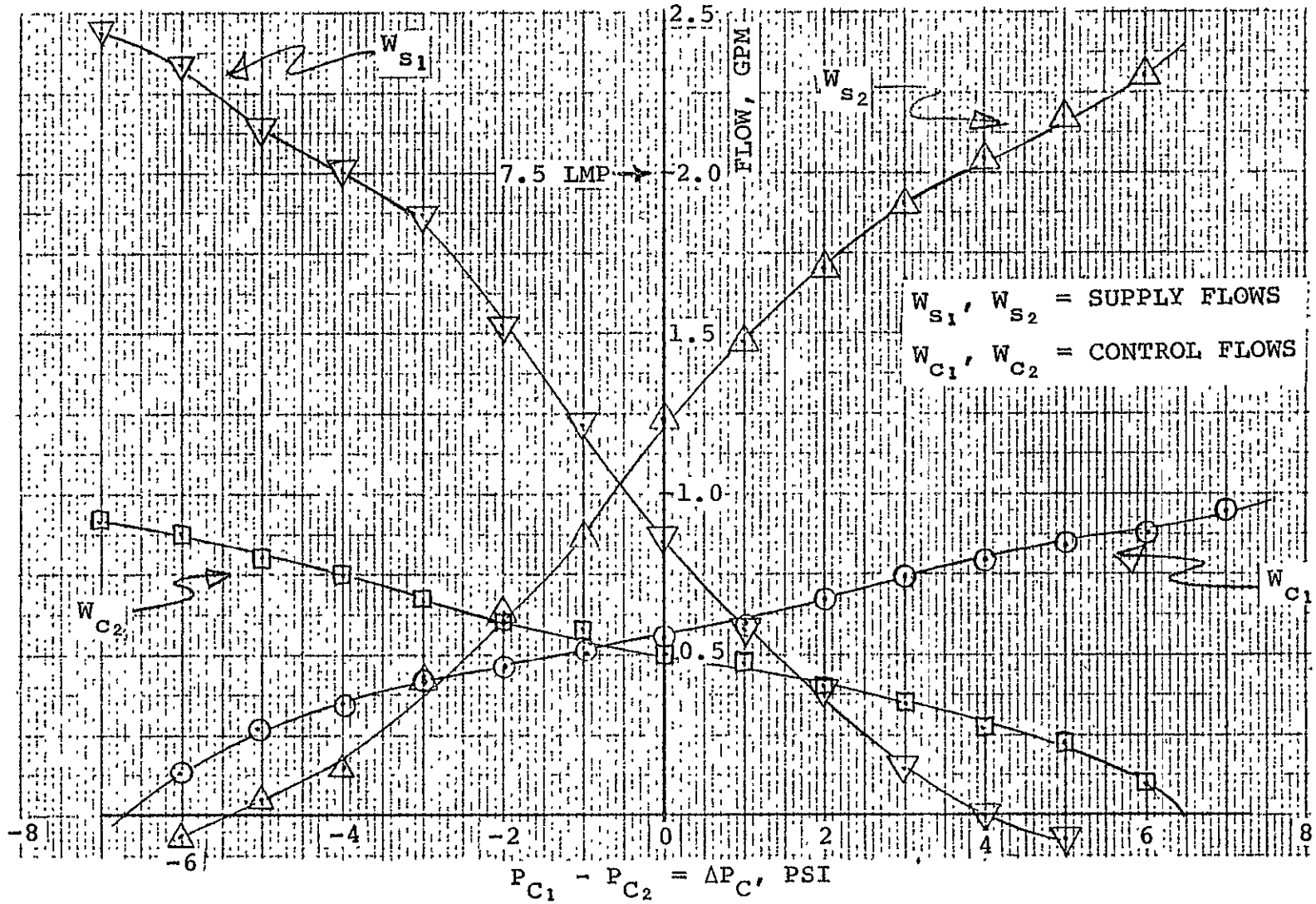

FIGURE 46

VORTEX MIXING VALVE FLOW CHARACTERISTICS

Figure 47 represents the same data, only in a different form. In this figure, the following three flow rates are represented:

$W_{s_1} + W_{c_2}$ - This sum of flows would represent $W_{sA} + W_{cB}$ as in Figure 44 or the total amount of hot flow.

$W_{s_2} + W_{c_1}$ - This sum of flows would represent $W_{sB} + W_{cA}$ as in Figure 44 or the total amount of cold flow.

$W_m = W_{s_1} + W_{s_2} + W_{c_1} + W_{c_2}$ - This sum of flows represent the total amount of mixed flow over the range of modulation.

Figure 47 clearly indicates that the vortex valves coupled in this manner can be controlled so as to mix flow ratios of greater than 20:1 of either hot flow and cold flow or cold flow and hot flow, as well as any ratio of hot and cold flow in between these two extremes. It should also be noted that the total mixed flow (W_m) remains essentially constant during the modulation of the valves.

3.2.1.4 Development Testing and Test Results of the Proportional-Vortex Combination Mixing Valves - With minor modification, the vortex valve test setup was modified to the configuration shown in Figure 48. This test setup is equivalent to Amplifier No. 4, Vortex A, and Vortex B of Figure 39. The purpose of this test was to determine the approximate size of the proportional amplifier required to drive the vortex valves, then to determine the approximate flow efficiency of the system.

During testing, it was immediately determined that the output impedance of the proportional amplifier was much larger than the input impedances of the vortex valves. This would require that the flow area of the power nozzle of the proportional amplifier be approximately two to three times larger than the control port area of the vortex. With the hardware that was available at that time, AiResearch was unable to construct a proportional amplifier of the required flow area. As an alternative, a proportional amplifier was constructed with a power nozzle area equivalent to the control port area of the vortex. This amplifier was able to modulate the vortex valve with a ΔP_c of only ±3 psi. This was not enough to modulate the flow extremes as shown in Figure 47. Although this was not the performance required of the system, the relative magnitudes of the vent flow and control flows were observed so that approximations of a system meeting the required performance could be made.

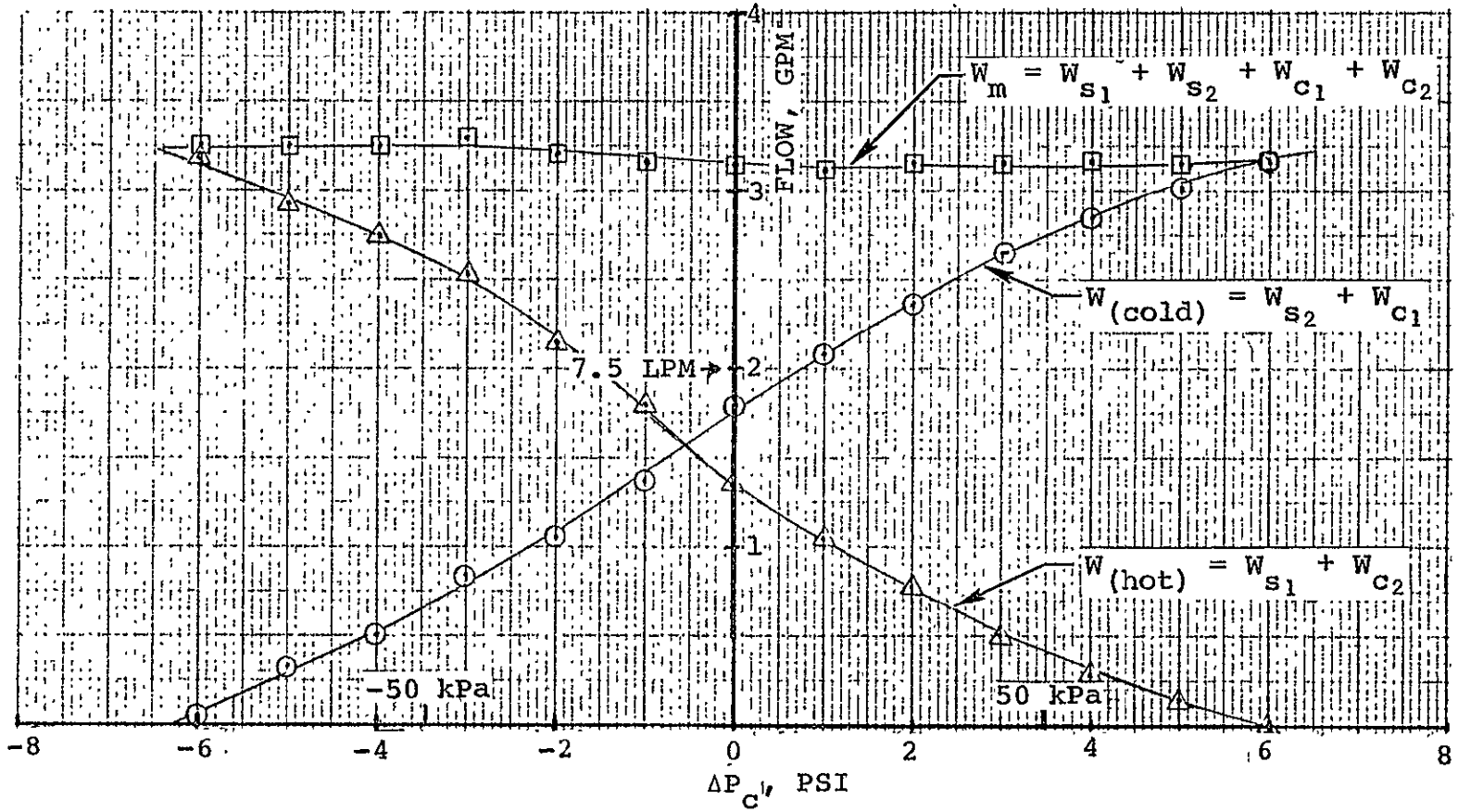

FIGURE 47

VORTEX MIXING VALVE
FLOW CHARACTERISTICS

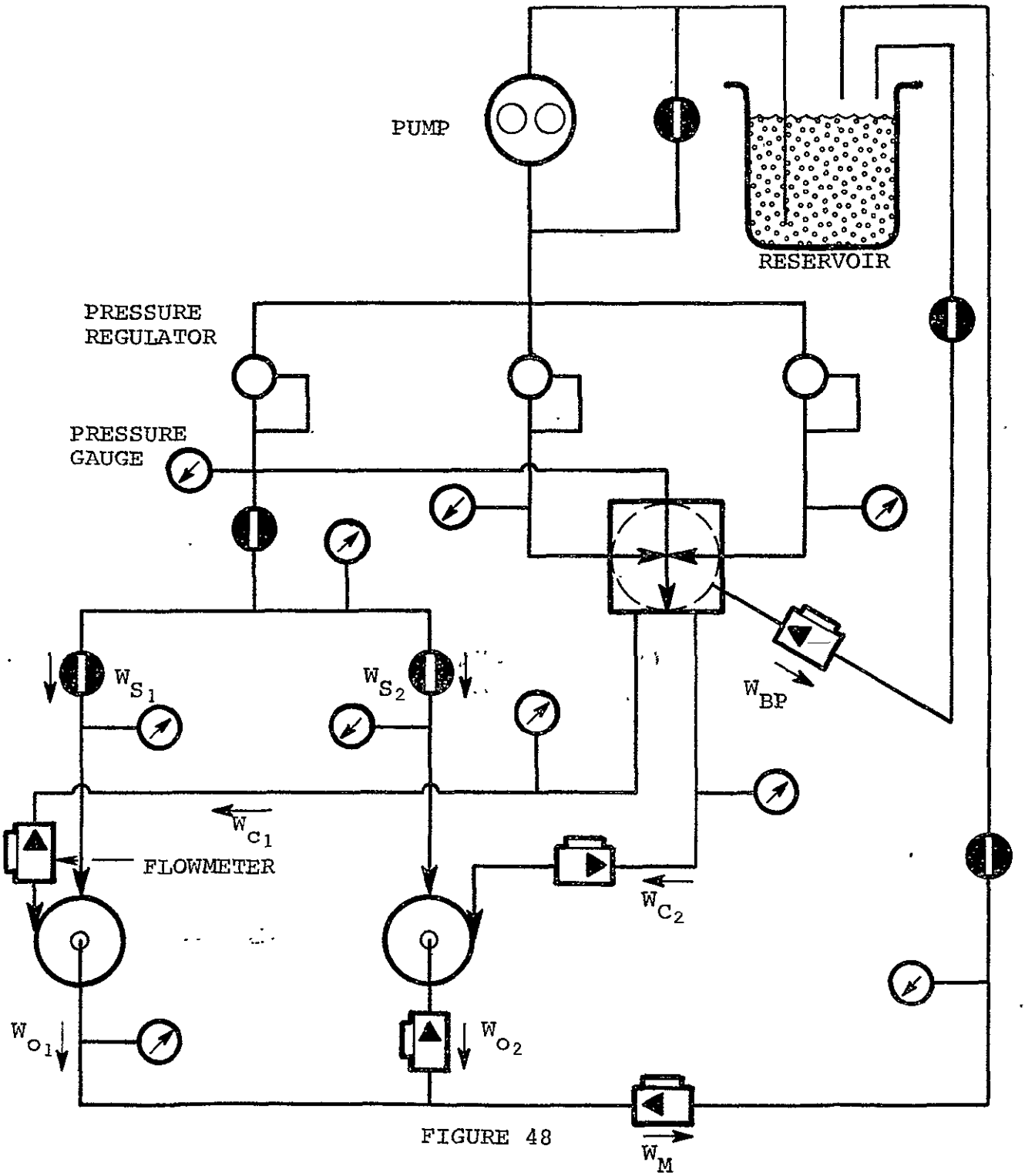

FIGURE 48

SCHEMATIC OF PROPORTIONAL-VORTEX COMBINATION MIXING VALVE TEST SETUP

The vent flow (W_{BP}) of the proportional amplifier in the system tested was approximately 60 percent of the power nozzle flow (W_{PN}) of the proportional amplifier. The tests run indicated that

$$W_{PN} = W_{BP} + W_{c_1(max)}$$

where $W_{BP} = 0.6\ W_{PN}$

$$W_{c_1(max)} = 0.4\ W_{PN}.$$

By doubling the area of the power nozzle to make the vortex valves meet performance requirements, W_{PN} would also double. Referring to Figure 46, it is seen that the control flow would only increase by about 20 percent.

This doubled flow (W^*_{PN}) would then be

$$W^*_{PN} = W^*_V + W^*_{c_1(max)}$$

and since

$$W^*_{PN} = 2\ W_{PN}$$

$$W^*_{c_1(max)} = 1.2\ W_{c_1(max)} = 0.48 \quad W_{PN} = 0.24\ W^*_{PN}$$

The vent flow of the larger amplifier would be

$$W^*_V = 0.76 \quad W^*_{PN} = 3.2\ W^*_{c_1(max)}$$

Assuming that the vent flow of amplifier Stages 1, 2, and 3 of Figure 39 would be approximately equal to the W^*_V or $W_{BP} = 6.4\ W^*_{c_1(max)}$, the overall flow efficiency of this system would be

$$\eta_W = \frac{W_m}{W_T} \times 100 \text{ percent} = \frac{W_s + W_c}{W_s + W_c + W_{BP}} \times 100 \text{ percent}$$

since

$$W_c \approx 0.25\ W_s$$

and

$$W_{BP} \approx 6.4\ W_{c_1(max)} = 6.4\ W_c$$

Then

$$\eta_W \approx 45 \text{ percent}.$$

3.2.1.5 Conclusion of Proportional-Vortex Combination Mixing Valve Testing - The overall flow efficiency of this system was somewhat lower than expected from the initial analysis of the system. This was due to the unexpected large output impedance required of the proportional amplifier. The flow efficiency of the proportional amplifier stages was approximately 16 percent. Since the vortex valves were operating with 100 percent flow efficiency, the flow efficiency of the device (in this case, the proportional amplifier), which controls the vortex valves, is the area of concern. If the flow efficiency of the vortex controller could be improved to as high as 80 percent, the overall flow efficiency of the system would be approximately 95 percent, rendering this system very acceptable for use in the thermal control loop.

Performance of the vortex mixing valves was as expected in the preliminary analysis. Test results have shown that this vortex mixing valve arrangement can be made to mix hot and cold flow in any proportion from zero percent cold, 100 percent hot flow to 100 percent cold, zero percent hot flow.

3.2.2 Development and Testing of the PDM Diverter Valve

Development and testing of this diverter valve concept was accomplished in three phases. First, the bistable diverter valve was sized, manufactured, and tested to determine the operating characteristics and performance. Then, the pulse duration modulator was designed, built, and tested. Finally, the PDM was coupled with the bistable diverter valve for testing of the complete valve.

3.2.2.1 Bistable Diverter Valve Design and Development - The bistable diverter valve was designed to operate without venting the interaction region. A previously designed nonvented bistable diverter valve was scaled down to meet the flow requirement for this system.

This diverter valve maintained 100 percent flow diversion when backpressurized to 60 percent of the supply to off-leg pressure differential. The diverter valve was operated with water, with the off leg of the valve able to asperate ambient air. The bistable diverter valve used in the thermal control loop could do this since the system would be a Freon-charged closed loop. This led to re-evaluation of the expected performance of the diverter valve operating in the thermal control system.

The newly designed bistable diverter valve was manufactured and assembled for testing. Figure 49 shows the schematic of the test setup. Figure 50 shows the bistable diverter valve mounted in its test fixture for testing. This test fixture was designed for visual observation of the flow patterns created in the valve.

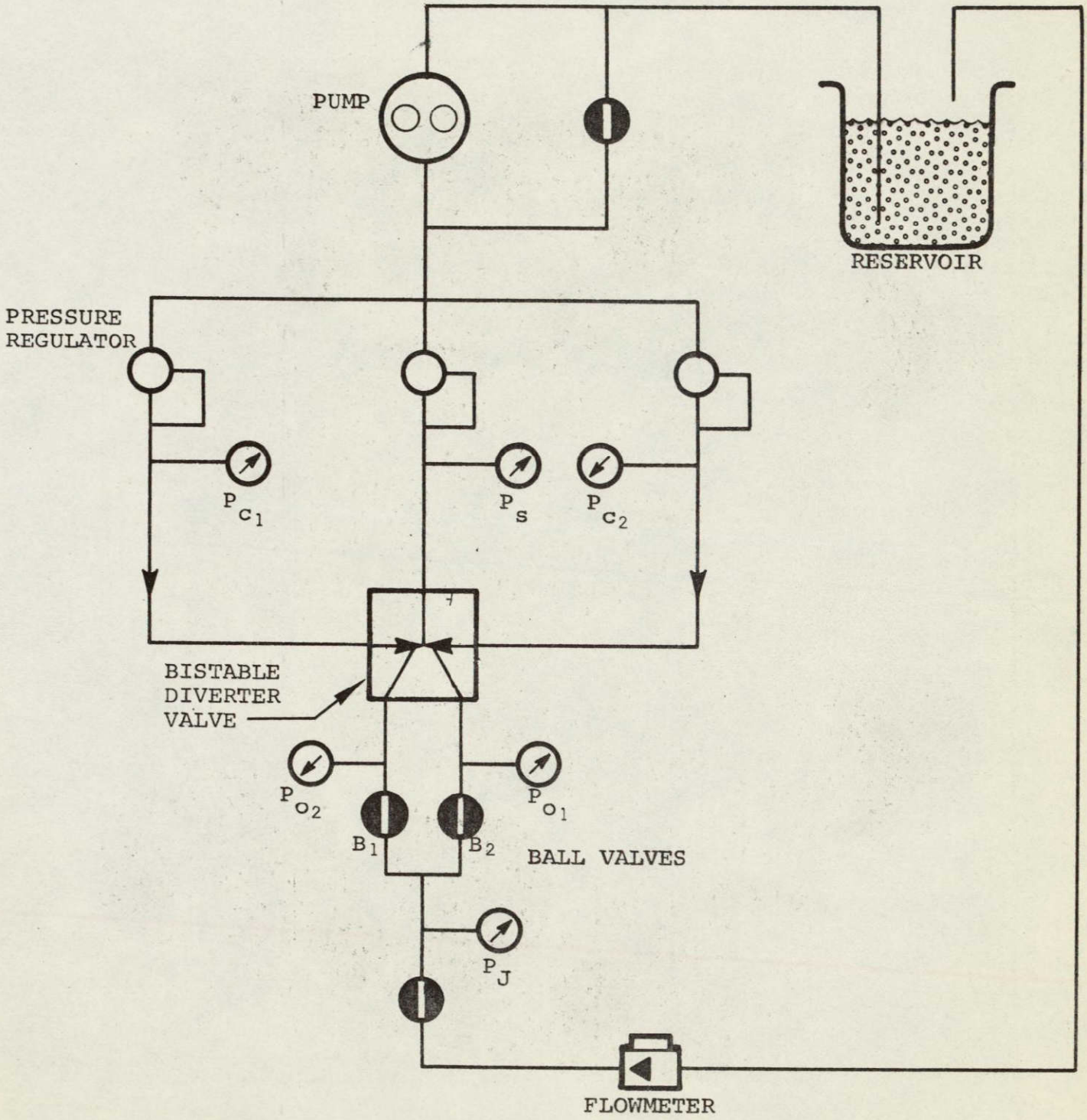

FIGURE 49

SCHEMATIC OF
BISTABLE DIVERTER VALVE TEST SETUP

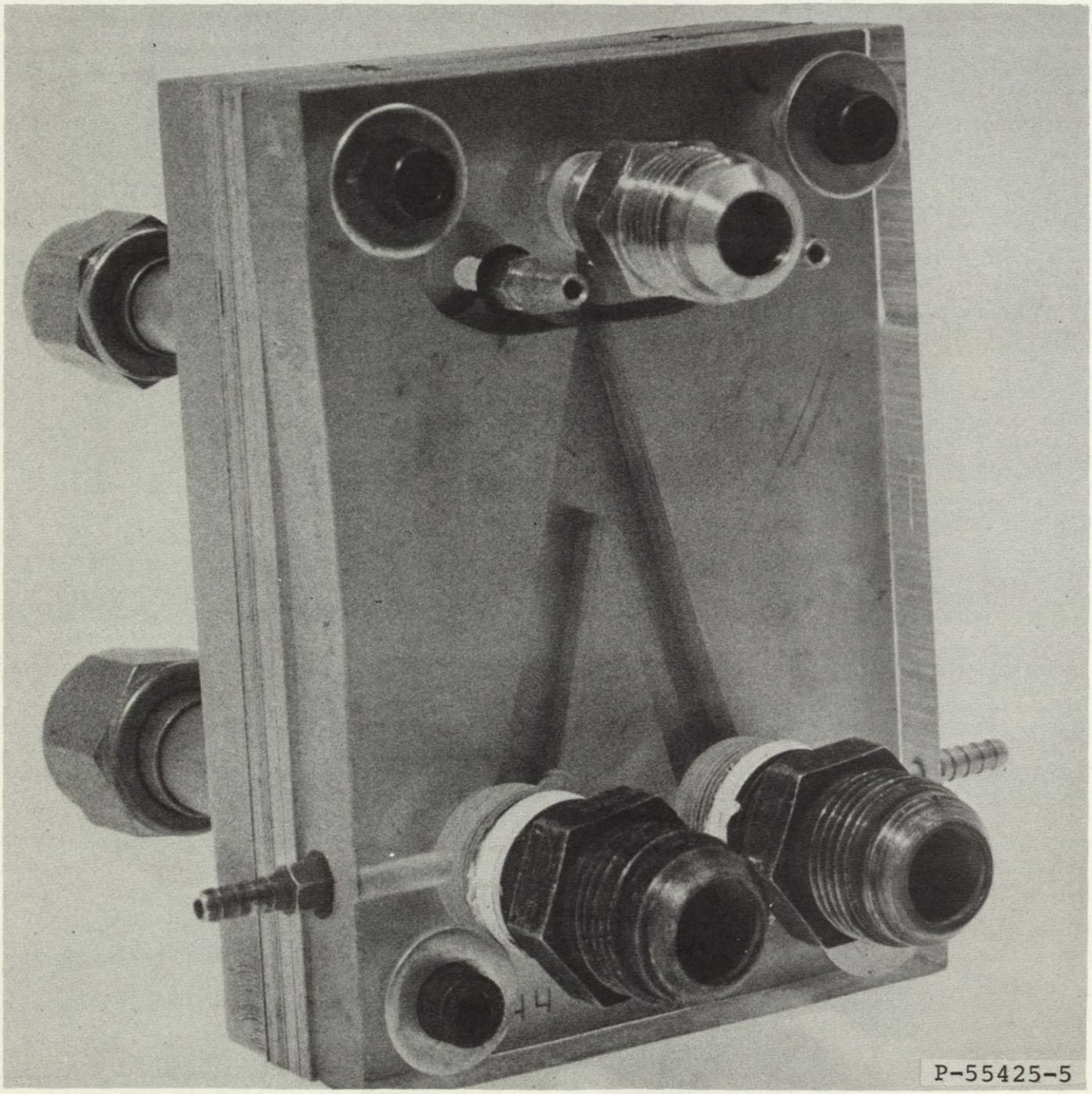

FIGURE 50

BISTABLE DIVERTER VALVE
MOUNTED IN A TEST FIXTURE

The primary purpose of testing this valve was to determine to what extent the valve could be backpressured and maintain 100-percent flow diversion. It was discovered that the backpressure applied to the system was a function of control pressure differential and the mean level of the control pressure ($P_{c(mean)}$).

$$\Delta P_c = P_{c_1} - P_{c_2}$$

$$P_{cc(mean)} = \frac{P_{c_1} + P_{c_2}}{2}$$

$$\Delta P_o = P_{o_1} - P_{o_2}$$

Figure 51 presents the data which indicate the conditions for which 100-percent flow diversion can be achieved. Notice that the percent of backpressure that can be placed on the valve, while maintaining 100-percent flow diversion, increases with control pressure mean ($P_{c(mean)}$) as well as with the control pressure differential (ΔP_c). It should be noted that the off-leg pressure (P_{o_1} or P_{o_2}) during 100-percent flow diversion condition will be equal (P_j) since the flow in the off leg is zero.

The importance of the backpressure capability of the diverter valve may be better understood by refering to Figures 49 and 35. Ball Valves B_1 and B_1 were in the test setup to simulate the pressure drop of the heat exchanger and the compensation restrictor of the actual system, as well as to backpressure the valve. The greater the backpressure capability of the valve, the more flexibility there will be in the design of the cooling heat exchanger, in that the heat exchanger may be more flow restrictive or have higher pressure drop.

3.2.2.2 Design and Development of the Pulse Duration Modulator - The design of the pulse duration modulator is shown in Figure 52. This design was assembled and tested. The PDM circuitry, when bonded, will appear as in Figures 53 and 54 with the porting on the bottom of the stack (seen in Figure 54) interfacing the PDM circuitry with the bistable diverter valve, temperature sensor, and power supply of the system. This circuitry is considered to be quite compact, requiring low flow relative to the system requirements.

The oscillator portion of the PDM was constructed using five stages of proportional amplifier and 24 sets of vortex restrictors in the feedback. The large number of amplifiers and vortex restrictors were required to add transport lag in the oscillator loop and to generate a 50-Hz oscillation. This oscillation is the base frequency of the PDM. The output of the oscillator is shown in Figure 55.

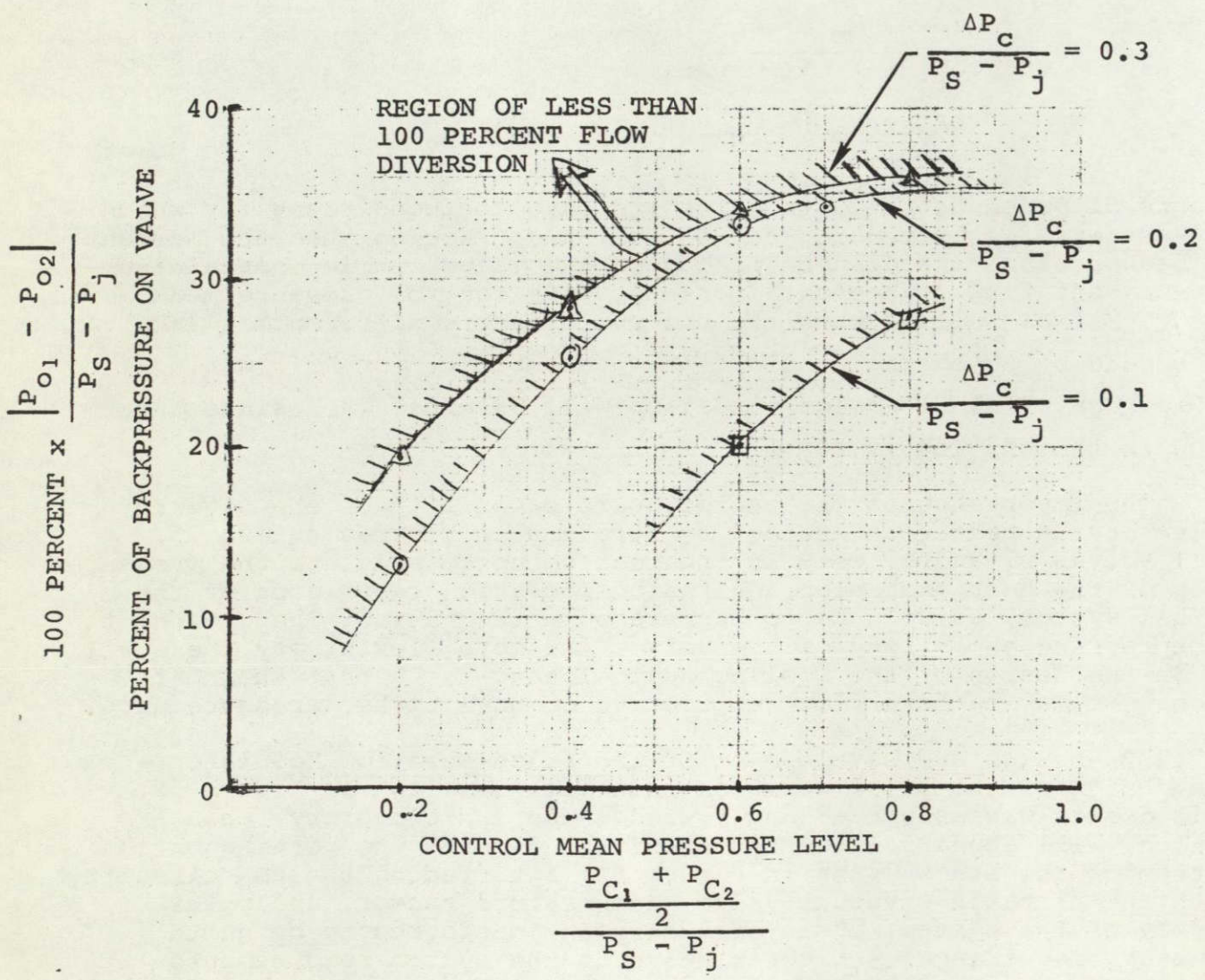

FIGURE 51

BISTABLE DIVERTER VALVE
BACKPRESSURE CHARACTERISTICS

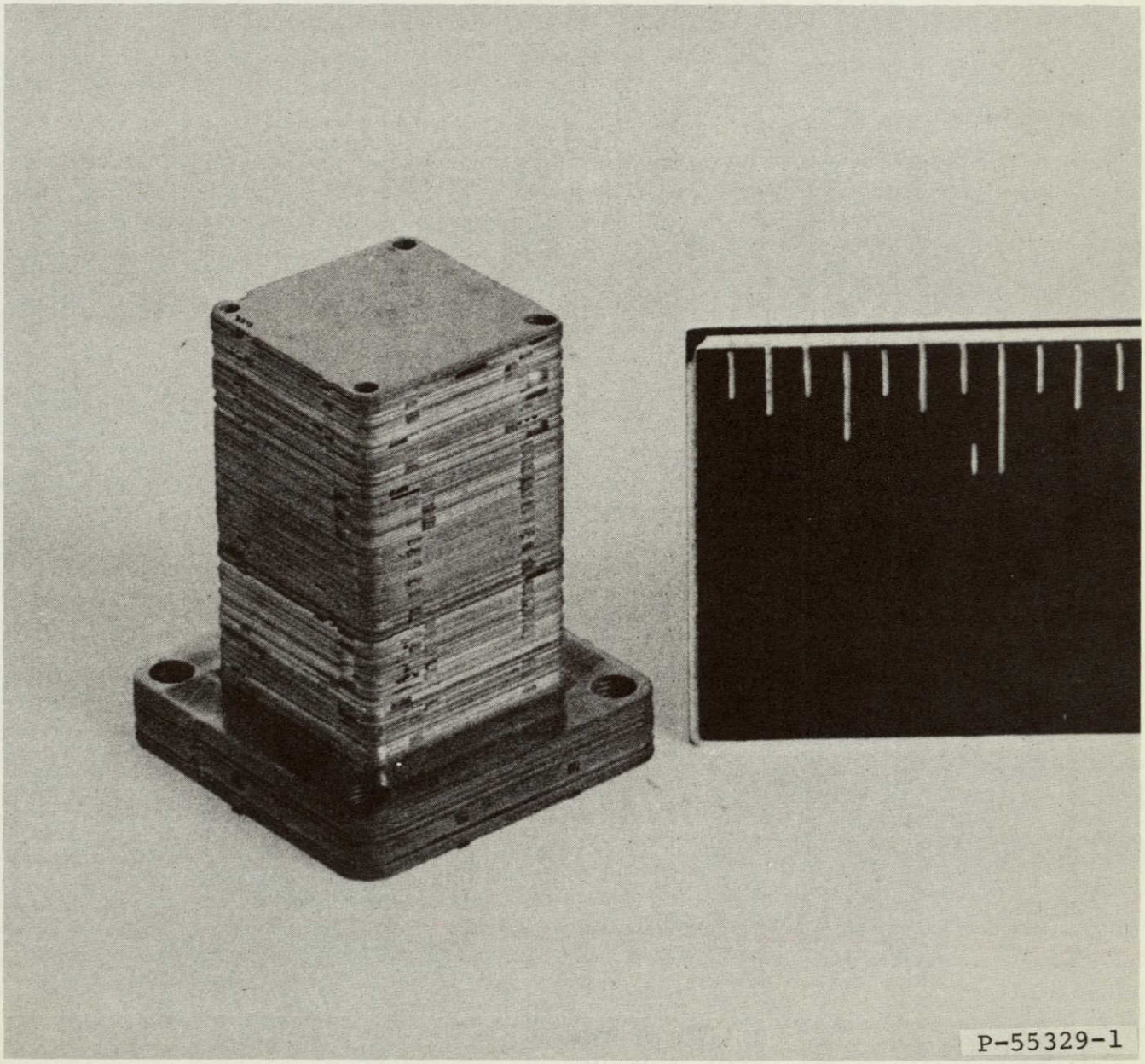

FIGURE 53

PHOTOGRAPH OF A PULSE
DURATION MODULATOR STACK

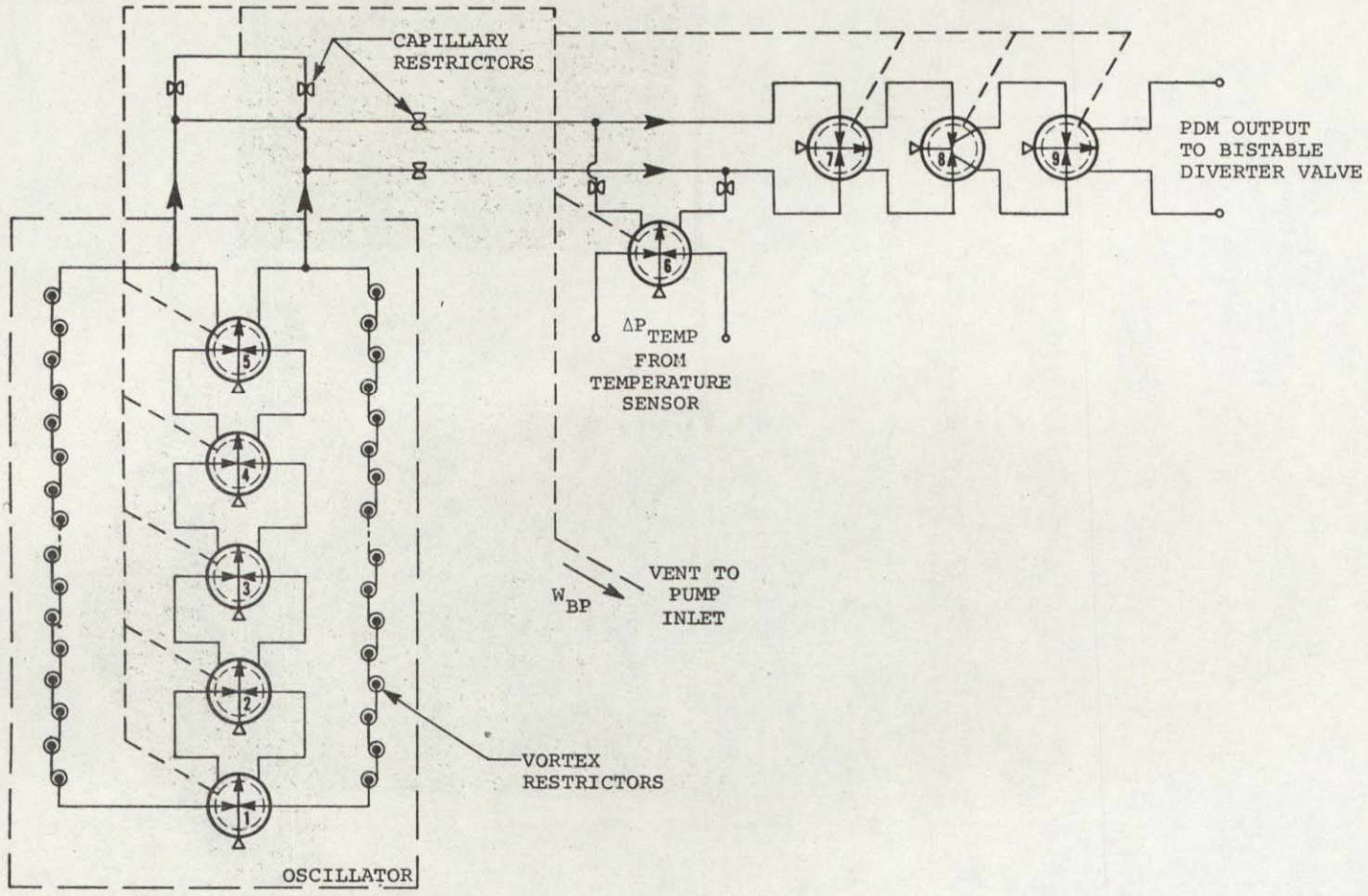

FIGURE 52

SCHEMATIC OF THE PULSE DURATION MODULATOR

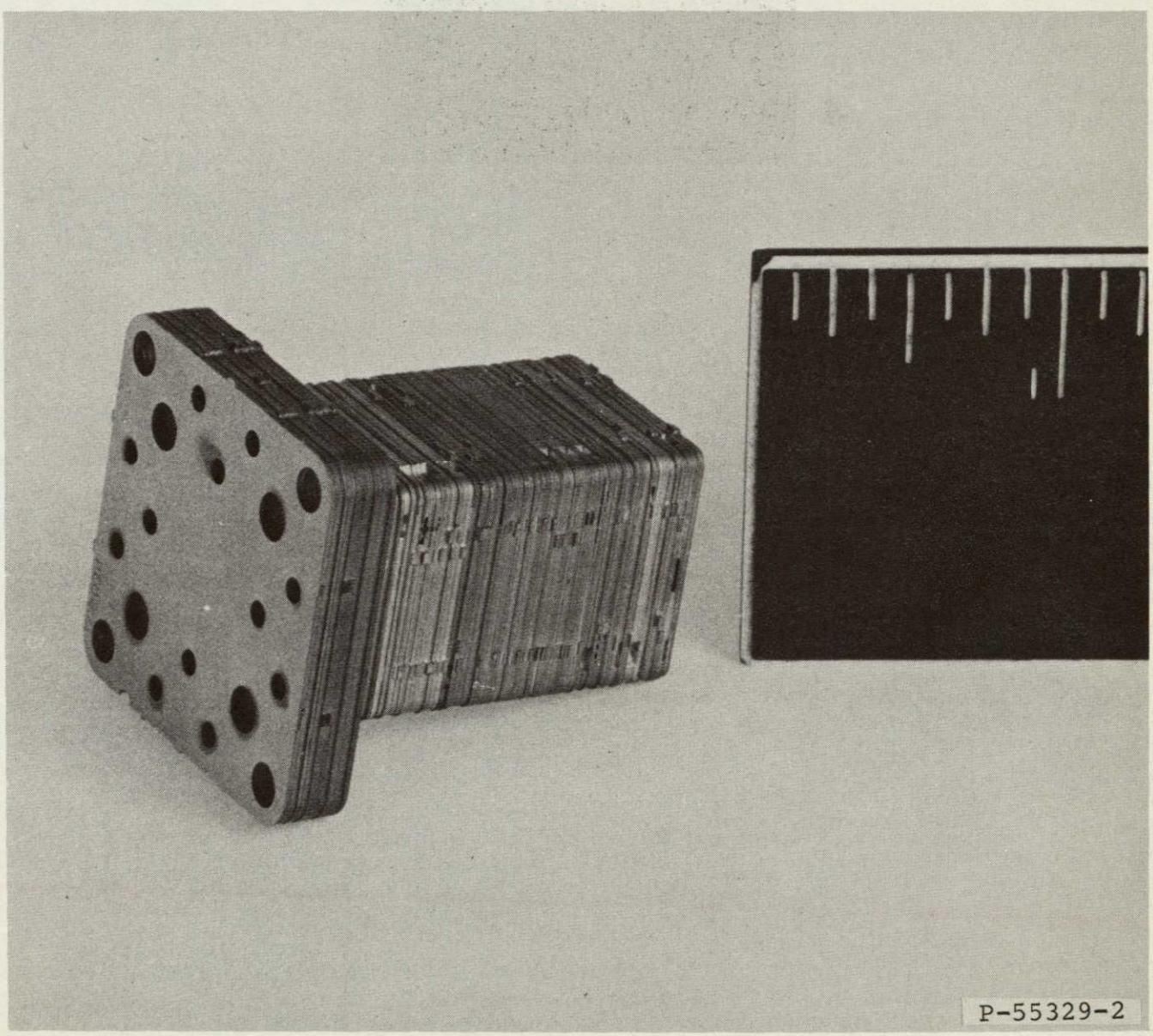

FIGURE 54

PHOTOGRAPH OF A PULSE DURATION MODULATOR STACK

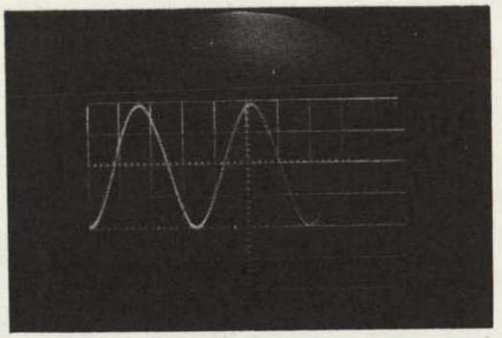

FIGURE 55

OSCILLATOR OUTPUT

The oscillator output and temperature sensor signal, when resistively summed, drive the output stages of the PDM (Amplifiers No. 7, 8, and 9). The gain of the PDM is presently set such that ±2 psi (13.8 kPa) ΔP_{Temp} signal will drive the PDM output into full saturation of the nonswitching condition.

3.2.2.3 Pulse Duration Modulation Diverter Valve Testing - The purpose of testing the PDM diverter valve was to establish the approximate flow staging of the diverter valve such that it could be driven by the PDM. The test setup schematic shown in Figure 56 was used to test the circuitry. No modifications were made to the PDM. Flow staging of the diverter valve was provided by bistable diverter valves (Nos. 10, 11, and 12 of Figure 57). Two sizes of bistable diverter valves were used in this staging, as are shown in Figure 58.

When staging the nonvented bistable diverter valves, the control pressure on the valve cannot be lower than the output pressures. This meant that the output pressure of a diverter valve stage would be lower than that of the previous staged diverter valve and so on throughout the valve staging. With this in mind, and the fact that the last stages of the diverter valve needed a high control pressure mean relative to its supply pressure to maintain increased levels of backpressure at the 100-percent flow diversion condition, the supply

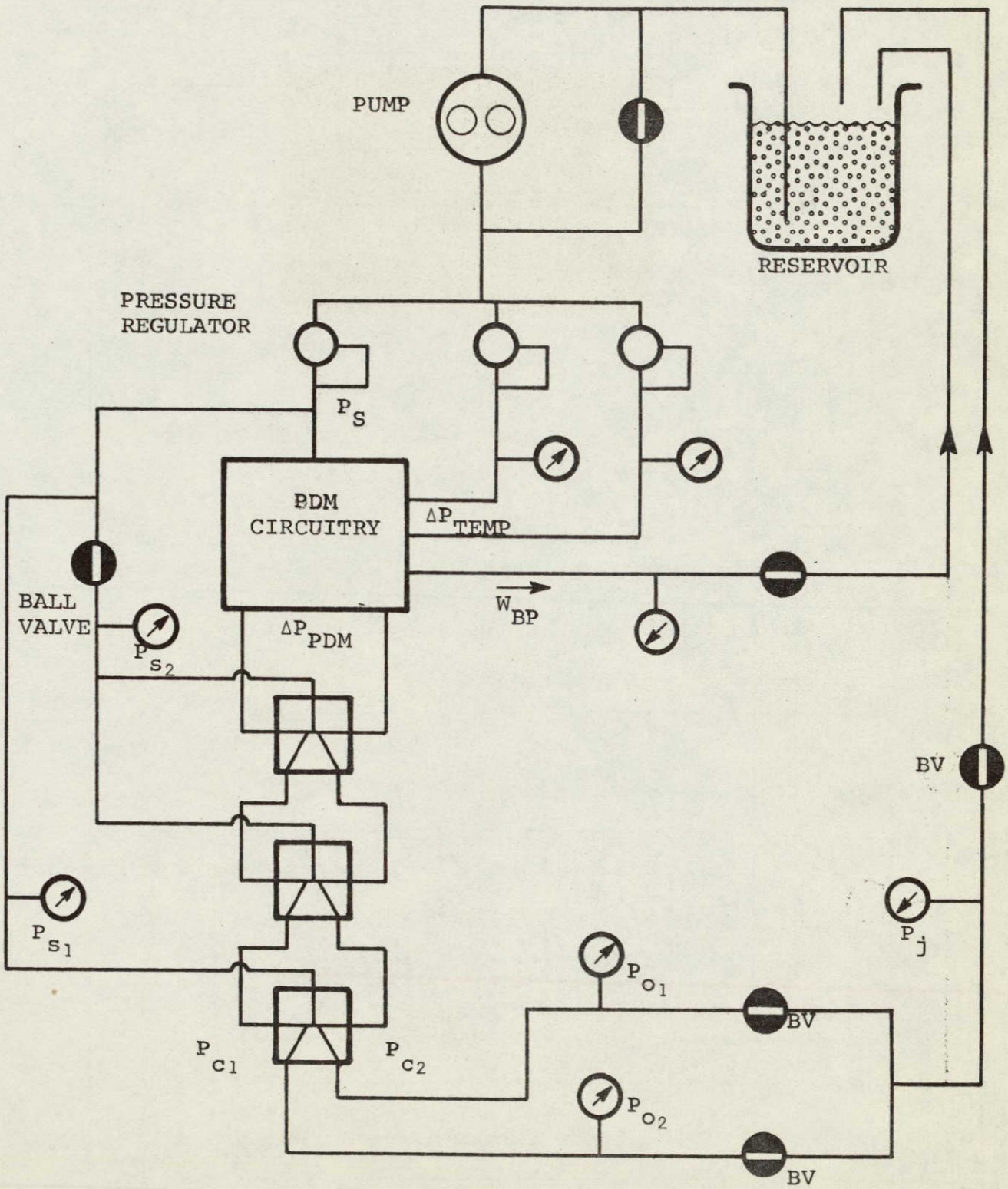

FIGURE 56

SCHEMATIC OF PDM DIVERTER VALVE TEST SETUP

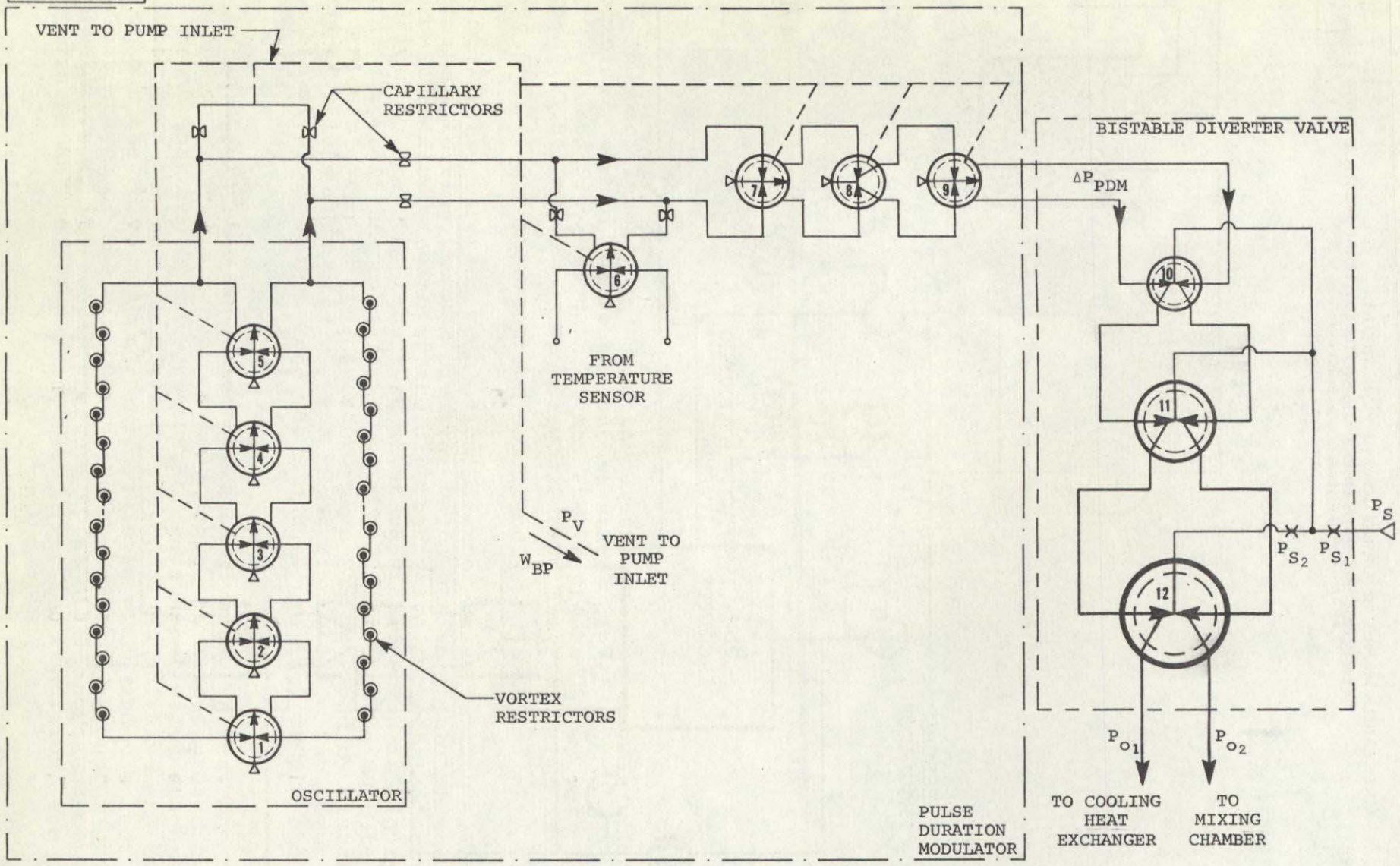

FIGURE 57

SCHEMATIC OF PDM DIVERTER VALVE

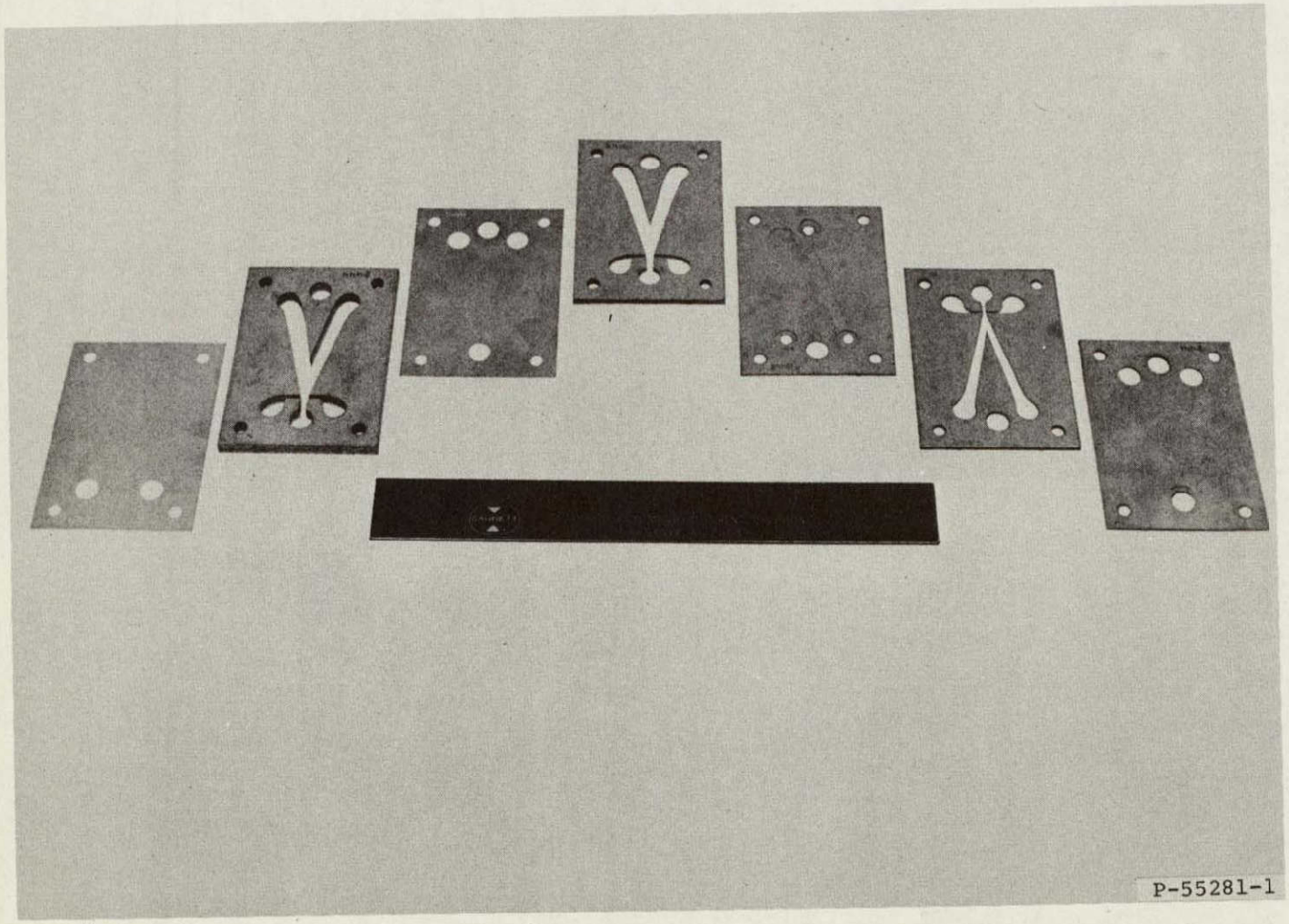

FIGURE 58

TWO SIZES OF
BISTABLE DIVERTER VALVES

pressures to the diverter valve stages were also staged (as shown in Figure 57) by Restrictor R_1 and R_2. This action enabled each stage of the bistable diverter valve to have higher pressure drops between supply and output, which increased the flow amplification capabilities of each bistable diverter stage.

The PDM diverter valve was installed in the test setup of Figure 56 and staged to operate under the following conditions using water as the working fluid:

$$P_s - P_j = 20 \text{ psi } (138 \text{ kPa})$$

$$P_s - P_{s_1} = 5 \text{ psi } (34 \text{ kPa})$$

$$P_s - P_{s_2} = 10 \text{ psi } (69 \text{ kPa})$$

$$P_s - P_v = 10 \text{ psi } (69 \text{ kPa})$$

$$\frac{P_{c_1} + P_{c_2}}{2} - P_j = 7 \text{ psi } (48 \text{ kPa})$$

$$\Delta P_{c(max)} = 2 \text{ psi } (13.8 \text{ kPa})$$

Figures 59 and 58 show the unbonded PDM stack and a breakaway view of the staged bistable diverter valve used in this test.

Visual observations were made of the flow patterns in the last stage of the bistable diverter valve to determine if 100-percent flow diversion was being achieved when the PDM was fully saturated. One-hundred percent flow diversion was maintained in the diverter valve when $|\Delta P_c|$ remained below 3.5 psi (24 kPa), which was as expected from backpressure characteristics (Figure 51) of the bistable diverter. During this test, visual observation of the last stage of the bistable diverter valve, while the PDM was operating under unsaturated modulating conditions ($|\Delta P_{Temp}| \leq 2$), indicated that the bistable diverter valve was being driven by the PDM. Further investigation of the diverter valve output pressures revealed that the bistable diverter valve was not being driven adequately by the PDM, in that not all the pulses transmitted by the PDM carried through the bistable diverter valve. This problem can be corrected by improving the flow staging of the diverter valves. No further staging development was accomplished at this time.

AIRESEARCH MANUFACTURING COMPANY OF ARIZONA
A DIVISION OF THE GARRETT CORPORATION

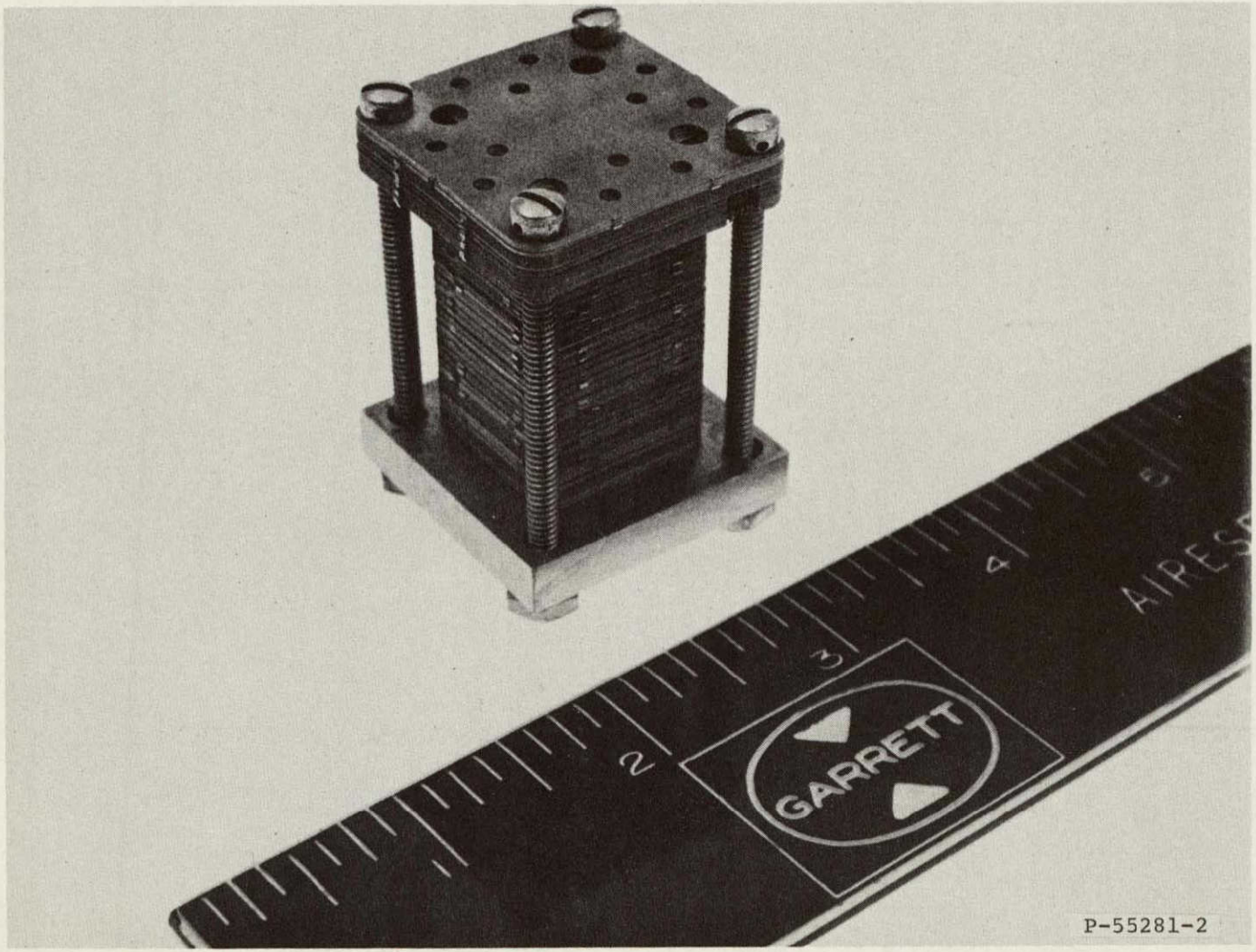

FIGURE 59

UNBONDED PDM STACK

The flow efficiency of this valve concept is determined by the ratio of the flow bypassed to pump inlet, to the supply flow to the fluidic valve, where

$$\eta_w = (1 - \frac{W_{BP}}{W_s}) \times 100 \text{ percent}$$

However, if the PDM vent pressure (P_v) can be maintained at the same pressure as the supply to the last stage of the bistable amplifier (P_{s_2}), as was the case during the PDM diverter valve testing, the vent flow could be channeled through the last stage of the bistable diverter valve without being bypassed to pump inlet. Thus, W_{BP} would be zero and the flow efficiency (η_w) of the PDM diverter valve would be 100 percent.

3.2.2.4 Conclusion of the Pulse Duration Modulation Diverter Valve Testing - The PDM diverter valve can meet and exceed the flow diversion requirement of the thermal control system. The bistable diverter valve in this system is capable of diverting 100 percent of the supply and control flow entering the last stage of the diverter valve to either of the two flow paths (one to the cooling heat exchanger and the other bypassing the cooling heat exchanger) if the pressure drop across the cooling heat exchanger does not exceed approximately 35 percent of the supply to off-leg pressure differential of the last stage in the bistable diverter valve. It also appears that, with proper supply staging of the PDM diverter valve, a 100-percent flow efficient system can be developed.

SECTION 4

CONCLUSIONS AND RECOMMENDATIONS

4.1 CONCLUSIONS OF PHASE I, TEMPERATURE SENSOR DEVELOPMENT

The orifice bridge viscosity change temperature sensor, when operated with a noise-free power supply, demonstrated the temperature sensitivity required for operating a thermal controller. The output of this device, with a noise-free power supply, is shown on Figure 3.

Two characteristics of the thermal control system affect the performance of the orifice bridge temperature sensor to the extent that it cannot meet the accuracy requirement of the thermal control system. The characteristics that are involved are: the viscosity properties of Freon 21 and the output characteristics of the Freon power supply. For most cases, the Freon power supply is a centrifugal pump that generates high-pressure fluctuations in the supply flow. Because the orifice bridge temperature sensor is also sensitive to supply-pressure fluctuations, this high-pressure fluctuation or noise will carry through to the output of the temperature sensor. The relative sensitivities to pressure and viscosity are such that the viscosity changes over the range of operation cannot be distinguished from the noise generated by the pump, even with the use of the most effective means of noise attenuation.

There are, however, two possible solutions that would make this sensor acceptable for this range of temperature control in a system of this type. Both of these involve the selection of the working fluid.

By increasing the temperature sensitivity of the bridge circuit, the noise generated by the pump would not be as significant, thereby providing a higher signal-to-noise ratio and an acceptable temperature signal. The temperature sensitivity of the bridge circuit is due to the viscosity change of the fluid with temperature. Therefore, by using a fluid with a greater viscosity change per temperature change than Freon 21, the temperature sensitivity of the orifice bridge temperature sensor would be larger.

The second solution would be to use a lower viscosity working fluid such that the pump noise may be diminished by viscous force that would become more prevalent. This characteristic was evidenced when the orifice bridge circuit was tested with water as the working fluid.

The filled bellows-driven pin amplifier temperature sensor produced remarkable temperature sentivities. This temperature sensor has been selected for use in Phase III of this program because of its superior performance over the orifice bridge viscosity change temperature sensor. Temperature changes as low as 0.25F have been sensed. The design of this temperature sensor provides the following characteristics and options if desired.

a. Low sensitivity to pressure present in the temperature sensing cavity

b. High temperature gains can be achieved

c. Can be operated on a wide range of fluids

d. The fluids being sensed may be isolated from the fluid in the pin amplifier

e. Wide range of set-point adjustability

f. The gain of the temperature sensor may be widely changed by modifying the fluid in the filled bellows and/or modifying the pin amplifier design.

g. Relatively low sensitivity to pump-generated noise

4.2 CONCLUSIONS OF PHASE II, VALVE DEVELOPMENT

Two valve concepts were developed in this phase of the program, both of which were capable of operating in this system. However, the pulse duration modulation diverter valve was selected for use in the system because it exceeded all flow diversion requirements, had the highest flow efficiency at the values tested, and is completely flueric, having no moving parts.

The proportional-vortex combination mixing valve, which was constructed and tested but was not selected for further implementation in the thermal control-mixing control system, easily satisfied the flow mixing requirements of the system; however, the flow efficiency of this valve concept was low. The low flow efficiency was due to the flow efficiency of the proportional amplifier which drove the vortex mixing valves. The vortex mixing valves operated with full flow recovery. The flow efficiency of the proportional amplifier was only approximately 15 percent.

The vortex mixing valve shows considerable promise for future applications since the valve has no moving parts and attained 100-percent flow mixing. For this valve to operate efficiently, the device that drives the vortex valves must possess relatively good flow efficiency so as not to deteriorate the flow performance of the system as did the proportional amplifier used on the proportional-vortex combination mixing valve concept.

The pulse duration modulation diverter valve performed with 95-percent flow efficiency and 100-percent flow diversion. The flow diversion characteristic of the valve concept was found to be a function of the back pressure applied to the diverter valve, as well as the control-pressure level on the last stage of the diverter valve. In order to obtain a high back pressure capability, the diverter valve required valve supply staging to maintain a high control pressure level on the last stage of the diverter valve. This allowed the diverter valve to be back-pressured to approximately 35 percent of the supply to off-leg pressure differential and to maintain 100-percent flow diversion capabilities. It should be noted that, in this application, the back pressure is generated by the cooling heat exchanger and the pressure drop across the cooling heat exchanger will constitute approximately 18 percent of the Freon supply (pump outlet) to controlled temperature junction (mixing chamber) pressure differential (Refer to Figure 35). The PDM diverter valve was designed to operate with a 20-psi (138 kPa) pressure drop across the valve and cooling heat exchanger, of which 3.5 psi (29 kPa) drop is due to the cooling heat exchanger. These operating pressures were selected out of convenience; it is possible that these operating pressures could be lowered by resizing and modifying the PDM diverter valve circuit.

4.3 RECOMMENDATIONS FOR PHASE III

The filled bellows pin-amplifier temperature sensor and the pulse duration modulation diverter valve have been selected for coupling during Phase III. The designs of the temperature sensor and valve will remain essentially the same as those tested during Phases I and II. Additional hardware, such as filters and regulators, will be required to provide proper protection and operation of the control system. To protect the fluidics from contamination that may occur in the system, 50-micron filters will be used in the supply lines to the temperature sensor and valve. The design of the entire system will require some form of regulation to maintain the prescribed pressure drop across the PDM circuitry. The vent flow of the PDM will be channeled through the last stage of the diverter valve, which will allow the regulator to be of a relief type with minimum parts and movement. This regulator will maintain pressure drop across the PDM circuitry, as well as maintain supply pressure to the last stage of the diverter valve.

SECTION 5

SCHEDULE AND COST SUMMARY

5.1 SUMMARY SCHEDULE

Figure 60 depicts the estimated time schedule for various tasks in the program.

5.2 PROGRAM COST

The Contractor has requested that Freon 114 (CCl_2F - CCl_2F) be substituted for Freon 21 ($CHCL_2$) for the final testing under Phase III of the subject contract. This request was prompted by the cost increases of Freon 21 since the beginning of the contract. At the initiation of the program, Freon 21 costs were $590.00 per 150-pound cylinder. The present cost per 150-pound cylinder is $1,950.00.

Phase III testing would require a minimum of two and possibly three 150-pound cylinders. These cost increases, which were not estimated at the outset of the contract, would create a contract cost overrun. To prevent this cost overrun, the Contractor suggests Freon 114 at a cost of $130.00 per 150-pound cylinder be substituted for Freon 21. This substitution was selected based upon similar viscosity, boiling point and freezing point. Since the temperature sensor and mixing valve are not affected by viscous changes of the fluid, the performance of the thermal mixing control will be insignificantly affected.

Figure 61 presents a comparison of estimated and actual program costs to the end of the reporting period.

5.3 PROGRAM TIME EXPENDITURE

The total man-hours expended on the program to date are as follows:

Engineering man-hours	1468
Laboratory man-hours	506
TOTAL	1974

AIRESEARCH MANUFACTURING COMPANY OF ARIZONA
A DIVISION OF THE GARRETT CORPORATION
PHOENIX, ARIZONA

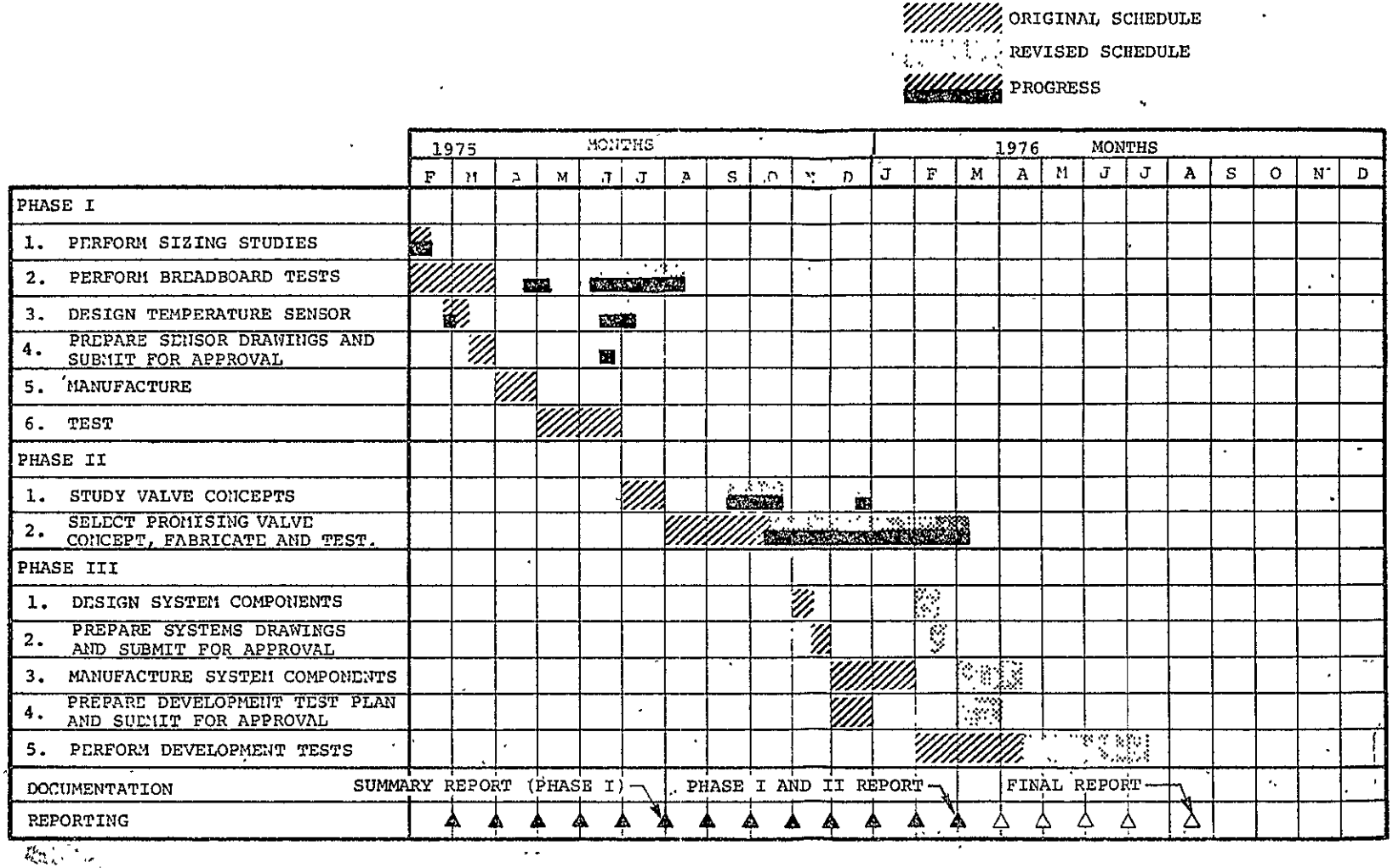

FIGURE 60

PROGRAM PLAN FOR THE DESIGN, FABRICATION, TESTING,
AND DELIVERY OF A THERMAL
CONTROL-MIXING CONTROL DEVICE

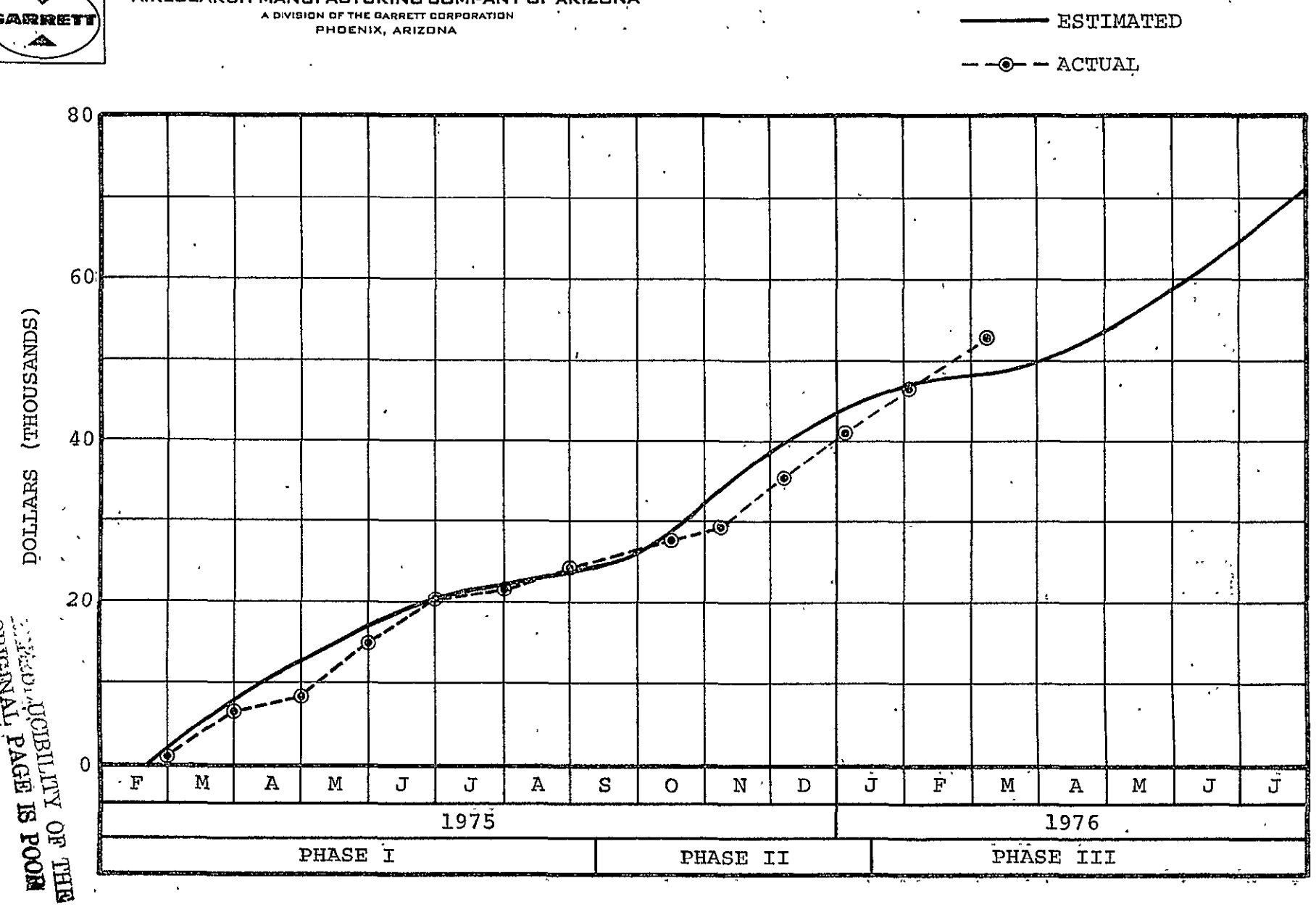

FIGURE 61

RATE OF EXPENDITURE
CONTRACT NO. NAS8-31289